Molecular Simulations of Deep Eutectic Solvents: A Perspective on Structure, Dynamics, and Physical Properties

Shalini J. Rukmani^{1,2,1}, Brian W. Doherty^{3,1}, Orlando Acevedo³, Coray M. Colina^{1,2,4}

¹Department of Materials Science and Engineering, University of Florida, Gainesville,
32611, USA

²George and Josephine Butler Polymer Research Laboratory, Department of Chemistry, University of Florida, Gainesville, 32611, USA

³Department of Chemistry, University of Miami, Coral Gables, 33146, USA

⁴Department of Chemistry, University of Florida, Gainesville, 32611, USA

These authors contributed equally to this work

1. Introduction

Sustainable solvents have attracted significant attention over the last three decades for the synthesis of functional materials in energy conversion, storage, and separation applications. ¹⁻⁵ For most applications, conventional organic solvents and inorganic electrolytes have proven to be expensive, energy-intensive, sensitive to moisture, and produce toxic effects harming the environment through formation of residual products and gaseous emissions into the atmosphere. ⁵⁻

To address these shortcomings, significant research efforts have focused on the development of green and sustainable solvents. ⁸⁻¹⁰ Deep eutectic solvents (DESs) have become attractive alternatives, and an increasing research effort to understand the structure-property relation in these solvents for diverse applications have grown since early 2000s. ¹¹⁻¹⁵ Many research studies have focused on the use of DESs as reaction media for the synthesis of functional materials in electrocatalysis, fuel cells, organic synthesis, biomass, and biodiesel purification. ^{2,16-18} DESs have also been investigated as a possible alternative for CO₂ scrubbing applications such as aqueous

amines, aqueous ammonia, and potassium carbonate due to their biodegradability, low cost of production, and low toxicity. 19-20 Other important applications of DES include liquid electrolyte alternatives for photovoltaic devices and nanostructured sensors, metal processing such as electrodeposition, metal extraction and processing of metal oxides, and electropolishing. 21-28

Several experimental and computational investigations have contributed towards the understanding of their complex structure and interaction between the constituents. ^{13,15,29} Molecular simulations have played a significant role in elucidating the intricacies present in DESs; in particular, the effect of intermolecular interactions on the observed macroscopic bulk properties. ³⁰⁻³⁶ Simulations have also been performed on DES in conjunction with other materials including metal surfaces, proteins and gas molecules with specific emphasis on the interaction between DES and molecules/surfaces, interfacial properties and gas sorption. ³⁷⁻³⁹ Rather than providing an overview of simulation studies performed to date on DESs, this review aims to accomplish three goals: (1) Provide the essential background to a novice modeler on the choice of simulation techniques used to model DESs, (2) Describe methods used to obtain important physical, thermodynamic, transport and structural properties of bulk DES systems including an evaluation of the strengths and drawbacks of the current simulation models, and (3) Discuss future directions for simulating DES-based systems.

In section 2, the molecular structure and types of DESs are described. Sections 3 to 7 provide an overview of atomistic simulation methods used to model DES systems with a discussion as to how physical, thermodynamic and transport properties are obtained from atomistic molecular simulations. Finally, a summary of the overall performance of current simulation models is provided that highlights the strengths and drawbacks of each method in representing the

structure and properties of DESs. Potential future directions for atomistic simulations of these unique solvent systems are discussed.

2. Deep Eutectic Solvents

2.1 Definition of Deep Eutectic Solvents

The term "deep eutectic solvents" was coined from the decrease observed in the melting temperature of a solvent mixture relative to the melting temperatures of the pure components prior to mixing. The *eutectic temperature* is thus defined as the lowest melting temperature for a given mixture and the corresponding composition is called the *eutectic composition*. DESs collectively denote liquids that are close to this eutectic composition. These solvents consist of large and asymmetric ions with low lattice energies. Abbott et al.¹¹ synthesized the first DES in 2001 by mixing metal chlorides (ZnCl₂, and/or SnCl₂) and quaternary ammonium salts. DESs are usually obtained by mixing a hydrogen bond acceptor (HBA) (such as quaternary ammonium halide salts) with a hydrogen bond donor (HBD) molecule that has the ability to form a complex with the halide, leading to a depression of the freezing point of the resulting mixture. Figure 1 shows as an example the freezing point curve of a DES system formed from a halide salt and a neutral organic compound, namely, choline chloride (ChCl) and urea.⁴⁰ The freezing point is the lowest (12 °C) at 65 mol% urea than the freezing point of the original constituents (ChCl = 302 °C and urea = 133 °C). In general, the freezing point of most DESs are less than 150 °C.^{13,41}

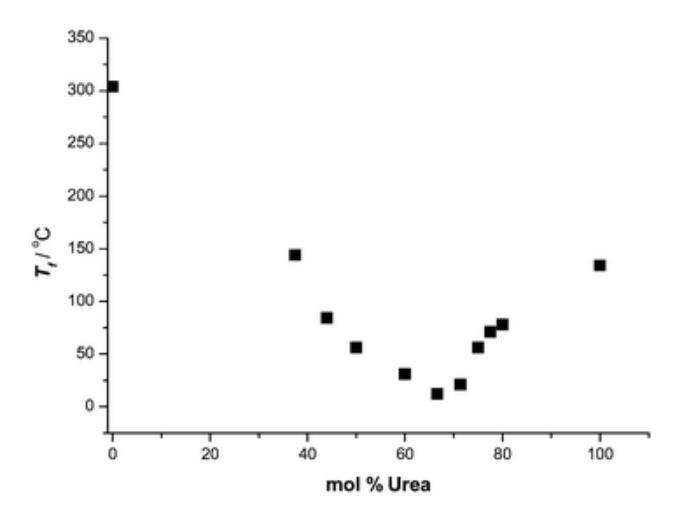


Figure 1. Freezing point of choline chloride (ChCl)-urea DES system as a function of composition. Republished with permission of the Royal Society of Chemistry, from Novel solvent properties of choline chloride/urea mixtures, A. P. Abbott, G. Capper, D. L. Davies, R. K. Rasheed and V. Tambyrajah, Vol 1, 2003; permission conveyed through Copyright Clearance Center, Inc.

2.2 DES as Ionic Liquid Analogues

The development of DESs by Abbott et al. 11 originated from their efforts to overcome the limitations associated with conventional imidazolium-based room temperature ionic liquids (RTILs). For example, the high cost of RTILs for bulk-scale applications and low moisture-stability associated with the use of salts such as aluminum chloride led to replacements featuring the combination of alternative metal chlorides with quaternary ammonium salts. It was observed that low symmetry cations in general led to a decrease in the freezing point, with ChCl showing the lowest freezing point among the systems tested. Subsequently, DESs based on ChCl and carboxylic acids were also synthesized by Abbott et al. and were shown to exhibit a similar depression in the freezing point. 42 These liquids share similar physical properties to RTILs, including high viscosity, large surface tension, low vapor pressure, and non-flammability. Consequently, DESs are often termed as ionic liquid analogues. Nevertheless, it is important to underscore the differences between DESs and ionic liquids (ILs) with respect to the constituents

and molecular interactions that govern their unique properties. One of the important differences between conventional ILs and DES is that ILs are made from discrete anions and cations, whereas DESs are synthesized by mixing two components that form a eutectic mixture which typically consists of cations, anions, and neutral organic compounds. The differences in the properties exhibited by DESs and ILs arise from the contribution of molecular interactions from different components. While ionic interactions dominate in ILs, molecular interactions have a significant contribution, starting from hydrogen bonding interactions in DESs. Moreover, an ease of synthesis in the pure state, moisture insensitivity, and biodegradability are some of the more attractive properties that differentiate DESs from ILs. Figure 2 shows an example of a DES system, reline, formed from ChCl and urea in a 1:2 ratio, respectively, where ChCl is the HBA and urea is the HBD. These components form a eutectic mixture primarily due to contributions from a network of hydrogen bonding interactions.

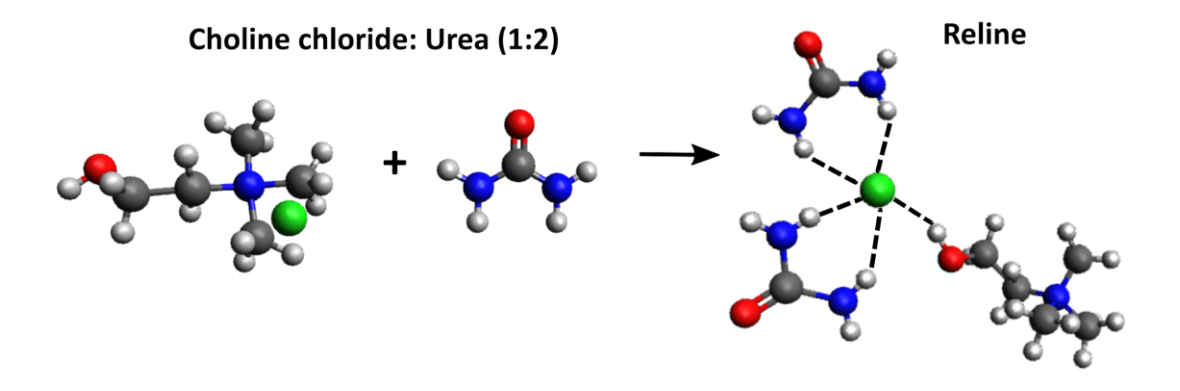


Figure 2. Schematic showing choline chloride (ChCl) and urea mixed in the ratio 1:2, respectively, to form reline. Elements are colored as ●carbon ●oxygen ●chloride ● nitrogen hydrogen. The dashed lines represent the formation of hydrogen bonds between different pairs including Cl⁻ and the hydrogen atom of the OH group in Ch⁺, and Cl⁻ and hydrogen atoms present in urea.

2.3 Molecular Structure of DESs and Type of Interactions

The properties of DESs are controlled primarily by hydrogen bonding between the different components of the mixture (cation and anion of HBA, and the HBD species). However, appreciable contributions from electrostatic interactions and van der Waals forces on some physical properties such as viscosity have been reported. 41,43-44 Figure 3 illustrates DES formation through a potential complexation of the Cl⁻ anion present in ChCl with urea (HBD)³³ and Table 1 shows the fraction of hydrogen bonds in four ChCl-based DES systems studied by Perkins, Painter, and Colina through atomistic molecular simulations.³¹ In three of the systems studied, namely, ethaline, glyceline, and maline, the fraction of hydrogen bonding interactions between the HBD and corresponding anion were found to be the largest. However, in the reline system, the urea-urea interactions were found to be significant. Despite the importance of intermolecular interactions within DESs, quantitatively reproducing the molecular structure of the systems has proven quite challenging for multiple simulation methods including classical MD, ab initio MD (AIMD), firstprinciples MD (FPMD), and mixed quantum and molecular mechanical (QM/MM) with deviations reported for properties such as radial distribution functions (RDFs) and hydrogen bonding behavior. 34-35,45-46

$$\begin{bmatrix} OH \\ OH \\ CI \\ H_2N \end{bmatrix} \overset{\odot}{=} \begin{bmatrix} OH \\ N-H \\ N-H \\ H-N \\ H \end{bmatrix} \overset{\odot}{=} \begin{bmatrix} Choline]CI + 2Urea & [Choline]^+ + [CI. Urea_2]^- \end{bmatrix}$$

Figure 3. Illustration of a possible complex formation in reline DES (ChCl-urea in 1:2 molar ratio). C. R. Ashworth, R. P. Matthews, T. Welton, P. A. Hunt, *Phys. Chem. Chem. Phys.*, 18,

(27), 18145-18160 (2016). Doubly Ionic Hydrogen Bond Interactions within the Choline Chloride–Urea Deep Eutectic Solvent. Published by the PCCP Owner Societies.

Table 1. Estimated Relative Contribution of Hydrogen Bonding Present in CCEtg, CCU, CCGly, and CCMal.

DES	Choline-Cl	Choline-HBD	HBD-Cl	HBD-HBD
CCEtg	0.15	0.05	0.57	0.23
CCU	0.08	0.08	0.32	0.52
CCGly	0.11	0.05	0.50	0.34
CCMal	0.30	0.05	0.51	0.14

- (a) Averaging was performed over a 1 ns trajectory with 2 ps between each frame.
- (b) System abbreviations are defined in Table 3.
- (c) Adapted with Permission from S. L. Perkins, P. Painter, C. M. Colina, *J. Chem. Eng. Data*, **59**, (11), 3652-3662 (2014). Experimental and Computational Studies of Choline Chloride-Based Deep Eutectic Solvents. Copyright 2014 American Chemical Society. Earlier experimental and simulation studies have suggested that negative charge

delocalization plays a major role in decreasing the melting point of the individual components, a consequence of hydrogen bonding between the mixture components, especially between the halide ion and the HBD moiety. 47-48 However, recent computational investigations based on *ab initio* and molecular mechanics (MM) calculations have shown that there are complex interactions present rather than a simple charge delocalization. For example, charge spreading in ChCl-based DES was investigated by Zahn, Kirchner, and Mollenhauer³⁴ where it was found that hydrogen bonding enhances negative charge spreading from the anion to the HBD, whereas the spreading of positive charge is decreased. However, in the case of ChCl-urea systems, negligible charge spreading was found between the anion and HBD as a result of increased hydrogen bonding between the Ch cation and the Cl anion as compared to Ch-urea. Ashworth et al. 33 also studied ChCl-urea as a model system to understand double ionic hydrogen bond interactions and found that urea forms a H-bonded complex with the cation, namely, urea[choline]⁺, which has been shown to form the

strongest H-bond identified between the hydrogen atom of the hydroxyl group of Ch⁺ and the oxygen atom of the urea molecule. This complex is energetically competitive with the [Cl(urea)₂]⁻ complex, which has been associated with the eutectic behavior observed in reline. The negative charge on the anion complex was found to be localized. To summarize, recent investigations have challenged the earlier explanation that negative charge delocalization between the HBD and anion is a predominant factor in decreasing the melting point of the DES mixture relative to the original components.

2.4 Types of DES

The general formula used to describe DESs is Cat⁺X⁻zY where Cat⁺ denotes the cation, which can be any ammonium, phosphonium, or sulfonium cation, and X is a Lewis base, usually a halide ion such as Cl⁻. Based on the complexing agent, DESs are commonly divided into four types as described in Table 2.

Table 2. Classification of DES Based on the General Formula Cat⁺X⁻zY.

Type	General formula
I	$Cat^{+}X^{-}zMCl_{X}$, $M = Zn$, Sn , Fe , Al , Ga
II	$Cat^{+}X^{-}zMCl_{X}.yH_{2}O, M = Cr, Co, Cu, Ni, Fe$
III	$Cat^{+}X^{-}zRZ$, $Z = CONH_2$, $COOH$, OH
IV	$MCl_x + RZ = MCl_{x-1}^+ \cdot RZ + MCl_{x+1}^-, M = Al, Zn$ and $Z = CONH_2, OH$

Adapted with permission from E. L. Smith, A. P. Abbott, K. S. Ryder, *Chem. Rev.*, **114**, (21), 11060-11082 (2014). Deep Eutectic Solvents (DESs) and Their Applications. Copyright 2014 American Chemical Society.

Type I is analogous to the ILs formed using metal-halide/imidazolium salts. The first DES synthesized by Abbott and coworkers^{11,13} by mixing quaternary ammonium salts and metal chloride salts belong to this category. Type II DESs are formed by mixing hydrated metal halides and ChCl. The inclusion of hydrated metal halides as one of the DES components is promising for

large-scale production due to lower costs and their ability to withstand moisture.¹³ Following their initial work on metal chloride salts, Abbott et. al.^{40,42} synthesized DESs based on quaternary ammonium salts and molecular HBDs such as urea, alcohols, and carboxylic acids giving rise to type III DESs. DESs formed from inorganic cations constitute type IV eutectics. Transition metal halides such as ZnCl₂ have been able to form eutectics with HBDs such as urea, ethylene glycol, and acetamide.⁴⁹

Type III DESs are one of the most commonly investigated classes, both experimentally and computationally, as they comprise eutectic mixtures formed from a variety of halide salts and neutral HBDs (Figure 4). Type III DESs based on ChCl has been of particular interest to researchers due to several advantages that include simple and versatile preparation from relatively inexpensive components, low toxicity, and biodegradability. 13,31,34,41-42,50-53 Additionally, they have enabled the study of the interactions between the ChCl cation and HBDs, and the effects of molecular interactions on bulk-phase thermodynamic and transport properties in general. Table 3 summarizes the names and composition of the most frequently used type III DESs; for consistency, the DES solvents will be referred to by their abbreviations for the remainder of this chapter.

Figure 4. Molecular structures of commonly used halide salts and hydrogen bond donors used in the formation of type III DES. Adapted with permission from E. L. Smith, A. P. Abbott, K. S. Ryder, *Chem. Rev.*, **114**, (21), 11060-11082 (2014). Deep Eutectic Solvents (DESs) and Their Applications. Copyright 2014 American Chemical Society.

Table 3. Deep Eutectic Solvents Composed of Choline Chloride (ChCl) and a Hydrogen Bond Donor (HBD) at Specific Ratios (e.g., ChCl:HBD of 1:1, 1:2, 1:3).

z siter (1122) w zpostite rewise	(0.8., 0.11011122 01 11.1, 11.2, 11.6	,
abbreviation	HBD	name
CCEtg	ethylene glycol	ethaline
CCGly	glycerol	glyceline
CCLev	levulinic acid	
CCMal	malonic acid	maline
CCOx	oxalic acid	oxaline
CCPhe	phenol	
CCPro	propylene glycol	propeline
CCU	urea	reline

3. Molecular Simulation Methods

The first molecular simulation investigations of DESs were performed in 2013, 31,54-55 a decade after DESs were first discovered by Abbott et al. 11,40 Molecular simulations have played a crucial role in conjunction with experimental investigations in elucidating the structure-property relationships of DESs. Simulation techniques capable of examining different time scales may be necessary depending on the specific property being investigated. In general, simulation studies in the DES field have focused on: (1) understanding negative charge delocalization and charge spreading in DES species to rationalize the lowering of melting temperatures; (2) unravelling complex interactions between different components in the systems (cations, anions and HBDs) that include contributions from hydrogen bonding and electrostatic interactions, e.g., doubly ionic bonds in different DES systems; and (3) simulating thermodynamic, physical, and transport properties in bulk-phase DES systems. 20,37-39,56 There has also been an increasing number of simulation studies for DES systems in combination with gases, solid interfaces, mixtures, and biomolecules. 20,37-39 This chapter describes efforts to reproduce thermodynamic, physical, and structural properties of bulk-phase DES systems using atomistic MD simulations, while also underscoring important conclusions made by ab initio methods. In sub-section 3.1, a brief overview of the *ab initio* investigations that have played an important role in understanding the molecular structure of DES is provided. Sub-section 3.2 discusses atomistic MD simulation methods and sub-section 3.3 provides a description of non-polarizable FFs used for DES simulations.

3.1 An Overview of *Ab Initio* Methods

One of the major thrust areas of *ab initio* investigations on DESs has been to provide a physical explanation for the observed low melting point in these systems and its effects on their

physicochemical properties. García et al.⁵⁷ studied the melting points of ChCl based DESs, where 29 HBDs were optimized at the B3LYP/6-31+G(d) level of theory. The quantitative structureactivity relationship methodology was then utilized to develop a model using a genetic function approximation. Later, similar methods were employed by the same research group³⁰ to rationalize potential correlations between the melting temperatures and the molecular structure for 45 different DES systems, mostly based on choline. A combination of density functional theory (DFT) and a topological analysis of electron density was employed to better understand intermolecular interactions, particularly for hydrogen bonding networks and their effect on the melting point of DESs. Functionals used to perform DFT calculations for DESs must account for dispersion forces given their importance in accurately describing long-range interactions for these ionic solvents. 58-⁶¹ For example, the DFT investigation by García, Atilhan, and Aparicio³⁰ used the B3LYP functional with Grimme's scheme⁶² that accounts for dispersion corrections (B3LYP-D2). Figure 5 provides B3YLP-D2/6-31+G(d,p) optimized structures for four selected DESs with the intermolecular hydrogen bonded network represented by dotted lines and the Bader cage critical points by points labeled "cp". Cage-like structures were formed by the HBD-chloride hydrogenbonded interactions and the HBD-cation and anion-cation interactions. This work represents one of the first contributions towards understanding the correlation between macroscopic properties, such as the experimentally observed lowering of melting points, and the molecular structure in terms of hydrogen bond networks.

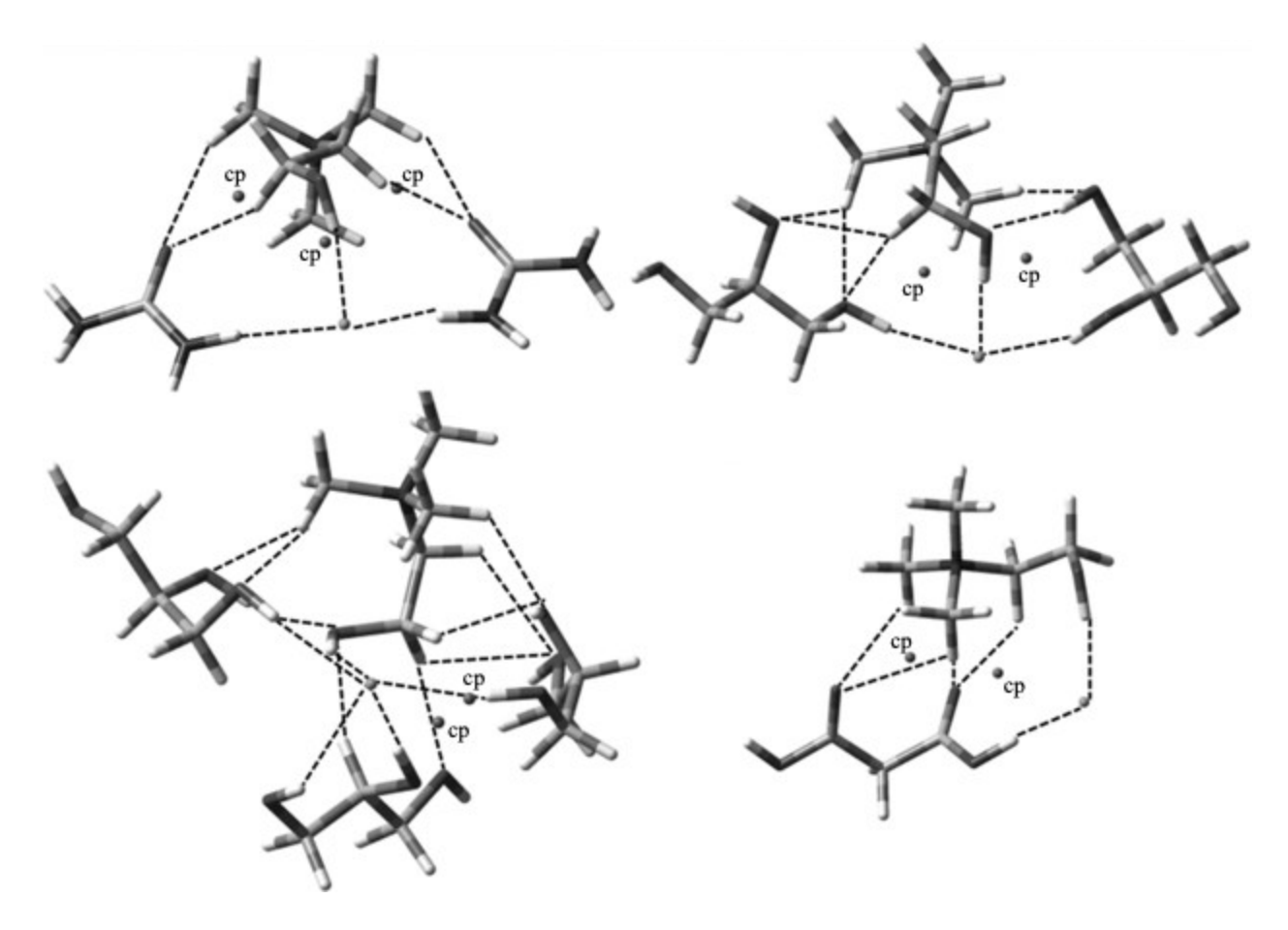


Figure 5. Optimized structures for selected DES systems: (top left) ChCl-Urea (1:2 molar ratio), (top right) ChCl-Glycerol (1:2 molar ratio), (bottom left) ChCl-Glycerol (1:3 molar ratio), and (bottom right) ChCl-Malonic acid (1:1 molar ratio). Intermolecular hydrogen bonds are represented by ---- and cage critical points are labeled cp. Reprinted from Chemical Physics Letters, Vol 634, G. Garcia, M. Atilhan, S. Aparicio, An approach for the rationalization of melting temperature for deep eutectic solvents from DFT, pages 151-155, Copyright 2015, with permission from Elsevier.

Wagle, Baker, and Mamontov also performed DFT calculations to study the mobility of different components in CCGly, in conjunction with quasielastic neutron scattering coupled with selective deuteration.⁶³ In this work, the M06-2X/6-31++G(d,p) level of theory was applied to study the local diffusion dynamics of glyceline's components. The M06-2X DFT functional was chosen as it has been reported to provide accurate descriptions of non-covalent interactions including dispersion effects.⁶⁴⁻⁶⁶ The calculations provided a physical explanation, i.e., the competitive nature of hydrogen bonding, for the observed higher local diffusion dynamics of Ch⁺

as compared to glycerol in CCGly (Figure 6). This contrasted with to the observed slower long-range diffusion dynamics of Ch⁺ in comparison to Cl⁻. Further *ab initio* calculations were performed on CCU, CCEtg, and CCMal.⁶⁷ Initial geometry optimizations and a subsequent reoptimization were done at the HF/6-311G(d,p) and M06-2X/6-31++G(d,p) levels, respectively. The DES species displayed a cage-like nanostructure due to cooperative H-bonding between HBDs, cations, and anions. A charge distribution analysis indicated higher charge transfer from Ch⁺ to the HBD as compared to that occurring from Cl⁻ to the HBD. The calculated sum of bond orders for Ch-Cl interactions correlated directly with the melting point of the DESs.

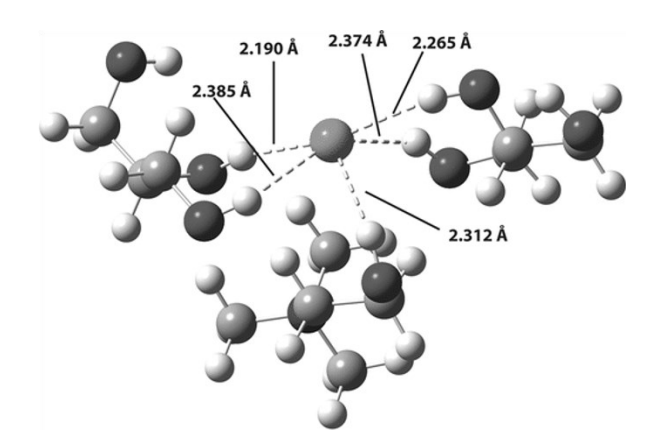


Figure 6. *Ab initio* calculations showing hydrogen bonds formed between glycerol molecules and chloride dominate over the ones occurring between the choline cation and chloride. Reprint with permission from D. V. Wagle, G. A. Baker, E. Mamontov, *J. Phys. Chem. Lett.*, **6**, (15), 2924-2928 (2015). Differential Microscopic Mobility of Components within a Deep Eutectic Solvent. Copyright 2015 American Chemical Society.

Zahn, Kirchner, and Mollenhauer³⁴ were the first to perform *ab initio* MD calculations to study charge spreading in the liquid state for CCU, CCGly, and CCOx. The Hirshfield-I partial charge analysis method, previously used for ionic systems,⁶⁸ was applied and it was found that increasing hydrogen bond interactions between the anion and the HBD compound increased the

negative charge spreading to the HBD with a reduction of the positive charge spreading for CCGly and CCOx. In contrast, negative charge spreading was negligible on CCU. The results obtained from this study challenged the commonly held notion that negative charge delocalization occurring between anion and HBD in DESs was responsible for the observed lowering of their melting points. Follow up studies further investigated the molecular structure and hydrogen bond dynamics of CCU,⁶⁹ alkali halide crystals,⁷⁰ and doubly-ionic bonds.³³

To summarize, *ab initio* simulations have provided a detailed description of the molecular structure of DESs that illustrate the complex nature of component interactions arising from hydrogen bond networks and electrostatic contributions. The charge transfer processes between the cation, anion, and HBD were examined for several ChCl-based DESs. The majority of these investigations have focused on unravelling the effect of molecular interactions on the "deep eutectic" behavior, i.e., a decrease in melting point near the eutectic composition. However, given the large computational cost of these *ab initio* methods in terms of both the time and computer resources required, the expansion of the QM-based methods towards large bulk-phase DES simulations is not feasible at present. Therefore, exploration of existing bulk-phase DES thermodynamic and transport properties and the design of new DES solvents for specific applications necessitates the use of molecular mechanics-based force fields. The subsequent sections provide a description of classical molecular dynamics (MD) simulation methods used to model larger sized, e.g., hundreds to thousands of ionic/molecular components, DES systems.

3.2 Classical Molecular Dynamics at the Atomic Level

Classical MD simulations that obey Newton's laws of motion use force fields (FFs) to calculate the potential energy of a system as a function of their atomic coordinates. The choice of FF plays an important role in the prediction of properties from atomistic molecular simulations

and must be chosen carefully depending on the type of system to model. Generalized FFs like GAFF⁷¹ and DREIDING⁷² can offer qualitative and quantitative information complementing experimental results for a wide range of small molecule and macromolecular systems. However, the application of these FFs to charged solvents such as ILs and DESs necessitates further refinement and development of new parameter sets to obtain good agreement with experimental data. To reproduce and predict thermodynamic, transport, and structural properties of DESs, it is important that the FF chosen accurately reproduces the molecular geometry, non-bonded interactions, and properly samples the conformational space of these systems. Therefore, any molecular simulations involving a new DES system must involve a thorough validation of the FF selected to provide confidence in the predictive results obtained for the properties of interest.

The majority of the DES simulation studies have used FFs such as GAFF⁷¹ and OPLS-AA, ⁷³⁻⁷⁷ which follow the general "class I" equation (equation 1), with the exception of molecular simulations of CCU^{32,78} that have employed the Merck molecular force field (MMFF)⁷⁹⁻⁸¹, a class II FF. The potential energy, U(r), in equation 1 is represented as the sum of bonded and non-bonded interactions present in a system. The bonded interactions typically comprise U_{bond} , U_{angle} , $U_{dihedral}$ and $U_{improper}$ terms as described in equations 2-5. The bond stretch interaction is described by a simple harmonic oscillator between atoms i and j as shown in equation 2a. K_{ij}^b denotes the force constant, r_{ij} represents the distance between atoms i and j, and r_{ij}^0 represents the equilibrium bond length. Similarly U_{angle} can be represented as a harmonic term ($U_{angle,h}$ as described in equation 3a) where K_{ijk}^0 , θ_{ijk} and θ_{ijk}^0 represent the angle force constant, angle between atoms i, j, and k, and equilibrium angle, respectively. A dihedral energy term is typically expressed as a cosine series as given by equation 4, where V_n represents the 'barrier height', n is the periodicity of the potential and γ is the phase angle. Energy contribution from impropers, or out of plane

bending, can also be taken explicitly into account, as given by equation 5 where K_{ω} is the force constant and ω_{ijk} - ω_{jkl}^0 is the out of the plane angle. Impropers can be also implemented using the Wilson wag angle that is the i-l bond angle with the j-k-l plane. Class II FFs such as COMPASS, 82 PCFF, 83 and MMFF $^{79-81}$ contain higher order force constants (typically cubic and quartic) for bond and angle terms, and also contain off-diagonal cross-coupling terms such as stretch-bend and bendbend interactions. For example, in the case of MMFF, cubic stretch and bend terms are used as shown in equations 2b and 3b where K_{ij}^b and K_{ijk}^{θ} are cubic-stretch and cubic-bend constants. Also, a stretch-bend cross-term is included as given in equation 6, where K_{ijk} and K_{kji} are the force constants for i-j and k-j stretching coupled to i-j-k bending, r_{ij} and r_{jk} represent the bond lengths between atoms i-j and j-k, and θ_{ijk} denotes the angle between i-j-k atoms.

$$U(r) = U_{bond} + U_{angle} + U_{dihedral} + U_{improper} + U_{van der Waals} + U_{electrostatics}$$
[1]

$$U_{bond,h} = K_{ij}^b (r_{ij} - r_{ij}^0)^2$$
 [2a]

$$U_{bond,q} = 143.9325 K_{ij}^{\prime b} / 2(r_{ij} - r_{ij}^{0}) \left(1 + cs(r_{ij} - r_{ij}^{0}) + \frac{7}{12} \left(cs^{2}(r_{ij} - r_{ij}^{0})^{2} \right) \right)$$
[2b]

$$U_{angle,h} = K_{ijk}^{\theta} \left(\theta_{ijk} - \theta_{ijkl}^{0}\right)^{2}$$
 [3a]

$$U_{angle,c} = 0.043844 K_{ijk}^{\prime \theta} / 2(\theta_{ijk} - \theta_{ijk}^{0})^{2} \left(1 + cb(\theta_{ijk} - \theta_{ijk}^{0}) \right)$$
[3b]

$$U_{dihedral} = \sum_{dihedrals} \frac{1}{2} V_n (1 + \cos(n\phi - \gamma))$$
 [4]

$$U_{improper} = 0.043844 K_{\omega}/2(\omega_{ijk} - \omega_{jkl}^{0})^{2}$$
 [5]

$$U_{stretch-bond} = 2.51210 \left(K_{ijk}^{sb} (r_{ij} - r_{ij}^{0}) + K_{kji}^{sb} (r_{kj} - r_{kj}^{0}) \right) \left(\theta_{ijk} - \theta_{ijk}^{0} \right)$$
 [6]

Non-bonded interactions are composed of van der Waals and electrostatic interactions. The electrostatic energy contribution is computed from the interactions between fixed partial charges in the case of non-polarizable FFs as given by equation 7. The weak dispersive or van der Waals interactions are typically represented with a 12-6 Lennard-Jones (LJ) potential, but 9-6 and buffered 14-7 LJ potentials can also be used. U_{LJ} in equation 8a represents the van der Waals energy contribution, where m and n values equal, for example, 12 and 6 or 9 and 6. ε_{ij} and σ represent the potential well depth and collision diameter, respectively. U_{vdW} (equation 8b) is

another form of the van der Waals term where a buffered 14-7 potential, as used in MMFF, is shown. The minimum interaction energy distance between atoms i and j is given by r_{ij} (or R_{ij}).

$$U_{coul} = \frac{q_i q_j}{4\pi \varepsilon_0 r_{ij}} \tag{7}$$

$$U_{LJ} = 4\varepsilon_{ij} \left[\left(\frac{\sigma}{r_{ij}} \right)^m - \left(\frac{\sigma}{r_{ij}} \right)^n \right]$$
 [8a]

$$U_{vdW} = \varepsilon_{ij} \left(\frac{1.07R_{ij}^*}{R_{ij} + 0.07R_{ij}^*} \right)^7 \left(\frac{1.12R_{ij}^{*7}}{R_{ij}^7 + 0.12R_{ij}^{*7}} - 2 \right)$$
 [8b]

In charged systems, such as DESs and ILs, tuning non-bonded parameters plays an important role in treating polarization implicitly to obtain better agreement with experimental data. The approaches used for implicit treatment for polarization include (1) scaling ionic charges and/or (2) adjusting LJ parameters. One of the earliest investigations to utilize scaled charges was performed by Morrow and Maginn, where overall cation and anion charges of +0.904 e and -0.904 e (as opposed to integer ±1 e values) were used for the 1-butyl-3-methylimidazolium hexafluorophosphate [bmim]⁺[PF₆]⁻ IL.⁸⁴ The charges on the fluorine atoms in the anion were found to be asymmetric, which implied polarization of the electron cloud. However, it was found that the anion did not show a preferential orientation close to the nearest cation. In addition, the computed properties did not show a significant difference when using symmetric charges on the anion. Following this work, there were two simulation studies of aqueous-IL interfaces where scaled charges showed better results in terms of interface formation and agreement with experimental values of ILs in humid conditions. $^{85\text{-}86}$ Refined potentials for $[bmim]^+[PF_6]^-$ IL by Bhargava and Balasubramanian 87 used charges of ± 0.8 e and tuned LJ parameters to match the RDFs obtained from ab initio simulations using the Car-Parrinello method. In particular, the emphasis was to reproduce the cation-anion H-bonding behavior. Liu et al. calculated a range of properties including density, heat capacity, thermal conductivity, shear viscosity and self-diffusion

coefficients for six ILs using GAFF parameters with scaled charges (±0.8 e). 88 Although other properties showed good agreement, shear viscosities were overestimated by an order of magnitude and self-diffusion coefficients were underestimated by a factor of 2 which has been attributed to the lack of treating polarizability in an explicit way. Consequently, a systematic investigation of different charge scaling factors was completed by Chaban, where an overall scaling factor between 0.7 and 0.8 worked best for imidazolium and pyridinium RTILs. 89 More recent studies have thoroughly investigated the use, advantages, and disadvantages of employing scaled charges in ILs. 90-92

Multiple molecular simulations of DESs have also utilized effective charge scaling to treat polarization implicitly. It is important to note that the choice of charge method, e.g., RESP, ChelpG, AIM, and Merz-Kollman, used during the development of FF partial charges can have a dramatic influence on the accuracy of IL and DES systems. 93-94 In addition, the development of atomic charges from either (1) clusters consisting of a 1:2 mole ratio, e.g., 1 ChCl and 2 urea in CCU, or (2) isolated molecules/ions can also have a profound effect on the predicted structural arrangement of the system. 94 Table 4 provides a comparison between different charge models and the use of small clusters versus individual molecules/ions. Overall, the ChelpG and Merz-Kollman charge models coupled to the minimal cluster optimization approach yielded the most accurate reproduction of DES properties. Similar to the IL simulations discussed previously, non-integer charges provided the best results, i.e., charges on Ch⁺ and Cl⁻ obtained from ChelpG were +0.8254 e and -0.8392 e, while the Merz-Kollman charges were +0.6849 e and -0.7158 e, respectively. 94 In addition, Ullah et al. reported a FF for CCLev that possessed non-integer cation and anion ChelpG-derived charges of +0.8254 e and -0.6849 e.37

Table 4. Evaluation of Different Charge Schemes for ChCl-levulinic Acid DES Employing Isolated Molecule and Cluster Approach.

Charge assignment method	Cluster	Isolated molecule
Mulliken	Poor	Poor
NPA	Fair	Poor
Löwdin	Poor	Poor
Mayer	Poor	Poor
ChelpG	Good	Fair
Merz–Kollman	Good	Fair
Atomic Polar Tensor	Fair	Poor
Hirshfeld	Fair	Poor
Voronoi deformation density	Poor	Poor
AIM	Fair	Poor

Reprinted from Journal of Molecular Liquids, Vol 211, G. García, M. Atilhan, S. Aparicio, The Impact of Charges in Force Field Parameterization for Molecular Dynamics Simulations of Deep Eutectic Solvents, pages 506-514, Copyright 2015, with permission from Elsevier.

Tuning of the van der Waals terms for better agreement in structural, thermodynamic, and transport properties in MD simulations has not been employed as extensively in DES simulations as compared to ILs. 95 Notably, Doherty and Acevedo adjusted LJ parameters and empirical charges during the development of an OPLS-AA force field for ChCl-based DES systems 55 to match RDFs reported by Hammond, Bowron, and Edler. 46 A potential drawback of this procedure is the transferability of these parameters to simulations featuring complex systems, e.g., additional species or heterogeneous environments. In the case of DES mixtures, even if one of the cationic/anionic species are common to both components, the chemical environment around the constituent atoms can lead to different charge descriptions. 96 This emphasizes that in the event of mixing DES systems, or simulating DESs with organic solvents or polymers, scaling of charges and FF parameters in general should be validated prior to the prediction of properties of interest.

Simulations featuring mixtures of DESs and conventional solvents have been reported but are limited in number. For example, Tanner et al. studied the effect of water addition to ILs

composed of choline and geranate at varying mole fractions using a combined experimental, atomistic MD, and coarse-grained MD approach.⁹⁷ Fetisov et al.⁴⁵ also performed a first principles molecular dynamics (FPMD) study between CCU and water to study the resultant molecular structure and transport properties for the mixture. Table 5 summarizes the non-polarizable FFs, with implicit treatment of polarization, used to simulate DES systems through charge scaling and/or LJ tuning and is discussed in greater detail in Section 3.3.

3.3 Non-polarizable Force Fields used for DES Simulations:

A variety of non-polarizable FFs have been used to study DESs. For example, Perkins, Painter, and Colina⁵⁵ performed molecular simulations on CCU with modified GAFF parameters at several temperatures. Good agreement with experimental densities (1% error) and heat capacities (1.3-1.4% error) was found with a reduced charge model (±0.8 e). However, transport properties such as self-diffusion coefficients were underestimated by 25-51% and 29-41% for Ch⁺ and urea at 298 K, respectively. Improvement was seen at the higher temperature of 330 K, which reduced the errors to 4-17% and 3-8% for the same species in comparison to experimental values. Subsequent work by the same group³¹ on CCEtg, CCGly, and CCMal also showed good agreement for physical and thermodynamic properties. Once again, the self-diffusion coefficients were difficult to reproduce for CCEtg where values were underestimated by 20-30% at 298 K and 5-25% for simulations at 330 K. For CCGly, the values were underestimated by 14–20 % and 17-27% at 298 K and 330 K, respectively.

Ferreira et al.⁹⁸ tested various FF combinations for each component in CCEtg including OPLS-AA,^{75,77} GAFF,⁷¹ and CHARMM27⁹⁹⁻¹⁰⁰ with varying charge schemes. Although they obtained good agreement for densities and thermal expansion coefficients using the unscaled charge scheme (±1e), self-diffusion coefficients of Ch⁺ and ethylene glycol were found to be

underestimated by a factor of 8 when compared against experimental values. After scaling the charges by a factor of 0.8, several properties including density, thermal expansion coefficient, enthalpy of vaporization, surface tension, shear viscosity, and structural properties were calculated over a temperature range of 298.15–373.15 K and compared to relevant experimental data. It was reported in this work that the self-diffusion coefficients displayed an improvement of 10% with the refined charges in comparison to the Perkins, Painter, and Colina simulations. Ferreira et al. 101 applied the same procedure to derive a system-specific FF for CCPro. The authors found success in reproducing experimental densities while combining existing parameters for choline, 75 chloride, 76 and propylene glycol. 102 Further refinement was achieved through AIMD simulations of the CCPro system and the restrained electrostatic charge potential (RESP) was utilized to generate new averaged charges on each species. With the newly produced charges, transport properties such as viscosity and diffusion coefficients were improved compared to experiment, however the errors associated with each property were still large at 19% and 16%, respectively.

Using the empirical potential structure refinement (EPSR) method that validates the sampling space to neutron diffraction data, Hammond, Bowron, and Edler⁴⁶ generated center-of-mass and partial atomic RDFs for CCU along with spatial distribution functions (SDFs) to characterize the solvation environment. To run the refinement simulations, harmonic potentials were used to maintain the geometry for each molecule of interest. A reference potential was either obtained from literature or generated to explore the desired configurational space. The parameters for urea molecules were derived from Soper, Castner, and Luzar¹⁰³ and OPLS-AA parameters were used for Ch⁺ and Cl⁻. The study found a complex H-bonding network consisting of strong HBD (urea)-Cl and Ch-Cl interactions, consistent with other experimental and simulation investigations. Besides being the first work to examine the liquid structure of CCU using neutron diffraction, this

work also provided a framework for refining existing atomistic FFs to simulate Ch-Cl DES systems.³⁵

Mainberger et al.³² tested two FFs, GAFF and MMFF, to simulate three ChCl-based DESs containing the HBDs of glycerol, 1,4-butanediol, and levulinic acid. An additional DES containing the zwitterion betaine was also investigated. Two sets of charges derived by the RESP methodology were used with GAFF to investigate the effect of charge scaling. Scaling atomic charges by 0.75 improved estimation of densities and heat capacities in comparison to experimental data for all systems. However, for the CCGly system where experimental self-diffusion coefficients are available, the predicted values were overestimated by an order of magnitude. The ±1 charge system underestimated the diffusion coefficients by 16% and 7% for glycerol and Ch⁺, respectively. Simulations with the MMFF did not utilize a charge scaling scheme, but still showed good agreement for densities and heat capacities (within ~3% of experimental values). However, the calculated self-diffusion coefficients for Ch⁺ and glycerol were underestimated by 43% and 92%, respectively.

Doherty and Acevedo³⁵ recently developed a set of custom OPLS-AA parameters (called OPLS-DES) to simulate the structural, thermodynamic, and transport properties of ChCl-based DESs. The nonbonded parameters for Ch⁺ and Cl⁻ were adjusted to match the RDFs obtained from the work of Hammond, Bowron, and Edler,⁴⁶ and Zahn, Kirchner and Mollenhauer.^{34,46} Torsional parameters for the Ch cation were originally adjusted in a previous IL study to fit conformational energy minima from LMP2/cc-pVTZ(-f) calculations.⁷⁵ For the HBDs, parameters were taken from OPLS-AA⁷⁷ and nonbonded terms were adjusted to match liquid structure and bulk properties from experimental data and AIMD based calculations.^{34,46,69} Physical and thermodynamic properties such as density, shear viscosity, heat capacities, and surface tension showed excellent

agreement with experimental data while self-diffusion coefficients showed higher error percentages. The overall mean absolute errors (MAEs) obtained in this work were 1.1%, 1.6%, 5.5%, and 1.5% for the above-mentioned properties, respectively. Self-diffusion coefficients estimated in this work showed error percentages of 31.4% and 78.8% for Ch⁺ and urea at 298 K. The % error values decrease with temperature (28.1% and 0.3% respectively at 328 K) similar to the behavior observed in other simulation investigations. ^{31,55,98} In recent simulations performed by Salehi et al., ¹⁰⁴ the OPLS-AA parameters from Doherty and Acevedo³⁵ and GAFF parameters from Perkins, Painter and Colina^{31,55} were used to calculate Hildebrand and Hansen solubility parameters for CCU, CCGly, CCMal, and CCOx. A charge scaling of 0.8 was applied to the simulated systems for both FFs tested. Additional modifications included the removal of intramolecular exclusion terms between hydrogen and oxygen atoms in OH groups of the HBDs and the inclusion of LJ parameters ($\sigma = 0.1$ Å and $\epsilon = 0.001$ kcal/ mol) for hydrogen atoms to avoid overlaps. Solubility parameters and enthalpies of vaporization were computed taking into consideration HBD, HBA, and cluster (comprising both HBD and HBA) vaporization. Based on the calculated vaporization enthalpy contributions, the HBD is suggested to vaporize first and the large values similar to ILs emphasize the polar nature of DESs. As a brief comparison between the GAFF and OPLS-AA parameter sets, in CCU, GAFF overestimated the experimental enthalpies of vaporization by 25 kJ/mol, whereas OPLS-AA showed close agreement.

Beyond generalized FFs that have been modified to simulate DESs, e.g., GAFF and OPLS-AA, additional work has been reported for FFs parameterized specifically to simulate DES systems.^{20,37,94} For example, parameterization efforts on CCU, CCGly, and CCMal by García, Atilhan, and Aparicio²⁰ developed partial charges by using a minimal cluster approach, where ChCl:HBD clusters (in the ratio 1:1, 1:2, and 1:2 for malonic acid, ethylene glycol, and urea,

respectively) were optimized at the B3LYP/6-311+G(d) theory level. Their DFT calculations showed different charge distributions for two urea/ethylene glycol molecules depending on the positions through which the two atoms interact with ChCl. Thus, the two urea/ethylene glycol molecules were assigned different charges. The parameterization effort reported liquid density deviations of 1.68%, 0.29%, and 1.56% for CCU, CCGly, and CCMal, respectively; however, viscosities obtained from these simulations showed large deviations. A similar parametrization procedure was followed by Ullah et al.³⁷ for CCLev where two types of levulinic acid molecules were developed with different ChelpG-based charges. This work showed good agreement with experimental data for density and thermal expansion coefficients (less than 0.8% and 2.8% respectively) but gave poor shear viscosity reproduction with a deviation of 16.8% compared to the experiment. Experimental data was not available to compare self-diffusion coefficients for CCLev; however, their predictions were comparable to GAFF simulations with no charge scaling.³²

Table 5 provides a summary of bulk properties and liquid structures predicted using the previously discussed non-polarizable FFs developed for DES systems. Liquid density and thermal expansion coefficient predictions of multiple DES systems showed good agreement with experimental data for all the FFs mentioned in the table. In particular, liquid density shows less than 3% deviation from experiments with the exception of CCU (OPLS-AA)³⁵ with 4.0 % at 298 K. This has been attributed to the scaling of LJ parameters to reproduce other properties such as heat capacity, surface tension, and molecular interactions. Viscosities calculated by García, Atilhan, and Aparicio²⁰ and Ullah et al.³⁷ using the Green-Kubo method showed higher error percentages (ranging from 16.8% to 35.4%) as compared to the nonequilibrium periodic perturbation method,^{35,98} where error percentages are less than 3%. Surface tension for most

systems have only been calculated by OPLS-AA with <2% deviations from experimental data.³⁵ For CCEtg, OPLS-AA parametrized by Doherty and Acevedo³⁵ displayed better performance than surface tensions computed using a combination of multiple FF parameters, i.e., GAFF (Ch⁺) + OPLS-AA(Cl⁻) + CHARMM27(ethylene glycol).⁹⁸ All non-polarizable FFs showed large deviations in self-diffusion coefficients at 298 K compared to experimental data (typically > 15%, but as high as >50% in several cases). During the development of the non-polarizable DES FFs, the predicted molecular structures and intermolecular interactions of the solvents were often compared to relevant QM-based calculations and experimental data. For example, the local interactions in CCU predicted by OPLS-AA-based simulations³⁵ were extensively characterized by examining combined distribution functions (CDFs), RDFs, and SDFs, and comparing them in detail to reported AIMD simulations.³⁴ Additional liquid structure properties, such as H-bond residence times were calculated by García and coworkers.^{20,37} Detailed comparisons of physical, thermodynamic, and transport properties, and molecular structure and interactions are provided in the subsequent sections 4 to 7.

Table 5. Comparison of DES Bulk Properties from Atomistic MD Simulations using Non-polarizable Force Fields.

Auth Force		Liquid density	Thermal expansion coefficient	Surface tension	Heat capacity	Viscosity	Self-diffusion coefficients	Liquid structure ^(a)
				CCU				
Perkins, Painter and Colina ⁵⁵	GAFF (0.8) ^(b)	++(c)	++	Na	++	na	_(d)	+
Doherty and Acevedo ³⁵	OPLS-AA (0.8)	++	na	++	+	++	-	++
Shah and Mjalli ⁷⁸	MMFF	++	++	Na	na	na		+
García, Atilhan and	MDynaMix	++	na	Na	na	-	na	+

	T	1	ı	1	1	I	T	1	
Aparicio ²⁰									
CCEtg									
Perkins, Painter and Colina ³¹	GAFF (0.8)	++	+	Na	+	na	-	+	
Zhang et al. ³⁶	GAFF(0.9)	++	na	Na	na	+	-	++	
Doherty and Acevedo ³⁵	OPLS-AA (0.8)	++	na	++	++	++	-	++	
Ferreira et al. ⁹⁸	Mixed ^(e)	++	+	+	na	+	-	+	
				CCGly					
Perkins, Painter and Colina ³¹	GAFF (0.8)	++	++	Na	+	na	-	+	
Doherty and Acevedo ³⁵	OPLS-AA (0.8)	++	na	++	+	++	-	++	
Mainberger et al. ³²	MMFF	++	na	Na	++	na		+	
García, Atilhan and Aparicio ²⁰	MDynaMix	++	na	Na	na	-	na	++	
				CCMal					
Perkins, Painter and Colina ³¹	GAFF (0.8)	++	+	Na	na	na	na	+	
Doherty and Acevedo ³⁵	OPLS-AA (0.8)	++	na	++	na	++	na	+	
García, Atilhan and Aparicio ²⁰	MDynaMix	++	na	Na	na	-	na	++	
CCLev									
Ullah et al. ³⁷	MDynaMix	++	++	Na	na	-	na	++	
Doherty and Acevedo ³⁵	OPLS-AA (0.8)	++	na	Na	na	++	na	+	
Mainberger et al. ³²	MMFF	++	na	Na	na	na	na	+	

Mainberger et al. ³²	GAFF (0.75)	++	na	Na	na	na	na	+
				CCPro				
Ferreira et al. 101	OPLS-AA	++	na	Na	na			+

- (a) Liquid structure was compared considering the breadth of properties calculated (RDFs, CDFs, SDFs, H-bond analysis, and intermolecular energies) and comparison with *ab initio* simulations or neutron diffraction data.
- (b) Values in parentheses 0.75, 0.8 and 0.9 indicate charge scaling factor in the given FF.
- (c) + and ++ denote reasonable and good agreement with experimental data (deviations < 10% and < 5%, respectively).
- (d) and -- denote deviations > 10% and > 20%, respectively.
- (e) Mixed GAFF, OPLS-AA and CHARMM27 were used for Ch⁺, Cl⁻, and ethylene glycol, respectively.

From Table 5, it is clear that accurately reproducing transport properties, such as self-diffusion coefficients, was a challenge for all parameterization efforts. The use of polarizable force fields has been advocated for improving agreement with diffusivity experimental data.³⁵ However, to our knowledge, polarizable FFs have not been developed/utilized to simulate bulk properties of DES systems.

4. Physical Properties

4.1 Liquid Density

Liquid density is an important physical property that has served as a starting point for the validation of DES FFs at a wide range of temperatures. 31-32,35,55 It should be noted that density by itself is not sufficient for validating the accuracy of a FF as multiple combinations of parameters can give similar densities within error bars while showing remarkable differences in other predicted thermodynamic, structural, and transport properties. Problematically, experimental solvent characterization data, such as cohesive energy and enthalpy of vaporization, are not readily available for DES systems. 104 Hence, liquid densities have been used for preliminary validation in the literature. Densities obtained from MD simulations have been compared against experimental data 32,44,105-115 for (a) CCU, (b) CCEtg, (c) CCGly, (d) CCMal, and (e) CCLev in Figure 7. A major

caveat is that large deviations are prevalent between the reported experimental densities themselves. These differences have been attributed to several factors that include water absorption by samples and the method of measurement. 41,55,116

For CCU (Figure 7a), MD simulations by Shah and Mjalli that utilized MMFF showed the closest agreement with experimental densities across a temperature range of 290 K to 330 K.⁷⁸ Reasonably close agreement (≤1%) was also found when using GAFF.⁵⁵ However, the OPLS-AA underestimated liquid densities with errors ranging from 3.9 to 4.2%; this was a consequence of scaling Lennard-Jones parameters to obtain better agreement with other properties that included surface tension, heat capacity and molecular structure at the expense of increased deviations in density. 35 For CCEtg (Figure 7b), GAFF, OPLS-AA, and a mixture of parameters (GAFF(choline) + OPLS-AA(chloride) + CHARMM27(ethylene glycol))⁹⁸ all exhibited good agreement with less than 3% deviation from experimental densities. As a general comparison, GAFF and the mixed parameters underestimated the experimental densities, whereas the OPLS-AA overestimated the values. However, the maximum absolute error for all FF predictions of CCEtg were usually < 0.01 g/cm³. Density simulations of CCGly (Figure 7c) reported deviations of less than 1.1% with experiment when utilizing either the GAFF (Perkins, Painter, and Colina³¹) or OPLS-AA³⁵ FFs. However, parameters from Mainberger et al.³² overestimated and underestimated experimental liquid densities at 298 K using GAFF and MMFF, respectively. For CCMal (Figure 7d), both GAFF and OPLS-AA overestimated the densities, except at 298 K where OPLS-AA showed near perfect agreement (0.1% deviation³⁵). Finally, for the CCLev DES (Figure 7e), OPLS-AA³⁵ showed the closest agreement with experimental data (0.2-0.4% error) as compared to GAFF,³² MMFF,³² and MDynaMix.³⁷

An important consideration when developing DES FF parameters is the role of charge scaling to improve agreement in densities. The results presented in Figure 7a-d for the model used by Perkins, Painter, and Colina employed a charge scaling factor of ±0.8 e with default GAFF parameters. 31,55 This was found to reproduce density better than unscaled charges (i.e., +1 for cations and -1 for anions) or a scaling of ± 0.9 e. Similarly, scaling by ± 0.75 e was found to yield better results for CCGly and CCLev modeled using GAFF (Mainberger et al.³²) when compared to unscaled charges. Simulations with MMFF^{32,78} employed full charges (Figure 7a,c,e) and OPLS-AA 35 simulations used a scaling factor of ± 0.8 e. As an alternative, FFs developed by García, Atilhan, and Aparicio²⁰ and Ullah et al.³⁷ featured charges calculated from small DES clusters. For example, instead of ± 1 e for the cation/anion and a neutral charge for the HBD molecules, charges of +0.8254 e, -0.6849 e, -0.0663 e, and -0.0743 e were used for choline, chloride, and the two levulinic acid molecules respectively.³⁷ Ferreira et al.¹⁰¹ also derived charges from bulk AIMD simulations for the CCPro system that resulted in a scaling of 0.74 and found good agreement (3% error) with a very specific combination of existing FFs. 75-76,102 Finally, Mainberger et al.³² included LJ parameters for hydrogen atoms, but their addition did not show a remarkable improvement in liquid density compared to the other FFs discussed. It is worth mentioning that with respect to DESs, due to a lack of reported experimental densities for many systems, research groups have used alternative methods to predict densities that include empirical group contribution methods and neural network models. 105,117

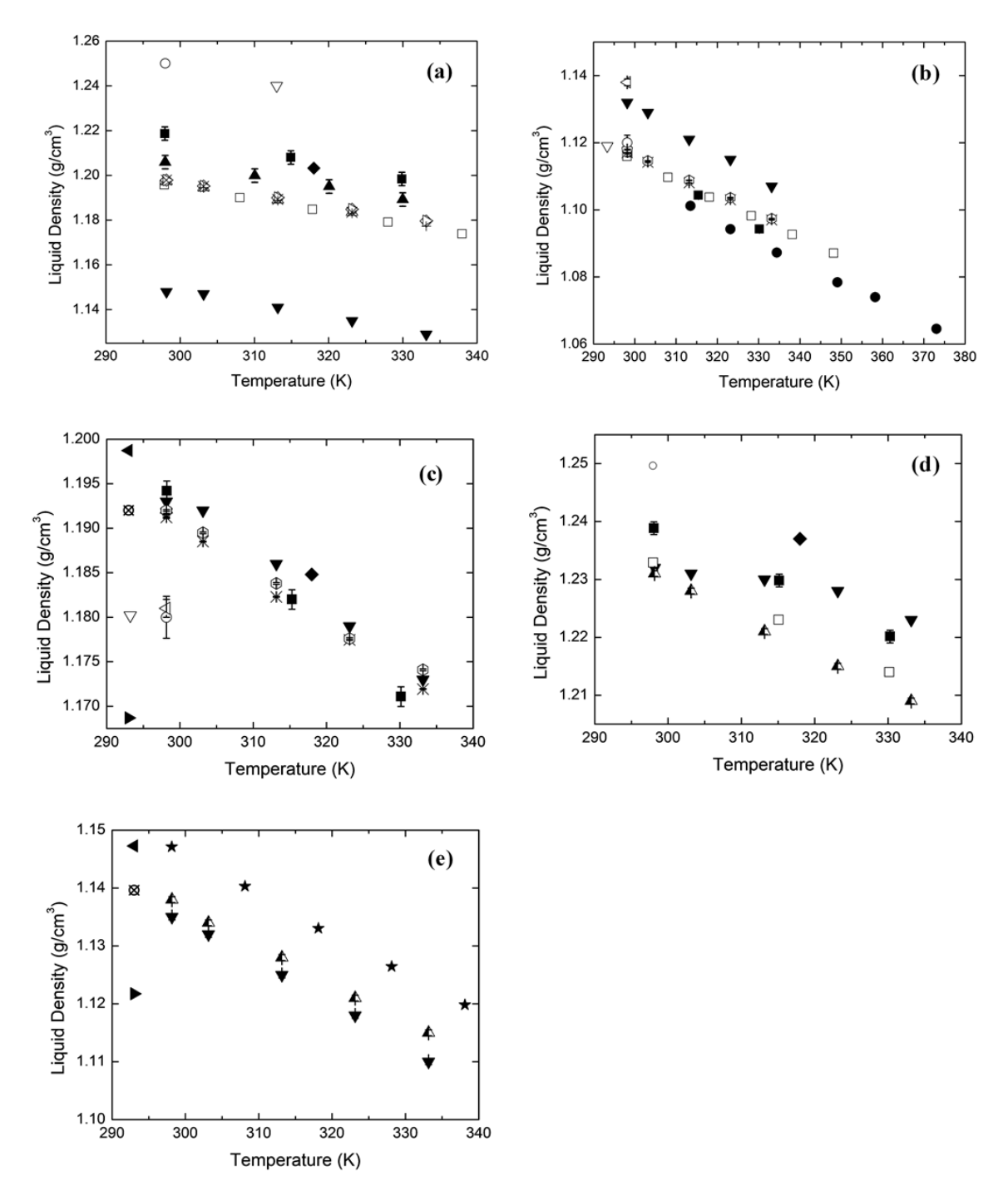


Figure 7. Comparison of liquid density data obtained from simulations (solid symbols) and experimental data (half-open symbols) for (a) CCU, (b) CCEtg, (c) CCGly (d) CCMal, and (e) CCLev. Simulations: ■ Perkins, Painter and Colina^{31,55} ▼ Doherty and Acevedo³⁵ ▲ Shah and Mjalli⁷⁸ ● Ferreira et al.⁹⁸ ◆ García, Atilhan and Aparicio²⁰ ► Mainberger et al. (MMFF)³² ◆ Mainberger et al. (GAFF)³² ★ Ullah et al.³⁷ Experimental: □ Ciocirlan et al.¹¹⁵ ○ D'Agostino et al.⁴⁴ + Yadav et al.^{111,118} × Leron and Li¹⁰⁶ △ Shekaari, Zafarani-Moattar and Mohammadi¹¹²

 \triangleright Xie et al. ¹⁰⁸ ∇ Abbott et al. ¹¹⁹ \diamond Chemat et al. ¹⁰⁹ \diamond Shahbaz et al. ¹⁰⁵ \diamond Mjalli et al. ¹¹⁴ \diamond Mjalli and Abdel Jabbar ¹¹³ \blacktriangle Leron, Wong and Li ¹⁰⁷ \otimes Mainberger et al. ³² \blacktriangle Florindo et al. ¹¹⁰

4.2 Volume Expansivity

Volume expansivity is calculated from the slope of the molar volume versus temperature curve as described in equation 9. Table 6 provides a comparison between computed DES volume expansivity values from multiple FFs and experimental measurements. Perkins, Painter, and Colina^{31,55} computed the volume expansivity for four different DESs using GAFF parameters with ± 0.8 e scaled charges. Their simulations yielded close agreement with most experimental measurements, ^{78,118} with the notable exception of CCGly, which was overestimated. The MMFF⁷⁸ and the MDynaMix³⁷ FFs also yielded excellent volume expansivity predictions. Finally, the use of mixed FF parameters by Ferreira et al. ⁹⁸ for CCEtg provided values at the lower and upper bounds of experimental measurements.

$$\alpha_P = \frac{1}{V} \left(\frac{\partial V}{\partial T} \right) \tag{9}$$

Table 6. Comparison of Average Volume Expansivity $\alpha_P \times 10^4$ (K⁻¹) for Deep Eutectic Solvents.

DES	Authors/Force Field		Simulations	Experiments ^{78,118}
CCU	Perkins, Painter and Colina ⁵⁵	GAFF (0.8)	5.32	4.378 to 6.0
	Shah & Mijalli ⁷⁸	MMFF	4.278	
CCEtg	Perkins, Painter and Colina ³¹	GAFF (0.8)	6.45±0.05	5 to 7
	Ferreira et al. ⁹⁸	Mixed	5.48±0.02, 7.67±0.02	
CCGly	Perkins, Painter and Colina ³¹	GAFF (0.8)	6.09±0.07	4.6 to 4.7
CCMal	Perkins, Painter and Colina ³¹	GAFF (0.8)	4.91±0.29	5 to 6

CCLev	Ullah et al. ³⁷	MDynaMix	5.76	5.83 to 5.93
-------	----------------------------	----------	------	--------------

4.3 Surface Tension

The reproduction of DES surface tension is important for several industrially relevant applications involving separation, distillation and extraction. Unfortunately, the availability of experimental DES surface tension data is limited due to measurement difficulties; consequently, predictive models have often been employed as an alternative. 117,120 Macleod proposed a relation to estimate the surface tension as given by equation $10^{121-122}$ where ρ_L and ρ_V represent liquid and vapor density, σ_M is the surface tension and K is a constant. This relation was modified (equation $(11a)^{121,123}$ where the constant K in Macleod's equation was replaced by a new constant known as the parachor (P) expressed in terms of molar quantities. In cases where the vapor density is negligible in comparison to the liquid density, P is given by equation 11b where M_W is the molecular weight and ρ is the liquid density. P can be expressed as a sum of the contributions from its constituents, comprising atoms or groups in the molecule, as shown in equation 11b, where P_i denotes individual contributions. 124 σ_S can be calculated by using the known density of a given compound. The parachor contribution values were later improved for neutral compounds. 124-125 Knotts et al. developed a quantitative structure-property relationship for P from data for neutral organic compounds available in the DIPPR database. 126 This model was then extended to charged systems such as ionic liquids. 127-128 The percent error obtained for CCGly and CCEtg using the parachor method at 298 K were 3.74% and 5.91 respectively. 121

$$\sigma_M = K(\rho_L - \rho_V)^4 \tag{10}$$

$$\sigma_{\mathcal{S}} = [P(\rho_L - \rho_V)]^4 \tag{11a}$$

$$P = \frac{M_W \sigma_s^{1/4}}{\rho} = \sum_i P_i$$
 [11b]

An alternative approach for estimating surface tension is to employ the Othmer equation (equation 12),¹¹⁷ where the surface tension at a given temperature T can be calculated using the critical temperature (T_C) and a reference surface tension (σ_{ref}) at another temperature (T_{ref}). Deviations between values predicted from the Othmer relation and experimental measurements worsen with increasing temperature.¹¹⁷ Nevertheless, the overall percent error for 9 DES systems was 2.57%, highlighting the empirical Othmer model as a good approach for predicting surface tensions.¹²¹

$$\sigma(T) = \sigma_{ref} \left[\frac{(T_c - T)}{T_c - T_{ref}} \right]^{\frac{11}{9}}$$
 [12]

Employing MD simulations to calculate surface tensions of DESs. Only two simulation studies to date have been reported. Doherty and Acevedo (OPLS-AA)³⁵ calculated the surface tension for four DES systems: CCU, CCEtg, CCGly, and CCMal. Ferreira et al. (mixed CHARMM27+OPLS-AA+GAFF)⁹⁸ calculated the surface tension for CCEtg. The *z*-axis of the simulation boxes was elongated by a factor of 3 and 2 by Doherty and Acevedo, and Ferreira et al., respectively. The surface tension was computed from the directional components of the pressure tensor as given by equation 13 where σ_{MD} and L_Z represent the surface tension and length of the box along the *z*-direction respectively. P_{ZZ} , P_{XX} and P_{YY} represent the directional components of the pressure tensor.

$$\sigma_{MD} = \frac{1}{2} L_z \left[P_{ZZ} - \frac{1}{2} (P_{XX} + P_{YY}) \right]$$
 [13]

Table 7 provides a comparison of surface tension values for DESs computed using MD simulations and the analogous experimental data/empirical models. Notably, the surface tension computed from OPLS-AA simulations were calculated at 425 K.³⁵ Due to the absence of

experimental data at this temperature, MD predictions were compared to surface tensions calculated using the Othmer equation at 425 K utilizing experimental data at 298 K as the reference point. The OPLS-AA FF provided excellent performance yielding small deviations ranging from 0.5 to 2.0%. In the work of Ferreira et al., surface tensions were directly compared with experimental data available at similar temperatures (298 K to 323 K) and yielded larger deviations of 3.5-5.7%.

Table 7. Comparison of Surface Tension (mN/m) for Deep Eutectic Solvents.

DES	Authors/Force Field		Simulation	Experiment ^{98,117}
CCEtg (298 K)	Ferreira et al. ⁹⁸	Mixed	48 ± 3	48.91 ± 0.1
CCEtg (313 K)			47 ± 3	47.50 ± 0.1
CCEtg (323 K)			45 ± 6	46.67 ± 0.1
CCU (425 K)	Doherty and Acevedo ³⁵	OPLS-AA (0.8)	38.9	38.7
CCEtg (425 K)			35.9	35.4
CCGly (425 K)			43.2	44.1
CCMal (425 K)			51.3	52.3

5. Thermodynamic Properties

5.1 Heat Capacity

Heat capacity at constant pressure (C_P) is defined by Equation 14a, where H represents the enthalpy (equation 14b), U_{inter} and U_{intra} are the intermolecular and intramolecular potential energies, respectively, and KE denotes the kinetic energy. The enthalpy is often expressed as a sum of ideal (H^{id}) and residual (H^{res}) contributions, as described by Lagache et al. ¹²⁹ and Cadena et al. ¹³⁰ (equations 15a-c). Therefore, C_p is written as the sum of ideal and residual contributions (equation 16a-c).

$$C_p(T, P) = \left(\frac{\partial \langle H \rangle}{\partial T}\right)_P$$
 [14a]

$$H = U^{inter} + U^{intra} + KE + PV$$
 [14b]

$$\langle H \rangle = \langle H^{id} \rangle + \langle H^{res} \rangle \tag{15a}$$

$$H^{id} = U^{intra} + KE + Nk_bT ag{15b}$$

$$H^{res} = U^{inter} + PV - Nk_bT ag{15c}$$

$$C_p(T, P) = C_p^{id}(T) + C_p^{res}(T, P)$$
[16a]

$$C_p^{id}(T) = \left(\frac{\partial \langle H^{id} \rangle}{\partial T}\right)_P$$
 [16b]

$$C_p^{res}(T, P) = \left(\frac{\partial \langle H^{res} \rangle}{\partial T}\right)$$
 [16c]

The residual, C_P^{res} , and ideal, C_P^{id} , contributions to the heat capacity are typically obtained from MD simulations and experiments, respectively. 129,131 For example, DES C_P^{res} values are typically derived from the slope of a plot featuring H^{res} (equation 15c) at multiple temperatures. 31,55 As mentioned, C_P^{id} should be measured experimentally, but when unavailable, *ab initio* calculation-derived values may be substituted. 31,55,88,130-131 For example, Perkins, Painter, and Colina 31,55 carried out gas-phase DFT calculations to optimize isolated ChCl and HBD moieties and then performed a vibrational frequency analysis to obtain C_P^{id} . It is important to emphasize that the C_P^{id} values obtained in this manner were significantly overestimated compared to

experimental values for multiple systems, including water and DESs. 130,132-133 This can be attributed to the fact that classical FFs use simple harmonic approximations, which overestimate the vibrational energy of molecules. 131,133-134 The need for further refinement of FF parameters to accurately reproduce heat capacities has been acknowledged. 55,130-131 A simple correction is to apply a scaling factor to the computed QM vibrational frequencies that is consistent with the level of theory employed. 88,130-131

An alternative approach for computing heat capacity is a two-phase model proposed by Lin, Blanco, and Goddard III¹³⁴ where the vibrational density of states (DoS) is calculated to account for QM corrections to the thermodynamic properties of liquids. DoS represents the distribution of the vibrational normal modes of a system, expressed as a function of the normalmode frequency (ν) . The DoS, denoted by $S(\nu)$, can be obtained from the Fourier transform of the mass weighted sum of the atomic velocity autocorrelation functions. The distributions obtained are then normalized to the total number of degrees of freedom in the given system; thermodynamic properties such as heat capacities can then be calculated by assuming each normal mode to be a quantum mechanical oscillator with a frequency ν . This method was employed to compute heat capacities for several IL and DES systems. 35,91-92,133 The corrected heat capacity is described in equation 17a, where C_P^{corr} and C_P^{class} represent the corrected and classical heat capacities at constant pressure. δC_v^{QM} denotes the QM-corrected heat capacity at constant volume and is given by equation 17b, where W is a weighting function. In DES simulations by Doherty and Acevedo, 35 an additional term $N_c k_b$ was added to the C_P term to account for neglected contributions due to bond constraints present in the simulations.

$$C_P^{corr} = C_P^{class} + \partial C_v^{QM}$$
 [17a]

$$\partial_{v}^{QM} = k_b \int_{0}^{\infty} (W(v) - 1)S(v)dv$$
 [17b]

A comparison of heat capacities computed from DES molecular simulations has been provided in Table 8. However, given the multiple methods employed and the differences in temperature reported in the simulations, direct comparison between the force field parameters is not straightforward. Perkins, Painter, and Colina. Teported heat capacities derived from GAFF simulations to be within the range of experimental data for CCU; however, 7% errors were computed for the CCEtg and CCGly DESs. Simulations by Mainberger et al. We using their custom GAFF and MMFF parameters found relatively lower percent errors of 2.6% and 3.6% respectively for CCGly. Finally, OPLS-AA simulations by Doherty and Acevedo are gave error percentages of 5.8, 5.6 and 4.9% for CCU, CCEtg, and CCGly, respectively. An alternative to FF predictions was developed by Taherzadeh et al. Using a correlation model trained on 505 C_p values from 28 DES that yielded an absolute average relative deviation of 4.7% for all investigated data points.

Table 8. Comparison of C_p (J/mol K) for Deep Eutectic Solvents.

DES	Authors/Fo	orce Field	Temp. (K)	Simulation	Experiment ¹⁰⁶
CCU	Perkins, Painter and Colina ⁵⁵	GAFF (0.8) ^(a)	298-330	184	181.4±0.5 to 186.4±0.5
	Doherty & Acevedo ³⁵	OPLS-AA (0.8)	353	201.9	190.8±0.8
CCEtg	Perkins, Painter and Colina ³¹	GAFF (0.8)	298-330	209.27±1.55	190.8±0.4 to 199.2±0.3
	Doherty & Acevedo ³⁵	OPLS-AA (0.8)	353	215.8	205.6±0.2
CCGly	Perkins, Painter and Colina ³¹	GAFF (0.8)	298-330	259.15±2.87	237.7±0.6 to 246.9±0.1
	Mainberger et al. ³²	GAFF (0.75)	303	244.0±2.9	237.7±0.6
	Mainberger et al. ³²	MMFF	303	246.3±8.6	237.7±0.6
	Doherty & Acevedo ³⁵	OPLS-AA (0.8)	353	240.1	254.3±0.4

(a) Values in parentheses (0.75 or 0.8) indicate charge scaling factor in the given force field.

5.2 Heats of Vaporization

Heats of vaporization (ΔH_{vap}) are calculated according to equation 18, where ΔE_{vap} is the difference between the total energies of the gas and liquid phase, T is the temperature, and R is the universal gas constant.

$$\Delta H_{vap} = \Delta E_{vap} + RT \tag{18}$$

With respect to DES simulations, calculating ΔH_{vap} is very challenging as the vapor phase composition is experimentally unknown. A thorough investigation by Salehi et al. 104 computed the ΔH_{vap} for CCU, CCEtg, CCGly, CCMal, and CCOx using OPLS-AA parameters by Doherty and Acevedo³⁵ and for CCU using GAFF parameters from Perkins, Painter, and Colina³¹ by utilizing three different vaporization clusters: HBD, HBA, and a cluster from the DES mixture. For the CCU solvent, the ΔH_{vap} derived from the vaporization of urea, ChCl, and a ChCl-urea cluster using OPLS-AA was 82, 165, and 228 kJ/mol, respectively. Comparison to the experimentally estimated ΔH_{vap} values of 46.9 and 79.0 kJ/mol obtained from vapor pressure data of Shabaz et al. and Ravula et al., ¹³⁶⁻¹³⁷ suggests that it is more likely for HBD molecules to vaporize from the DES mixture and dominate the vapor phase. Similar results and agreement with experiment were computed by Salehi et al. for the CCEtg and CCGly DESs using OPLS-AA. 104 However, the GAFF parameters yielded less accurate ΔH_{vap} values for CCU. In separate work, Ferreira et al. utilized their mixed FF parameter set to compute ΔH_{vap} for CCEtg⁹⁸ and CCPro¹⁰¹ and found the values ranged from 167.5±0.3-179.5±0.5 kJ/mol and 161-210 kJ/mol, respectively. Finally, Ullah et al.³⁷ calculated the ΔH_{vap} value for CCLev using their custom MDynaMix parameters and reported an energy of 52.05 kJ/mol.

5.3 Isothermal Compressibility

Isothermal compressibility (κ_T) can be expressed as a change in molar volume (V) with pressure (P) at a given temperature, or, alternatively, in terms of fluid density (ρ) as given in equation 19.

$$\kappa_T = -\frac{1}{V} \left(\frac{\partial V}{\partial P} \right)_T = \frac{1}{\rho} \left(\frac{\partial \rho}{\partial P} \right)_T$$
 [19]

To compute κ_T using MD simulations, the relationship between V (or ρ) and P could be obtained by fitting an equation of molar volume at varying pressures (at constant temperature). However, a simpler approach was developed by Motakabbir and Berkowitz (equation 20), ¹³⁸ where a linear isotherm was assumed in the pressure range used to calculate κ_T . Here, ρ_I and ρ_2 represent the densities at pressure P_I and P_2 , respectively. The simulations can be divided into smaller blocks in order to obtain multiple values of κ_T at the desired temperature.

$$\kappa_T = \frac{1}{\rho} \left(\frac{\partial \rho}{\partial P} \right)_T \approx \frac{\Delta \ln(\rho)}{\Delta P} = \frac{\ln(\frac{\rho_2}{\rho_1})}{P_2 - P_1}$$
 [20]

It is important to emphasize that a linear approximation may not be appropriate for different classes of liquids or within specific pressure/temperature ranges, and may lead to inaccurate estimation of κ_T . Alternatively, the Tait equation¹³⁹ can be substituted to fit molar volumes/densities obtained from MD simulations to provide a correlation to pressure. In this method, κ_T is calculated using the fluctuations formula as given by equation 21, where FFs $\langle \delta V^2 \rangle_{NPT}$ and $\langle V \rangle_{NPT}$ denote the volume fluctuations and average volume of the simulation box in the NPT ensemble, respectively. The volume fluctuations method has been used widely to compute κ_T for several charged liquid systems including ILs. $^{84,143-146}$

$$\kappa_T = \frac{\langle \delta V^2 \rangle_{NPT}}{\langle V \rangle_{NPT} \kappa_b T}$$
 [21]

Both methods, i.e., equations 20 and 21, were compared by computing κ_T values using the SPC/E water model and provided similar κ_T values of 38.47 ± 1.16 and 34.07 ± 5.21 in 10⁻¹¹ Pa⁻¹, respectively. Simulations at 323K and 0.98 bar for the IL [bmim][PF₆] performed by Shah, Brennecke, and Maginn¹⁴⁰ also gave similar error percentages, 40.3% and 41.1%, for the linear approximation and Tait equation methods, respectively. With respect to DES simulations, κ_T values have been reported for CCEtg by Ferreira et al.⁹⁸ at 298, 313 and 323 K using equation 21. Multiple FFs were tested, but the mixed parameter set termed 0.8FFM (i.e., GAFF (Ch⁺)³¹ + OPLS-AA/AMBER (Cl⁻)⁷⁶ + OPLS-AA (ethylene glycol)¹⁴⁷), yielded the closest agreement with error percentages of 11%, 1.5%, and 0.1% at 298, 313, and 323 K respectively. Notably, FF combinations that displayed better agreement for κ_T did not necessarily show good performance for other DES solvent properties including self-diffusion coefficients, surface tension, and viscosity.

6. Transport Properties

6.1 Viscosity

Viscosity is an important property for evaluating FF parameters, particularly when gauging the accuracy of computed intermolecular interactions. Fortunately, due to the relative ease of measurement and the importance of DESs in industrial processes,⁵⁷ experimental viscosities are often readily available for comparison. However, the highly viscous nature of DESs⁴¹ often leads to major discrepancies in reported values under the same conditions. For example, viscosities for CCU at ambient conditions have been reported to range from 152 cP⁴⁰ to 527.28 cP.¹¹¹ The cause of such large deviations may stem in part from differences in the experimental methods,¹¹⁰ but more likely arise from the presence of impurities during the preparation process.⁵⁷ Many classes of DESs are highly hygroscopic and water has been found to have a dramatic effect on the

viscosities of these solvents. For example, the viscosity of CCU was shown to decrease by approximately 60% when shifting from pure DES to 0.1 mole fraction of water. Additionally, Florindo et al. 10 found that CCOx has a considerable affinity for atmospheric water, citing a 19.40% water content that dropped the viscosity from 5363 cP to 44.49 cP at 303.15 K. The cause of such dramatic decreases in viscosity is believed to be from the disruption of the complex hydrogen bond network that is attributed to DES's highly viscous nature. 41,110

Along with impurities, increasing the molar ratio of HBDs present in a DES can also decrease the viscosity as a consequence of disrupting the hydrogen bond network of the solvent. For example, the viscosities for CCPhe at 1:2, 1:3, and 1:6 molar ratios are reported as 90.33 cP, 44.64 cP, and 21.43 cP respectively. Al, 148 As more phenol was added it is suggested that the HBD eventually acts as an organic solvent which disrupts the Coulomb interaction between the cation and anion, leading to the same effect seen when water is introduced to the system. However, for CCGly the opposite effect was observed, as the molar ratio increased from 1:2 to 1:3 to 1:4 the reported viscosity values (at 293.15 K) also increased, i.e., 376, 450, and 503 cP respectively. Al, 148-149 This phenomena is attributed to the strong cohesive energy between glycerol molecules that generates a strong hydrogen bond network limiting ion mobility and thus increasing the viscosity. Considering these examples, it is important to consider the ratios used during the construction of DESs when studying their viscosities.

Temperature also has a significant effect on the viscosity of DESs. ^{110,150} For example, substantial decreases in viscosity going from 298 K to 328 K were reported for CCU (1:2 molar ratio): 750 to 95 cP, CCGly (1:2 molar ratio): 259 to 52 cP, and CCMal (1:1 molar ratio): 1124 to 161 cP, respectively. ^{44,110} A strong relationship between the temperature dependence of the DES viscosity and the strength of the ion-HBD intermolecular forces has been suggested based on

fittings to an Arrhenius model which allows for activation energies (E_a) to be calculated. ¹¹⁰ In this correlation, DESs that exhibit low viscosities have a low E_a, whereas systems with high viscosity values have a relatively higher E_a. For example, CCEtg (1:2 molar ratio) which has a reported viscosity of 39.7 cP at 298.15 K has an E_a of -11.26 kJ/mol, while CCOx (1:1 molar ratio) which has a reported viscosity of 208.3 at 348.15K has an E_a of -65.20 kJ/mol. ^{41,57} This trend further highlights the dramatic effect of ion-HBD interactions upon the overall viscosity.

When calculating the viscosity of a system computationally, the type of simulation falls under two categories: equilibrium MD and non-equilibrium molecular dynamics (NEMD). MD is desirable because the viscosity can be calculated from either pressure or momentum fluctuations in an equilibrium trajectory via a single simulation. A common approach to relating pressure fluctuations to viscosity uses the Green-Kubo formula (equation 22).¹⁵¹

$$\eta = \frac{V}{k_B T} \int_0^\infty \langle P_{\chi z}(t_0) P_{\chi z}(t_0 + t) \rangle_{t_0} dt$$
 [22]

Here, V is the volume, T is the temperature, V is the Boltzmann constant, and V is the off-diagonal element of the stress tensor. To reduce uncertainties arising from large pressure fluctuations, the integral is often fit to a pressure tensor autocorrelation function. However, due to the slow dynamics and relaxation times of the highly viscous solvents, the Green-Kubo method struggles to accurately sample pressure tensors unless very long simulations are performed. V

Alternatively, NEMD methods have been shown to properly treat highly viscous solvents^{91-92,155-156} by applying an external force to the solvent and relating the resulting flux back to the viscosity. As a result, additional simulations are required beyond the equilibrium trajectory. One method that has been used extensively is the periodic perturbation method.¹⁵⁷ In this method an external force of a chosen amplitude is applied in the x direction, a_x , to three-dimensional periodic cells to create a velocity field a_x . The velocity field can then be described using the Navier-Stokes

equation (Equation 23) where a_y and a_z are equal to zero, resulting in velocity fields in the y and z direction to also be zero. The equation for the velocity field then becomes

$$\rho \frac{\delta u_{x}(z)}{\delta t} = \rho a_{x}(z) + \eta \frac{\delta^{2} u_{x}(z)}{\delta z^{2}}$$
 [23]

where ρ is the mass density. The velocity field is easily calculated throughout the simulation with the use of a velocity profile, V. The velocity profile is then related to the viscosity of the system using the Equations 24 and 25, where l_z is the height of the box and Λ is the acceleration amplitude of the external force, $a_x(z)$ (eq. 26).

$$\eta = \frac{\Lambda}{V} \frac{\rho}{k^2} \tag{24}$$

$$k = \frac{2\pi}{l_z} \tag{25}$$

To ensure a smooth velocity profile with small local shear rates, the external force is controlled with a cosine function.

$$a_x(z) = \Lambda \cos(kz) \tag{26}$$

The selection of a proper acceleration amplitude is crucial, as it should be large enough to properly probe the system, but small enough so that the equilibrium of the system is not completely destroyed. Multiple simulations are then required at varying amplitudes, typically ranging between 0.02 to 0.25 nm/ps², in order to get point viscosities at each amplitude. Extrapolation to an undisturbed system where, Λ =0, is taken as the viscosity of the system.

An alternative NEMD, called the D-base method, was recently tested on a highly viscous ionic liquid system [Bmim][Tf₂N].¹⁵⁸ This method utilizes finite-size effects of self-diffusion coefficients to calculate the viscosity of a bulk system through the equation of Yeh and Hummer (equation 27).¹⁵⁹ Multiple simulations are required to provide diffusion coefficients at various system sizes.

$$D_{self}^{MD} = \left(\frac{1}{n}\right) \left(-\frac{\xi k_b T}{6\pi L}\right) + D_{self}^{\infty}$$
 [27]

From equation 27, ξ is a dimensionless constant equal to 2.837297, L is the length of the simulation box. Equation 27 is in a linear form, where D_{self}^{MD} is the independent variable and $-\xi k_B T/6\pi L$ is the dependent variable. D_{self}^{∞} is the intercept of the linear function, representing the thermodynamic limit in which $L \to \infty$. The inverse slope of the line is then taken as the viscosity of the system. In order to incorporate all species in the system, D_{self}^{MD} is replaced by an average of each self-diffusion coefficient weighted by their corresponding mole fraction (equation 28).

$$D_{avg} = \lim_{t \to \infty} \frac{1}{6t} \frac{1}{N} \left\langle \sum_{i=1}^{n} \sum_{j=1}^{N_i} \left(r_{j,i}(t) - r_{j,i}(0) \right)^2 \right\rangle$$
 [28]

Here n and N are the total number of species and molecules in the mixture, respectively. When used on the [Bmim][Tf₂N] ionic liquid system at increasing temperatures, the predicted viscosities matched well with Green-Kubo data reported by Zhang, Otani, and Maginn. Although the D-base method has not been applied to DESs to date, it does have considerable potential for future use with its ability to handle viscous mixtures possessing more than one molecular species.

Another potential avenue for computing the viscosities of DESs is the Müller-Plathe method, which has been successfully applied to the ionic liquid system [Emim][Tf₂N].¹⁶¹⁻¹⁶² The Müller-Plathe method uses a reverse NEMD approach (RNEMD), where a momentum flux causes the corresponding external field that is related to the viscosity using equation 29. This differs from the NEMD approach, where an external field elicits a flux within the system which is then related to the viscosity by the Navier-Stokes equation.

$$j_{y} = -\eta(\dot{\gamma}) \frac{\delta v_{x}}{\delta y}$$
 [29]

In equation 29, $^j{}_y$ is the momentum flux that is imposed, and $\dot{\gamma}$ is the velocity gradient which can be calculated using a velocity profile throughout a simulation. The momentum flux is arbitrarily chosen by dividing the simulation box into an N number of "slabs" in the y direction and then exchanging the largest momentum difference, $^p{}_{x,n_c}-^p{}_{x,n_1}$, in the x direction between 2 atoms from differing slabs. The total momentum exchange, $^p{}_{total}$, and resulting flux at a time t is calculated with equations 30 and 31.

$$P_{total} = \sum (P_{x,n_c} - P_{x,n_1})$$
 [30]

$$j_{y}(P_{x}) = \frac{P_{total}}{2tL_{x}L_{z}}$$
 [31]

 L_x and L_z are the lengths of the simulation boxes in the x and z direction. The resulting velocity gradients, which are calculated by the velocity profiles of the simulation, are then related back to equation 29 to obtain the viscosity. Calculated viscosities for the IL system [Emim][Tf₂N] gave a root mean squared error of 15% when compared to experimental values. Again, while this method has yet to be applied to DES systems it may present a viable option for future studies.

Errors between MD and NEMD methods have been highlighted in the DES system CCLev (1:2 molar ratio). Using the Green-Kubo method, a calculated viscosity of 265 cP at 298 K was overestimated compared to the weighted experimental value of 226.8 cP, a 16.8% error.³⁷ Comparatively, the periodic perturbation method proved to be more accurate yielding a viscosity of 220.8 cP, a 2.6% error.³⁵ Additional simulated viscosities featuring the Green-Kubo method have been reported for CCU (1:2 molar ratio), CCGly (1:2 molar ratio), and CCMal (1:1 molar ratio) at 318K with percent errors of 35.4%, 26.8%, and 31.8% respectively.²⁰ Simulated viscosities using the periodic perturbation method for these same systems gave percent errors of 1.1%, 3.3%, and 1.9%, respectively, at 303 K and 348 K.³⁵ Altamash et al. calculated the viscosity of the DES system choline chloride phenylacetic acid (1:2 molar ratio) using the Green-Kubo

method and found at 298 K the simulations performed modestly with percent error of 16.4%.¹⁶³ However, when the temperature increased to 345 K the percent errors became as high as 80.1% illustrating the importance of studying DESs systems within a wide range of temperatures. Alternatively, Zhang et al.³⁶ found using the time decomposition method¹⁶⁰ of the Green-Kubo theory for CCEtg (1:2) while utilizing the parameters of Perkins, Painter, and Colina³¹ performed better at elevated temperatures where calculated viscosities were overestimated by 5-8 cP. The periodic perturbation method when coupled to the OPLS-AA FF developed by Doherty and Acevedo³⁵ found that temperature had little effect on the accuracy of each prediction, where a mean absolute error of 14 data points was calculated to be 1.6% (Table 9). However, there are cases where the percent error did increase marginally as the temperature was raised by 5 degrees Kelvin, and further studies may be needed at higher temperatures for a full evaluation.

Table 9. Calculated and Experimental Viscosities (cP) at Various Temperatures.

DES	Simulation Experiment		% error						
298.15 K									
CCEtg	39.5	39.7	0.6						
CCGly	258.8	259.0	0.1						
CCLev	220.8	226.8	2.6						
CCPhe(1:2)	89.1	90.3	1.3						
CCPhe(1:3)	44.4	44.6	0.4						
CCU	753.1	749.9	0.4						
	303.	15 K							
CCEtg	35.0	35.0	0.0						
CCGly	246.8	238.9	3.3						
CCLev	164.0	164.5	0.3						
CCPhe(1:2)	64.7	68.4	5.4						

CCPhe(1:3)	36.5	35.2	3.7
CCU	520.5	514.8	1.1
	348.15 K		
CCMal	94.9	96.7	1.9
CCOx	205.2	208.3	1.5
MAE (%)			1.6

⁽a) Weighted experimental averages were computed at various temperatures where each weight was determined by the inverse of its reported uncertainty. Reprint with permission from B. Doherty, O. Acevedo, *J. Phys. Chem. B*, 122, (43), 9982-9993 (2018). OPLS Force Field for Choline Chloride-Based Deep Eutectic Solvents. Copyright 2018 American Chemical Society.

 Table 10. Viscosity Calculation Methods Utilized in DES Simulations.

Simulation by	DES Studied	Charge Assignment	Method
Ullah et al. ³⁷	CCLev(1:2)	Scaled	Green-Kubo
Doherty and Acevedo ³⁵	CCEtg (1:2), CCGly (1:2), CCLev (1:2), CCMal (1:1), CCOx (1:1), CCPhe (1:2), CCPhe (1:3), CCU (1:2)	Scaled	Periodic Perturbation
García, Atilhan and Aparicio ²⁰	CCGly (1:2), CCMal (1:1), CCU (1:2)	Scaled	Green-Kubo
Altamash et al. ¹⁶³	CCPhOAc (1:2)	Scaled	Green-Kubo
Zhang et al. ³⁶	CCEtg (1:2)	Scaled	Green-Kubo

Ferreira et al. ⁹⁸	CCEtg (1:2)	Unscaled, Scaled	Periodic Perturbation
Ferreira et al. 101	CCPro (1:2)	Unscaled, Scaled	Periodic Perturbation

Along with the calculated viscosity method, the quality of the FF can influence bulk-phase properties significantly. A list of FFs that have been used to simulate DES viscosities is given in Table 10. The importance of selecting a proper force field is emphasized by Ferreira et al. who tested 8 combinations of non-polarizable FF parameters from the literature for the different components of CCEtg (1:2 molar ratio). 98 This includes choline parameters from Sambasivarao and Acevedo,⁷⁵ Perkins, Painter, and Colina,⁵⁵ and OPLS-AA intramolecular parameters.⁷⁷ Chloride parameters were taken either directly from OPLS-AA⁷⁷ or from Canongia Lopes, Deschamps, and Pádua⁷⁶ which were developed for IL simulations. For ethylene glycol, the HBD parameters were taken from either OPLS-AA,⁷⁷ Szefczyk and Cordeiro,¹⁴⁷ or Gorny et al.⁹⁹ In addition, each combination was evaluated with integer charges (± 1 e) and scaled charges (± 0.8 e). Substantial improvement for self-diffusion coefficients were observed when the charges were scaled. While using the periodic perturbation method, five FF combinations struggled to match experimental viscosity values shown in Figure 8, where measurements were underestimated by a factor of 2.5 on average. However, at 298 K some FFs performed considerably better than others, stemming from the treatment of short-range interactions and hydrogen bonding that are governed by the quality of the parameters. Also worth noting is the ability to capture the temperature dependence of viscosity measurements, where calculated values normalized by the 298 K measurement are in very good agreement with experimental data. Overall, great care should be

taken when selecting (1) FF parameters and (2) viscosity calculation methods, as viscosity predictions derived from atomistic DES simulations have been shown to be highly sensitive to both choices.

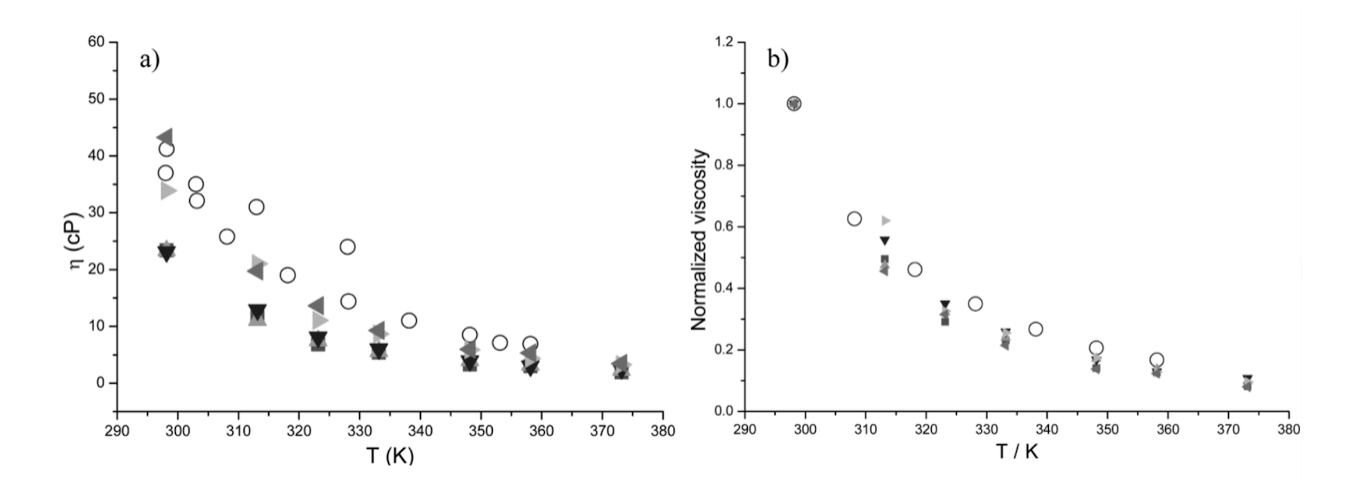


Figure 8. (a) Experimental and simulated viscosities from multiple FF combinations for CCEtg at 1 bar and (b) Experimental and simulated normalized viscosity by the temperature 298.15 K. Experimental values are depicted as empty black circles while simulated values are filled shapes. Reprinted with permission from E. S. C. Ferreira, I. V. Voroshylova, C. M. Pereira, M. N. D S Cordeiro, *J. Phys. Chem. B*, **120**, (38), 10124-10137 (2016). Improved Force Field Model for the Deep Eutectic Solvent Ethaline: Reliable Physicochemical Properties. Copyright 2016 American Chemical Society.

Aside from MD simulations, the viscosity of DES systems can also be calculated with equations of state models in combination with various friction theories which has been outlined in the review by González de Catilla, Bitter, and Müller. For example, Haghbakhsh et al. 165 used friction theory along with the cubic plus association and perturbed chain-statistical associating fluid theory to calculate the viscosity of 27 different DES systems and found an average relative deviation from experimental values of 4.4% for both models. A follow up version of the models were used by the same group where results were then improved to an average deviation of 2.7%. Additionally, Lloret, Vega, and Lovell 167 used a soft-SAFT with free volume theory for quaternary ammonium chloride containing DES systems and found good agreement with experimental trends.

6.2 Diffusion Coefficients

The importance of understanding the mechanism of how ions/molecules diffuse in DES systems has been discussed in the literature and tested experimentally. 44,57,168 Originally, DESs were thought to move similarly to ILs which have been characterized by Zhao, Lian, and Li using a modified hole theory. 169 In the modified hole theory, ions diffuse moving from one vacancy to another when an ion's hole size is smaller than the one adjacent to it. While it is still believed that the mobility of the holes are the dominant factor in an ion's diffusivity resulting in a jumping mechanism,⁴⁴ the hydrogen bond network between the ions and HBD should also be considered as it can hinder the mobility of each component. To our knowledge, only D'Agostino et al. 44 and Abbott et al. 168 have reported diffusion coefficients with the use of pulse field gradient nuclear magnetic resonance (PFG)-NMR for DES systems. D'Agostino et al. 44 found the HBD interactions to be important for CCMal, where it is believed that the carboxylic acid functional groups of maline create a dimerization through hydrogen bonding that leads to long chains and hinders the mobility of the ions within the system. Abbott et al. 168 also found that when more choline chloride was added to a CCGly system, the choline chloride would break up the intermolecular forces between glycerol molecules and increase their diffusivity, highlighting the importance of the hydrogen bond network established as well as the molar ratio in each DES system. Experimentally, cations are found to diffuse slower than HBDs for urea, glycerol, and ethylene glycol which can be explained by the hole theory. However, the opposite trend is seen with malonic acid due to its dimerization that was explained previously. The importance of temperature has also been stated in literature, 44 where results show an Arrhenius-type behavior. The temperature dependence is also crucial when considering simulated diffusion coefficients which is explained later.

For a simulated system, the diffusion coefficient is calculated by applying the Einstein relation and the average mean square displacement for each ion/molecular center of mass (equation 32).¹⁴²

$$D_{s} = \frac{1}{6} \lim_{t \to \infty} \frac{d}{dt} \frac{1}{N} \sum_{i=1}^{N} \langle |r_{i}(t) - r_{i}(0)|^{2} \rangle$$
 [32]

Here, $r_i^{(t)}$ is the center of mass of species i at time t, and N is the number of individual species. An important aspect of using the Einstein relation is that the system is studied within a proper diffusive regime where ions/molecules are moving freely. A way to monitor the diffusive regime is with the calculation of the beta-parameter (β), which has been previously discussed by Del Popolo and Voth¹⁷⁰ and applied to DES systems by Perkins, Painter, and Colina,^{31,55} Doherty and Acevedo,³⁵ Ferreira et al.,⁹⁸ and Mainberger et al..³²

$$\beta(t) = \frac{d \log_{10} \langle \Delta r(t)^2 \rangle}{d \log_{10} t}$$
 [33]

Here, $\langle \Delta r(t)^2 \rangle$ is the mean square displacement and t is the time. The beta-parameter can therefore be plotted versus time and when $\beta < 1$, the system is considered to be in the subdiffusive regime. When $\beta = 1$ the system is then considered in the diffusive regime and the diffusion coefficient can be properly calculated with equation 33.

Similar to viscosity calculations, diffusion coefficients are very sensitive to the treatment of charges assigned to each molecule/ion. For simulations that utilize a non-polarizable FF, the use of integer charges (±1 e) for the ions has shown to significantly underestimate the diffusion coefficients. For example, Mainberger et al.³² used MMFF parameters with unscaled charges and found that for CCGly the calculated diffusion coefficients at 328 K had percent errors as high as 92%. As an alternative, GAFF parameters in combination with RESP charges derived from a minimal cluster of ChCl/HBDs (1:2 ratio) were also tested. Due to charge transfer effects, the species Ch⁺, Cl⁻, and glycerol had scaled point charges of 0.7615 e, -0.6527 e, and -0.0544 e,

respectively. Diffusion coefficient results improved dramatically to 15.6% and 6.5% errors for choline cation and glycerol, respectively. Ferreira et al. 98 observed the same improvement when charges were scaled for CCEtg and CCPro. For example, using unscaled charges by Perkins, Painter, and Colina 55 for CCEtG combined with parameters from OPLS-AA, 77 calculated diffusion coefficients at 313.15 K had errors of 90.13% and 87.88% for choline and ethylene glycol, respectively. However, scaling the charges by a factor of 0.8, improved the errors to 11.8% and 2.8%, respectively. For CCPro, system specific charges resulted in a scaling factor of 0.74 that did not perform as well with errors of 17% and 15% for choline and propylene glycol, respectively. However, this was a major improvement over the unscaled systems that never reached the diffusive regime. Calculations of self-diffusivity using a variety of FFs are presented in Table 11 for multiple DESs.

Table 11. Calculated Self-Diffusion Coefficients (D^+ and D^{HBD} at 10^{-11} m² s⁻¹) at 298.15 K and 330.15 K for Deep Eutectic Solvents.

DES	Force Field	D ⁺	DHBD	% error D ⁺	% error D ^{HBD}
CCU				298.15 K	
	Doherty and Acevedo ³⁵	0.46	0.35	31.4	47.0
	Perkins, Painter and Colina ⁵⁵	0.17	0.39	51.4	40.9
	Experiment ⁴⁴	0.35	0.66		
				330.15 K	
	Doherty and Acevedo ^{35,*}	1.51	3.56	28.1	0.3

	Perkins, Painter and Colina ⁵⁵	2.18	3.67	3.8	3.4
	Experiment ⁴⁴	2.10	3.55		
CCEtg				298.15 K	
	Perkins, Painter and Colina ³¹	1.81	3.75	30.9	21.4
	Ferreira et al. ⁹⁸	2.08	4.15	20.6	13.0
	Experiment ⁴⁴	2.62	4.77		
				330.15 K	
	Perkins, Painter and Colina ³¹	7.44	15.3	24.0	6.7
	Ferreira et al. 98,*	14.9	-	52.2	-
	Experiment ⁴⁴	9.79	16.4		
CCGly				298.15 K	
	Perkins, Painter and Colina ³¹	0.30	0.45	21.1	13.5
	Experiment ⁴⁴	0.38	0.52		
				330.15 K	
	Perkins, Painter and Colina ³¹	2.11	3.12	17.9	27.3
	Mainberger et al. 32,*	2.07	2.61	15.6	6.5

	Experiment ⁴⁴	1.79	2.45			
CCPro				298.15K		
	Ferreira et al. ¹⁰¹	1.37	2.11	17.0	15.0	
	Experiment ¹⁰¹	1.66	2.49			

^{*} Measured at 328.15 K

Another important factor to consider is the temperature of the system. Typically, at room temperature (298.15 K) systems exhibit a sub-diffusive character where $\beta < 1$ due to the strongly correlated hydrogen bonding that occurs between the cation and anion creating a cage that the ions cannot escape until the temperature is raised.⁴⁴ Although scaling charges has shown to improve results, simulations at room temperature still struggle as shown by Perkins, Painter, and Colina. 31,55 where they analyzed diffusion coefficients at both 298 K and 330 K for CCU, CCEtg, and CCGly using the GAFF FF with RESP derived charges on isolated ions/molecules. Most noticeably for the CCU system, results at room temperature gave large errors of 51.4% and 40.9% for choline and urea, respectively. Results improved considerably however when the temperature was raised to 330 K, with calculated diffusion coefficients for choline and urea having 3.8% and 3.4% errors, respectively. Although improvement was seen when the temperature was raised to 330 K for every DES system, reported percent errors were still as high as 27.3%. Despite the errors, diffusive trends were adequately captured for all simulated results reported. Shown in Figure 9, Perkins, Painter, and Colina⁵⁵ found that urea diffuses faster than the heavier and larger choline ion for CCU which is consistent with experimental findings.

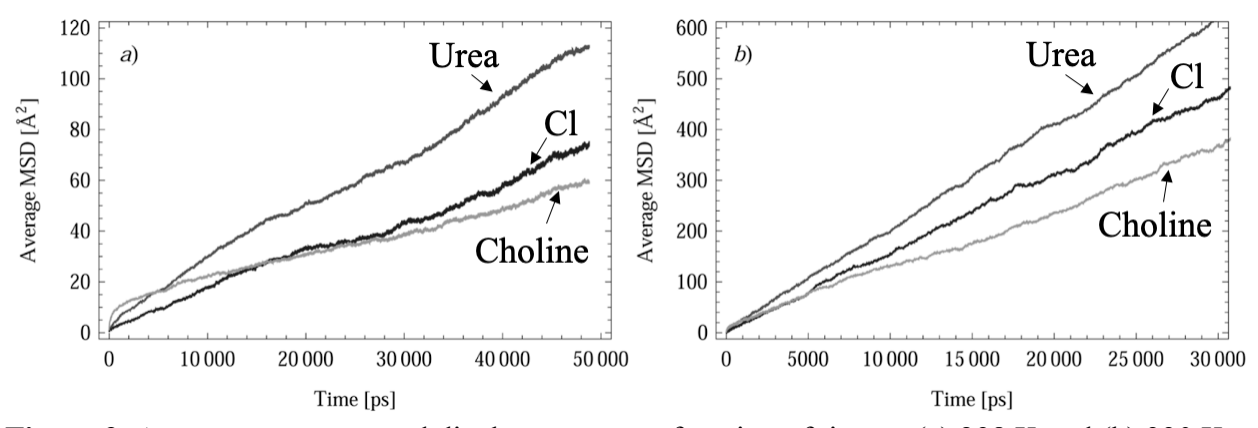


Figure 9. Average mean squared displacement as a function of time at (a) 298 K and (b) 330 K. Adapted with permission from S. L. Perkins, P. Painter, C. M. Colina, *J. Phys. Chem. B*, **117**, (35), 10250-10260 (2013). Molecular Dynamic Simulations and Vibrational Analysis of an Ionic Liquid Analogue. Copyright 2013 American Chemical Society.

As with any simulation, refinement of FF parameters can lead to more accurate predictions of bulk-phase and transport properties. Modest improvement was accomplished by Ferreira et al. 8 by testing various combinations of FF parameters for each component of CCEtg. After scaling the charges by 0.8 to the best performing parameter combination, predicted diffusion coefficients improved to an average error of 10% for the temperature range of 298.15-323.15 K. However, the results were inconsistent and for all combinations tested there was a parabola-like temperature dependence for each diffusion coefficient where percent errors more than doubled between temperatures. A similar trend was reported by Doherty and Acevedo³⁵ who developed OPLS-AA parameters utilizing a \pm 0.8 charge scaling for 8 different DES systems. At temperatures between 298.15-328.15 K a sub-diffusive regime was observed. Illustrated in Figure 10 are calculated beta-parameters for the choline chloride urea system at both 298.15 K and 420.15 K, clearly showing the temperature dependance where β < 1 is observed for the majority of the 298.15 K simulations and β = 1at 420.15 K. To compensate, simulations were performed at higher temperature (400.15-500.15 K) and calculated diffusion coefficients were extrapolated to room temperature. Results

varied substantially for the CCU system, where errors were reported as 31.4%, 0.0%, and 23.2% for 298.15 K, 308.15K, and 323.15 K, respectively.³⁵

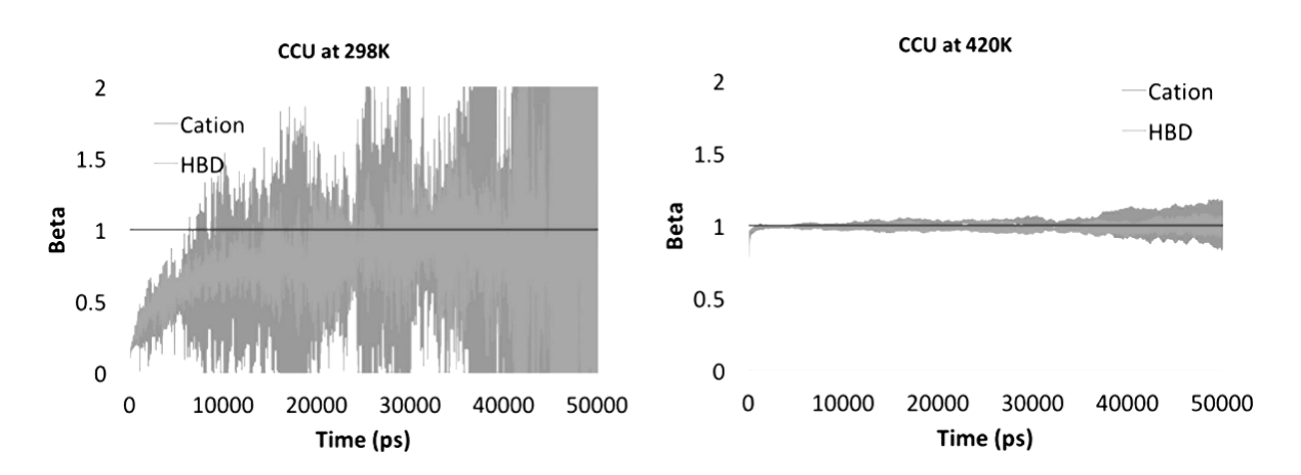


Figure 10. Calculated beta-parameter as a function of time for CCU at 298 K and 420 K. Reprint with permission from B. Doherty, O. Acevedo, *J. Phys. Chem. B*, **122**, (43), 9982-9993 (2018). OPLS Force Field for Choline Chloride-Based Deep Eutectic Solvents. Copyright 2018 American Chemical Society.

Although calculated self-diffusion coefficients can seem accurate at specific temperatures, there exists an inconsistency for all non-polarizable FFs when tested over a range of temperatures. At minimum, simulations should be run at higher temperatures with adequate lengths in order to ensure a diffusive regime is properly sampled. Polarizable FFs are likely required to adequately capture the charge fluctuations that have a large effect on transport properties.

7 Deep Eutectic Solvent Structure

7.1 Radial Distribution Functions

The driving force for DES melting point depression has often been linked to the complex hydrogen bond network formed between both the ions and HBDs. 44,54,168,171 In addition, physical properties such as viscosity and diffusion coefficients can be directly related to the DES local structure and interaction strengths between each component. 36,150 To clarify the liquid structuring

of various DES systems including CCU (1:2 molar ratio), CCOx (1:1 molar ratio), CCEtg (1:2 molar ratio), and CCGly (1:1 molar ratio), neutron diffraction^{36,46,63,172} and simulation studies^{31-32,34-36,45,55,69,78,150,173} have been performed. The existence of a H-bond network is well supported by HOESY NMR,⁴⁰ FT-IR,^{55,174-175} PFG-NMR,⁴⁴ and Quasi-elastic neutron scattering.⁶³ The use of ND/EPSR has been shown to provide specific atomic site-site interactions at an accurate level.^{46,172,176} From the ND/EPSR data, comparisons can be made to high-level computational methods such as FPMD,⁴⁵ AIMD,^{34,36,69,173} and QM/MD simulations.¹⁵⁰ MD simulations utilizing non-polarizable FFs have also been used to study the structure of CCU (1:2 molar ratio),^{20,35,54-55,177-178} CCEtg (1:2 molar ratio),^{31,35-36} CCLev (1:2 molar ratio),^{37,94} CCMal (1:2 molar ratio),²⁰ and CCGly (1:2 molar ratio)^{20,31-32,35} and compared to the previously mentioned methods when applicable.

Analyzing the center-of-mass (COM) RDFs provides insight into how each component of the DES system is coordinated to one another by integrating the first peak of each interaction. For the system CCU (1:2 molar ratio), the COM RDFs were computed using ND/EPSR⁴⁶ and MD^{35,54} at room temperature, as well as FPMD⁴⁵ at 333 K. Table 12 shows the COM RDF peak distances and coordination numbers computed from ND/EPSR, indicating the strongest interactions occurred between choline-chloride, urea-chloride, and urea-urea near 4 Å. Integration of the urea-chloride peak resulted in a coordination number of 2 urea molecules per chloride, which is expected due to the 2:1 urea:chloride ratio used to construct this particular DES. The choline-chloride peak shows a distinct shoulder around 5 Å implying that there exists multiple interaction sites within the first solvation shell in which a chloride ion can oscillate between. Meanwhile, the urea molecules are not only interacting with the chloride ions, but also with surrounding urea molecules with a coordination value of 6.77. These results suggest that the HBDs in DESs are

highly involved with the structural ordering of the system and that a complex hydrogen bond network exists between both the ion pair and HBDs. The importance of the HBD was also examined by Sun, Wu, and Li⁵⁴ who studied the effect of increasing mole percentages (0%, 25%, 67.7%, and 75%) of urea into choline chloride using MD. Pure ChCl exhibited strong long-range ordering between the ions, but when urea was added to the system the COM RDFs showed a gradual increase in the ion interaction distance and the second solvation layer decreasing. This is the result of the chloride ions interacting urea molecules that have inserted themselves within the ionic lattice and disrupting the long-range interactions.

Also provided in Table 12 are the coordination numbers calculated using FPMD and classical MD. Good agreement between all 3 methods was observed, with all coordination numbers within error of each other. Minimum and maximum distances are also in good agreement for each peak. It should be noted that for the MD simulations, the FF was fit specifically to reproduce the ND/EPSR data while maintaining accurate bulk property predictions. Significant tailoring of both the Lennard-Jones terms and charges were required to obtain accurate results and would be a necessary procedure for future DES systems.³⁵

Table 12. Average Coordination Number (N_{coord}) and Position (Å) of the First Maximum and Minimum in Center-of-Mass RDFs between Choline Cation (Ch), Chloride Anion (Cl), and Urea.

		Classi	cal MD	$(303 \text{ K})^{35}$	ND/ESPR (303 K) ⁴⁶		FPMD (333 K) ⁴⁵			
center	shell	$r_{ m max}$	r_{\min}	$N_{ m coord}$	$r_{\rm max}$	$r_{ m min}$	$N_{ m coord}$	$r_{ m max}$	$r_{ m min}$	$N_{ m coord}$
urea	Cl	4.3	5.4	1.90	4.0	5.5	2.08 ± 1.01	4.1	5.3	1.9 ± 0.4
Ch	Cl	4.1	6.4	3.49	4.2	6.7	4.35 ± 1.30	4.2	6.5	3.1 ± 0.6
Ch	urea	4.7	7.2	8.76	5.4	6.9	5.91 ± 2.84	5.1	7.1	8.6 ± 0.7
Ch	Ch	6.5	8.2	5.41	6.3	8.0	6.74 ± 2.16	-	-	-

urea ure	1 4.8	6.6	6.00	4.3	6.1	6.77 ± 3.05	4.7	6.3	4.9 ± 0.5
----------	-------	-----	------	-----	-----	-----------------	-----	-----	---------------

Adapted with permission from B. Doherty, O. Acevedo, *J. Phys. Chem. B*, **122**, (43), 9982-9993 (2018). OPLS Force Field for Choline Chloride-Based Deep Eutectic Solvents. Copyright 2018 American Chemical Society.

COM RDFs have also been computed for CCU (1:2 molar ratio) and CCOx (1:1 molar ratio) at 338 K using ND/EPSR (Table 13).¹⁷² When comparing the CCU (1:2 molar ratio) results to the room temperature ND/EPSR, the maximum peak positions were very similar, varying only by an average of 0.2 Å. There is a noticeable difference in the choline-chloride interaction where the shoulder indicating the presence of multiple binding motifs is now a singular broad peak, suggesting that the elevated temperature favors interactions with primarily the hydroxyl group and trimethylammonium region of choline. For the CCOx (1:1 molar ratio) system the same peak distances are observed as the CCU (1:2 molar ratio) system. Similar to the CCU system, the choline-HBD occurs at a shorter distance than the choline-choline interaction, which indicates an intercalation of oxalic acid within the ionic lattice. A prominent peak for the choline-chloride interaction over the oxalic acid-chloride interaction is worth noting, as an AIMD study performed at 375 K by Zahn, Kirchner, and Mollenhauer³⁴ found the opposite trend where preference was given to the HBD-chloride interaction. This could be a result of elevated temperatures but should be examined in future studies.

Table 13. Position of the First Peak in the COM Radial Distribution Functions for CCGly at 1:1 and 1:2 Molar Ratios.

	Peak Position (Å)			
RDF	CCU (1:2)	CCOx (1:1)		
Choline-choline	6.4	6.3		
Choline-Cl⁻	4.6	4.5		

Choline-HBD	5.4	5.7
HBD-HBD	4.3	5.0
HBD-Cl ⁻	3.7	3.7

Reprinted from M. Gilmore, L. M. Moura, A. H. Turner, M. Swadźba-Kwaśny, S. K. Callear, J. A. McCune, O. A. Scherman, J. D. Holbrey, *J. Chem. Phys.*, **148**, (19), 193823 (2018). A Comparison of Choline:Urea and Choline:Oxalic Acid Deep Eutectic Solvents at 338 K, with permission of AIP Publishing.

The importance of the HBD molar ratio has also been recently studied with the use of ND/EPSR for CCGly. 176 Looking at both the 1:1 and 1:2 ratios, Turner and Holbrey found through COM RDFs that there was no significant changes in the local structuring when choline chloride was added to the system (Table 14). However, by observing the partial site-site RDFs and the corresponding coordination numbers, it was found that the hydrogen bond network formed between glycerol molecules was disrupted as choline chloride was added. This may be the cause of the increase in distance seen in the glycerol-glycerol COM RDF from 5.3 to 5.5 angstroms. Site-site RDFs also showed that as the ratio of ions increases from 1:2 to 1:1, there was a significant reorganization that occurred to compensate for the excess choline chloride to the point where the system may be considered more of a choline chloride ionic liquid environment with glycerol clusters dispersed throughout.

Table 14. Position of the First Peak in the COM Radial Distribution Functions for CCGly at 1:1 and 1:2 Molar Ratios.

	Peak Position (Å)	
RDF	$\chi_{\rm chel} = 0.33$	$\chi_{\rm chel} = 0.50$
Choline-choline	6.5	6.3
Choline-Cl ⁻	4.1	4.1
Choline-glycerol	5.9	5.7

Glycerol-Cl ⁻	4.1	4.1
Glycerol-glycerol	5.3	5.5

Republished with permission of Royal Society of Chemistry, from Investigation of Glycerol Hydrogen-Bonding Networks in Choline Chloride/Glycerol Eutectic-Forming Liquids Using Neutron Diffraction, Adam H. Turner, John D. Holbrey, volume 39, 2019; permission conveyed through Copyright Clearance Center, Inc.

While COM RDFs provided insight into the general coordination between each component of a DES system, partial site-site RDFs allowed for further investigation on specific interactions between atoms of each species. From the COM RDFs for CCU (1:2 molar ratio), it is understood that within the first solvation shell there are close range interactions between the cation-anion, anion-HBD, and HBD-HBD creating a complex hydrogen bond network. From the ND/EPSR results of Hammond, Bowron, and Edler, 46 there was a clear preference for the chloride to interact with the hydroxyl hydrogen of choline for the ion pair. The interactions with the other hydrogens of choline showed a lower correlation with chloride, but still have significant peak heights which could be the reason why the shoulder was seen for the choline-chloride interaction in the COM RDFs. As for the anion-HBD and HBD-HBD interactions, differentiation between the hydrogens cis and trans to the urea oxygen is apparent when interacting with the chloride anion. The ND/EPSR data suggests that the chloride ion is more likely to interact with the cis hydrogens while the *trans* hydrogens have a stabilizing effect in interacting with surrounding urea molecules. This same trend is observed by Doherty and Acevedo³⁵ using a refined FF fitted to ND/EPSR data. Alternatively, both AIMD⁶⁹ and MD⁵⁵ studies have observed the opposite phenomena, where sitesite RDFs show the trans hydrogens prefer interactions with the oxygen of surrounding urea molecules and the *cis* hydrogens bond with the chloride anion.

Consistent among all DES systems is that the majority of the cation-anion interactions occurred between the hydroxyl hydrogen of choline and chloride, while the anion-HBD

interactions were dominated by the hydrogen bonding groups, i.e., OH or NH. Zahn, Kirchner, and Mollenhauer³⁴ studied the influence of the HBD group with AIMD when the hydrogen bonding ability of the organic compound varied from urea to ethylene glycol and oxalic acid (Figure 11). Site-site RDFs showed that as the HBD shifted from an amine to hydroxyl and eventually a carboxylic acid, the anion-HBD interaction became stronger as indicated by the increase of the peak height as well as the decrease in the hydrogen bond distance. These results match the partial charge analysis performed using the Hirshfield-I charge partitioning scheme,¹⁷⁹ where charge transfer was much more significant to oxalic acid when compared to urea indicating a stronger hydrogen bond to the carboxylic acid group. Interestingly, Ullah et al.³⁷ found through MD simulations that the cation-anion interaction through the hydroxyl group of choline was still the dominating interaction when compared to the anion-HBD interaction between Cl⁻ and the carboxylate containing levulinic acid through site-site RDFs. This is likely due to the fact that oxalic acid has 2 sites where the chloride can hydrogen bond to as opposed to levulinic acid's single site.

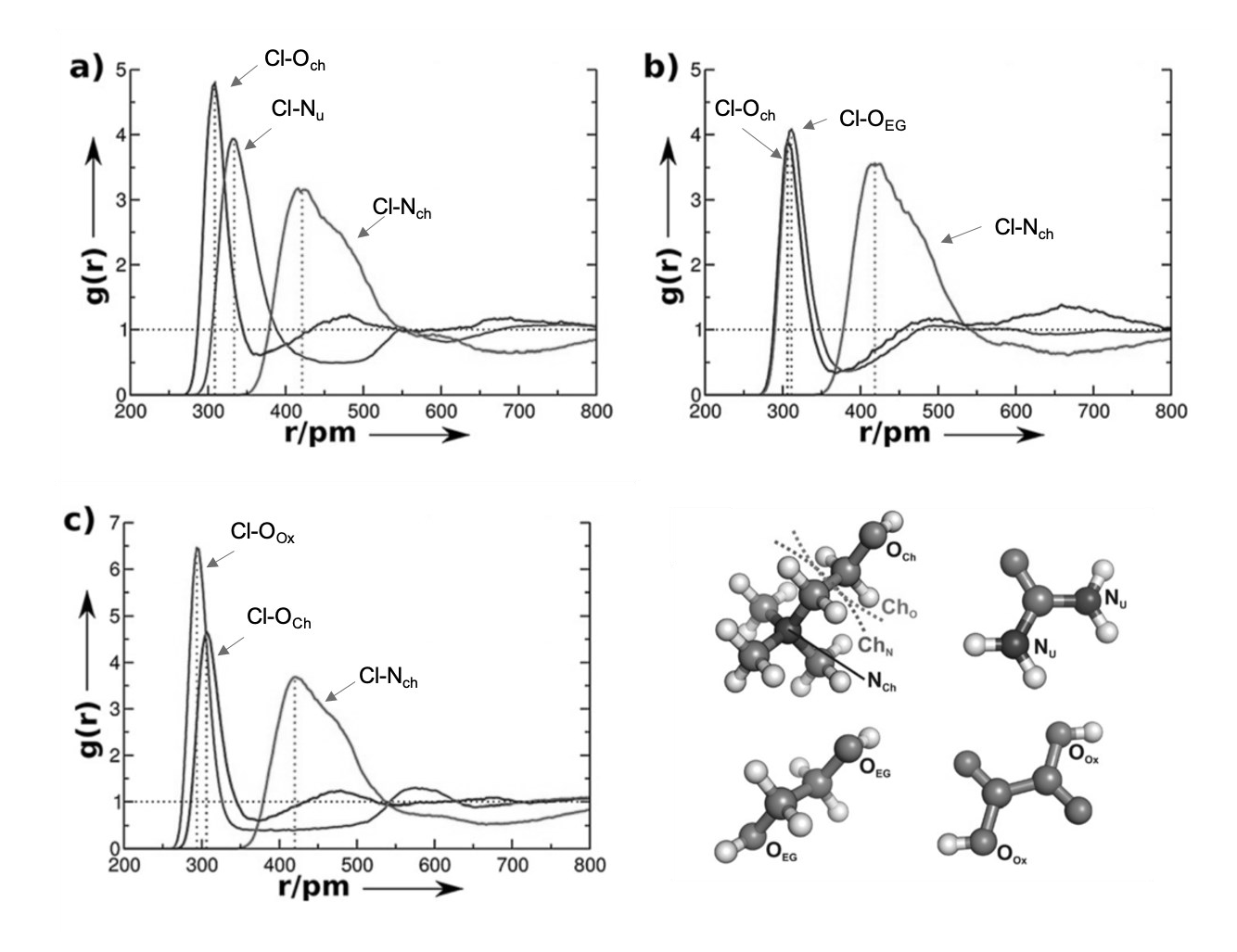


Figure 11. Radial distribution functions of selective interactions for (a) urea, (b) ethylene glycol, and (c) oxalic acid for choline chloride deep eutectic solvents. Adapted with labels from S. Zahn, B. Kirchner, D. Mollenhauer, *Chemphyschem*, 17, (21), 3354-3358 (2016). Charge Spreading in Deep Eutectic Solvents. This figure is licensed under the Creative Commons Attribution License.

The importance of the HBD is also showcased in the AIMD simulation of CCGly (1:1 molar ratio).¹⁷³ The strongest hydrogen bonding occurred between the OH groups of glycerol and Cl⁻, with the middle hydroxyl group being the most dominant while the peripheral OH groups hydrogen bonded with surrounding glycerol molecules. Considerable interactions were also observed between choline and glycerol through the hydroxyl groups of both moieties.

A comprehensive look into the structure of CCEtg (1:2 molar ratio) was recently studied by Zhang et al. where a combination of classical MD, AIMD, and neutron scattering experiments

were utilized.³⁶ The FF used by Perkins, Painter, and Colina³¹ was validated as a means to simulate the solvation environment by matching experimental neutron scattering structure factors, S(q), as well as computed S(q) through AIMD. RDFs were also compared to AIMD results at 400 K, and although there were discrepancies in peak height and position the overall structure features were captured. Further analysis was provided by the MD simulations, where calculated coordination number probabilities showed that on average, the chloride anion is surrounded by either 1 or 2 ethylene glycol molecules while the choline acts more as an observer. However, once the chloride anion interacts with the hydroxyl group of the choline, calculated hydrogen bond lifetimes and peak heights in the RDFs indicate that the cation-anion interaction is the strongest.

The use of non-polarizable FFs to recreate the site-site RDFs from AIMD data has proven to be a difficult task. While Doherty and Acevedo³⁵ were able to match RDFs of ND/EPSR data for CCU,⁴⁶ the systems CCEtg, CCOx, and CCGly were less successful. Mainberger et al.³² also reported problems in obtaining consistent site-site RDFs when comparing the GAFF and MMFF with scaled charges for CCEtg and CCLev. The source of this difficulty likely arises from the charge assignment given to each atom in the deep eutectic system. García, Atilhan, and Aparicio⁹⁴ found that using a variety of different charge partitioning schemes resulted in considerably different site-site RDFs for CCLev, and the atoms involved in hydrogen bonding were particularly sensitive to the charges assigned. Zahn, Kirchner, and Mollenhauer³⁴ suggested that depending on the HBD involved, different scaling factors should be used for non-polarizable FFs, and strongly recommended the use of polarizable FFs as an alternative.

7.2 Hydrogen Bond Analysis

In order to perform a hydrogen bond analysis, distances and angles characteristic to DES donors and acceptors need to be defined, e.g., donor-acceptor distances that range between 2.95

and 3.5 Å and X-H-Y angles ranging between a starting point of 130-150 degrees (Table 15). An additional criterion was proposed by Fetisov et al.⁴⁵ and Wernet et al.¹⁸⁰ who defined hydrogen bonding in DES through a CDF resembling an ellipsoid as shown in Figure 13. This ellipsoid criterion has also been applied to CCU in MD simulations by Doherty and Acevedo.³⁵

Table 15. List of Hydrogen Bond Criteria for Various DES Systems.

			Donor-Acceptor	X-H-Y
	System	Simulation Method	Distance (Å)	angle cutoff
Perkins, Painter and Colina ³¹	CCEtg	Molecular Dynamics	3.5	150
García, Atilhan and Aparicio ⁹⁴	CCLev	Molecular Dynamics	3.0	130
Ullah et al. ³⁷	CCLev	Molecular Dynamics	3.0	130
García, Atilhan and Aparicio ²⁰	CCGly	Molecular Dynamics	3.0	130
Perkins, Painter and Colina ³¹	CCGly	Molecular Dynamics	3.5	150
Turner and Holbrey ¹⁷⁶	CCGly	ND/EPSR	3.4	135
García, Atilhan and Aparicio ²⁰	CCMal	Molecular Dynamics	3.0	130
Perkins, Painter and Colina ³¹	CCMal	Molecular Dynamics	3.5	150
García, Atilhan and Aparicio ²⁰	CCU	Molecular Dynamics	3.0	130
Fetisov et al. ⁴⁵	CCU	First Principle Molecular Dynamics	3.5	150

Sun et al. ⁵⁴	CCU	Molecular Dynamics	2.95	150
Perkins, Painter and Colina ³¹	CCU	Molecular Dynamics	3.5	150

Using FPMD, Fetisov et al.⁴⁵ studied the effects of water in CCU (1:2 molar ratio). Hydrogen bonds were monitored with a combination of RDFs and CDFs, while also taking into account the average hydrogen bond types at each frame of the trajectory. For the pure CCU system, strong interactions between urea and chloride were observed through both the RDFs and average fraction of hydrogen bonds where the *trans* hydrogens of urea were found to prefer bonding with Cl⁻. Conversely, urea-urea hydrogen bonding of the NH--O=C type was primarily dominated by the cis hydrogens of urea. This same trend was also observed by Perkins, Painter, and Colina^{31,55} when the average fraction of hydrogen bonds were calculated between urea and chloride throughout an MD trajectory (Figure 12). Hydrogen bonds between choline and chloride were also observed through RDFs, however due to the 1:2 molar ratio the majority of hydrogen bonds involving Cl⁻ included interactions with urea. Raman spectroscopy and DFT calculations by Silva et al. also found hydrogen bonding between chloride and urea to be the most important interaction present in CCU.¹⁸¹ When water is introduced into the system, Cl-urea interactions become weaker as water begins to form new intermolecular interactions with each DES component. Figure 13 illustrates the CDFs of the X-H-Y interactions between choline, urea, water, and Cl⁻ that showcase the ellipsoid criterion that has been proposed by Wernet et al. 180 The ellipsoid criterion has also been used by Doherty and Acevedo³⁵ who used a non-polarizable FF to study a pure CCU (1:2 molar ratio) system. Shown in Figure 14, strong hydrogen bonding is evident between the cholinechloride and urea-chloride, whereas choline and urea rarely interacted through hydrogen bonding.

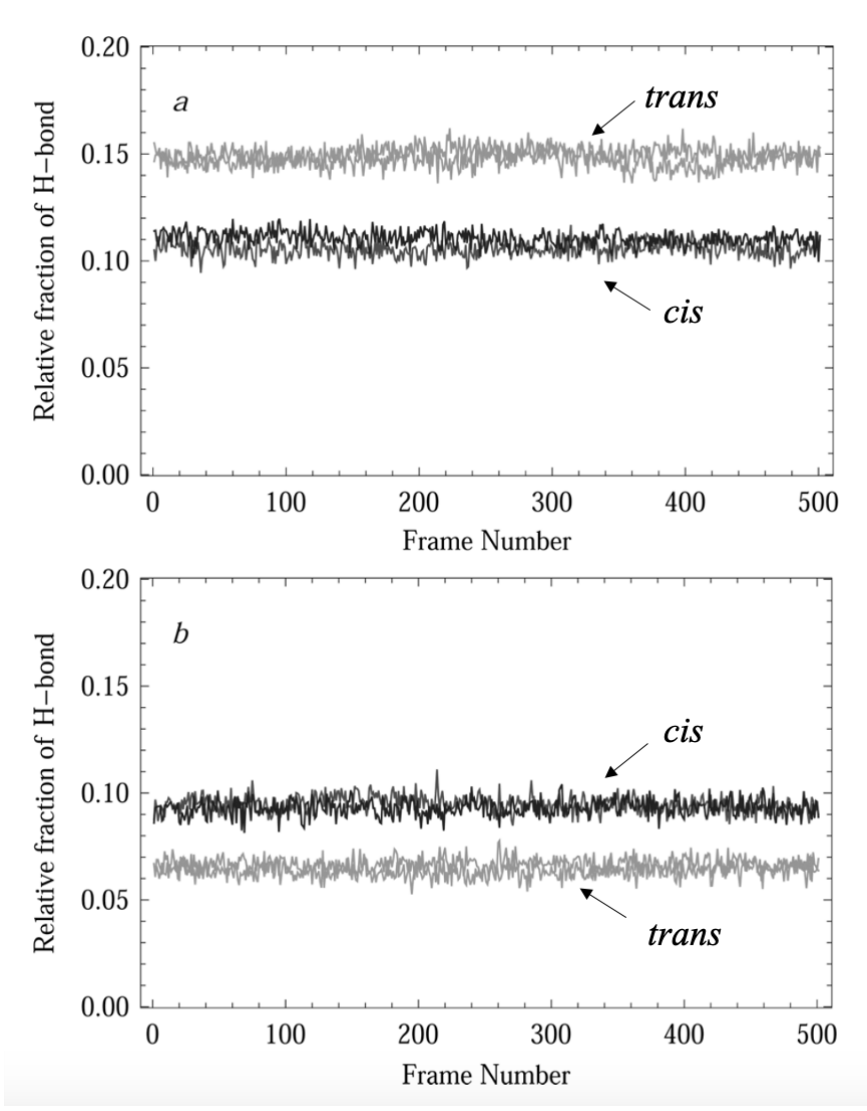


Figure 12. Average fraction of H-bonds of the type (a) NH--O=C and (b) NH--Cl⁻. Adapted with permission from S. L. Perkins, P. Painter, C. M. Colina, *J. Phys. Chem. B*, **117**, (35), 10250-10260 (2013). Molecular Dynamic Simulations and Vibrational Analysis of an Ionic Liquid Analogue. Copyright 2013 American Chemical Society.

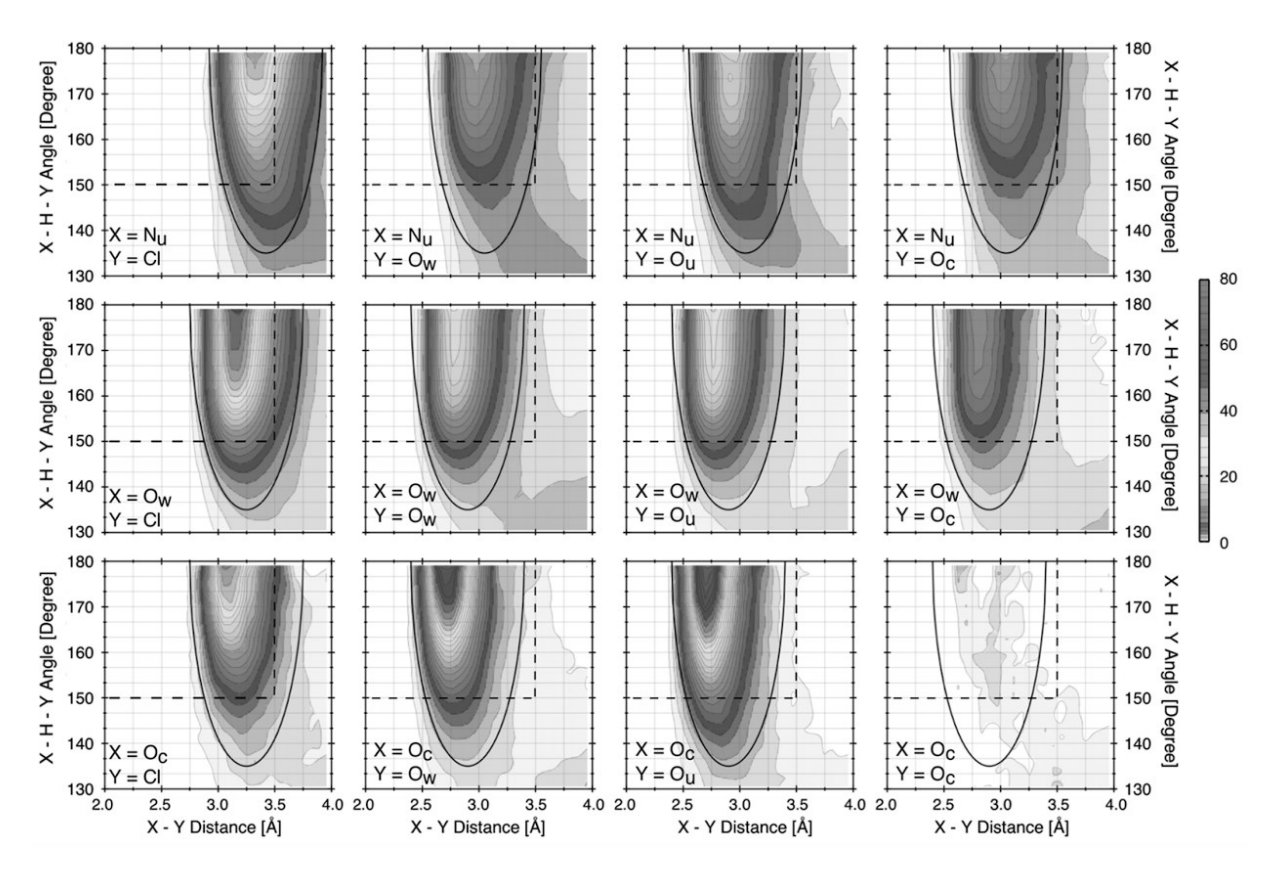


Figure 13. CDF to examine hydrogen bonding interactions in the aqueous reline system. Dashed lines show rectangular boundaries for the hydrogen bond criteria of Perkins, Painter and Colina⁵⁵ while the solid lines show the elliptical boundaries as defined by Wernet et al. ¹⁸⁰ Adapted from E. O. Fetisov, D. B. Harwood, I. F. W. Kuo, S. E. E. Warrag, M. C. Kroon, C. J. Peters, J. I. Siepmann, *J. Phys. Chem. B*, **122**, (3), 1245-1254 (2018). First-Principles Molecular Dynamics Study of a Deep Eutectic Solvent: Choline Chloride/Urea and Its Mixture with Water. (https://pubs.acs.org/doi/10.1021/acs.jpcb.7b10422). Further permission related to this material should be directed to the ACS.

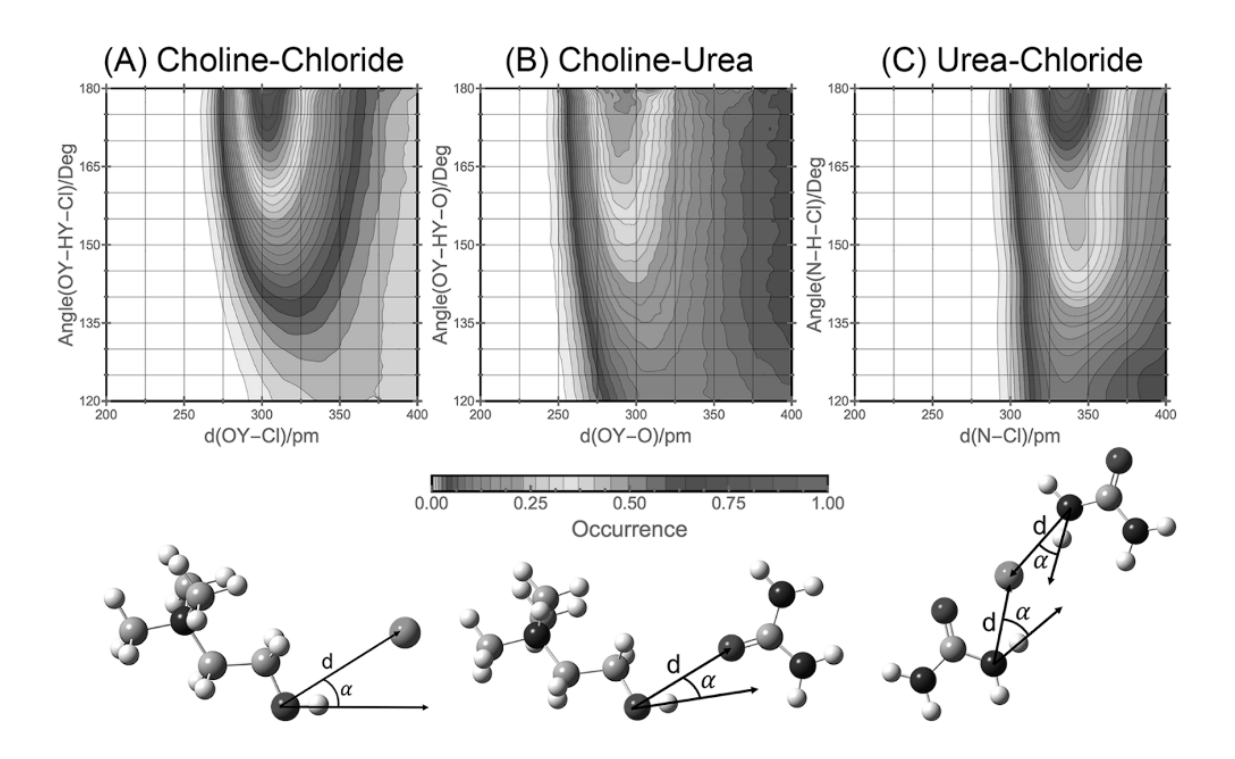


Figure 14. CDFs for selected interactions in reline. Reprint with permission from B. Doherty, O. Acevedo, *J. Phys. Chem. B*, **122**, (43), 9982-9993 (2018). OPLS Force Field for Choline Chloride-Based Deep Eutectic Solvents. Copyright 2018 American Chemical Society.

Perkins, Painter, and Colina^{31,55} also studied the systems CCEtG (1:2 molar ratio), CCGly (1:2 molar ratio), and CCMal (1:2 molar ratio) using the same methods as their CCU (1:2 molar ratio) simulations. Following the relative contributions of hydrogen bonds for a given hydrogen bond type, it was observed that the largest fraction of hydrogen bonds were between the HBD and the anion (see Figure 14). CCEtG and CCGly exhibited similar trends with the exception of HBD-HBD interactions due to the extra hydroxyl group of glyceline resulting in a higher fraction. Of these systems, CCMal has the highest viscosity, perhaps a consequence of the strong cation-anion and HBD-anion interactions present, which indicates a very stable hydrogen bond network and limited mobility within the system.

Additional hydrogen bond analysis can be observed through residence times calculated by the following autocorrelation functional (equation 34).

$$\tau_{HB} = 2 \cdot \int \frac{\langle h_i(t)h_i(0)\rangle}{\langle h_i(0)\rangle} dt$$
 [34]

Where h_i(0) and h_i(t) are hydrogen bonds at time 0 or time *t* when given a set criteria. Zahn focused on CCU (1:2 molar ratio) using AIMD⁶⁹ and found that the cation-anion hydrogen bonding occurring between the hydroxyl hydrogen and chloride contributed the longest hydrogen bond residence time of 10.3 ps. Interestingly, the second longest residence time was also between the hydroxyl hydrogen of choline and the oxygen of urea with a time of 6.4 ps. These results contradicted reports by Hammond, Bowron, and Edler⁴⁶ where the rotation of the OH group in choline was dynamic thus preventing rigid hydrogen bonding. Instead, it was discovered that choline preferred the *gauche* conformation, leading to longer residence times between the cation and both anion and HBD. Sun et al.⁵⁴ also discovered the longest hydrogen bonding between urea and chloride was about 5 times shorter (2.4 ps).

CCLev (1:2 molar ratio) hydrogen bond life-times were also monitored by García, Atilhan, and Aparicio⁹⁴ and Ullah et al.³⁷ through MD simulations. Ullah extended the hydrogen bonding criteria to the second solvation shell at a maximum distance of 6.0 Å, and found that the cationanion (Hc-Cl) interaction had the longest life-time followed by cation-HBD (H1-Oc) and anion-HBD (H1-O11). All other hydrogen bonds in the system were similar and ranged between 35-45 ps (Figure 15). García, Atilhan, and Aparicio found that the hydrogen bond life-times were highly dependent on the charge partitioning scheme to assign charges in the MD simulation.⁹⁴ When considering the top performing charge partitions however, it was discovered that the cation-anion interaction still remained as the longest hydrogen bond life-time.

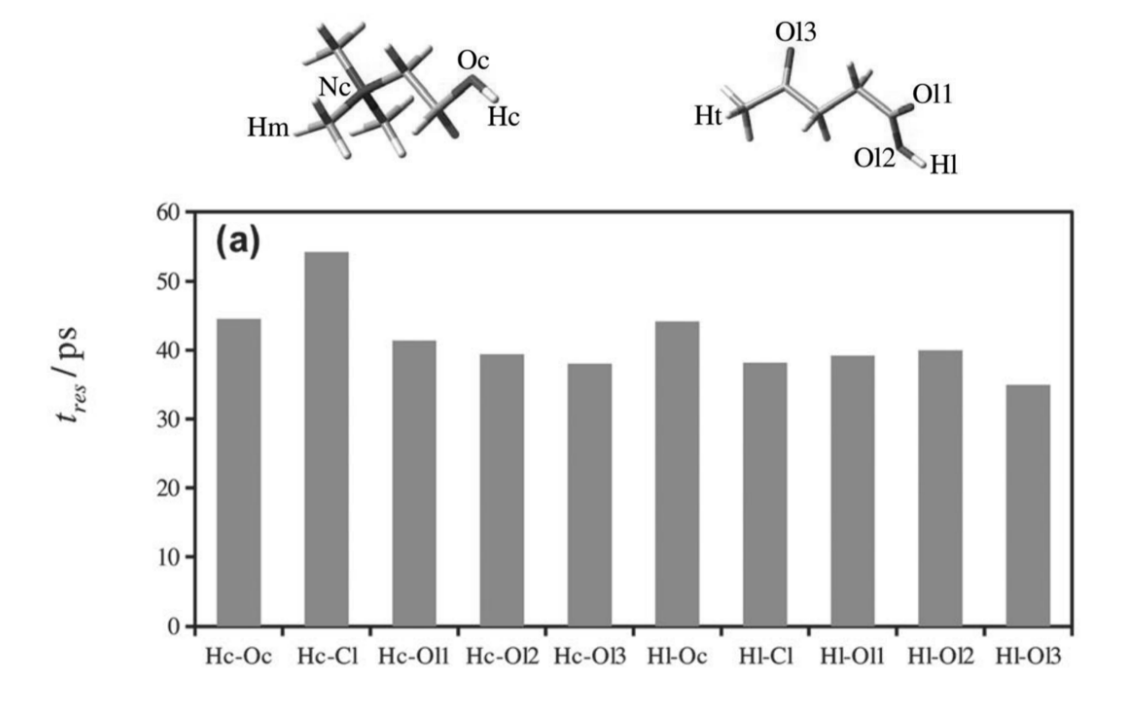


Figure 15. Hydrogen bond life-times, t_{res}, for selected atoms in CCLev system. R. Ullah, M. Atilhan, B. Anaya, M. Khraisheh, G. García, A. ElKhattat, M. Tariq, S. Aparicio, *Phys. Chem. Chem. Phys.*, **17**, (32), 20941-20960 (2015). A Detailed Study of Cholinium Chloride and Levulinic Acid Deep Eutectic Solvent System for CO₂ Capture Via Experimental and Molecular Simulation Approaches. Published by the PCCP Owner Societies.

Hydrogen bond lifetimes were also calculated by Zhang et al.³⁶ for CCEtg (1:2 molar ratio) using the same FF parameters as Perkins, Painter, and Colina.³¹ Interactions between chloride and choline were found to have considerably longer lifetimes compared to the studies mentioned above, with the hydroxyl group of Ch^+ and Cl^- having a lifetime of 1462.4 ± 56.0 ps. The second longest lifetime calculated was between ethylene glycol and chloride with a value of 972.4 ± 27.9 ps. All other hydrogen bond interactions fell into the same range, i.e., 24.1-80.5 ps, as the previous studies mentioned. These results match the same trend seen in other systems, where the cationanion interactions provide the longest lifetimes. Further detail into the dynamics of the CCEtg system was also provided by fitting of the molecular dipole moment correlation function for choline and ethylene glycol to the fractional kinetic Mittag-Leffler model.¹⁸² By using the fractional kinetic model, the dipole relaxation can be separated into a fast mode and slow mode.

The fast time process calculated was attributed to the weaker hydrogen bond interactions between choline and ethylene glycol which matches the hydrogen bond lifetimes, while the slower modes were partially attributed to the longer hydrogen bond lifetimes in the interactions with nearby chlorides. These results further connect the considerable influence that the hydrogen bond network has upon system dynamics in DESs.

7.3 Spatial Distribution Functions

General structuring of DES systems have been monitored with the help of spatial distribution functions (SDFs) which provide a three-dimensional visualization of the distribution of the nearest neighbor to a reference molecule. Systems studied include CCU (1:2 molar ratio), 20,35,45-46,69,178 CCLev (1:2 molar ratio), 37,94 CCEtg (1:2 molar ratio), CCGly (1:2 molar ratio), 35,176 CCPhe (1:2 and 1:3 molar ratio), CCMal (1:2 molar ratio), and CCOx (1:2 molar ratio). As expected from the RDFs, the chlorine anion resided near the hydrogen bond donating groups of both the cation and HBD, while the cation-HBD interactions resided in the remaining space surrounding the anion (Figure 16). Maintaining this ordering via favorable electrostatic interactions has been suggested to be the driving force for deep eutectic solvent formation. 46

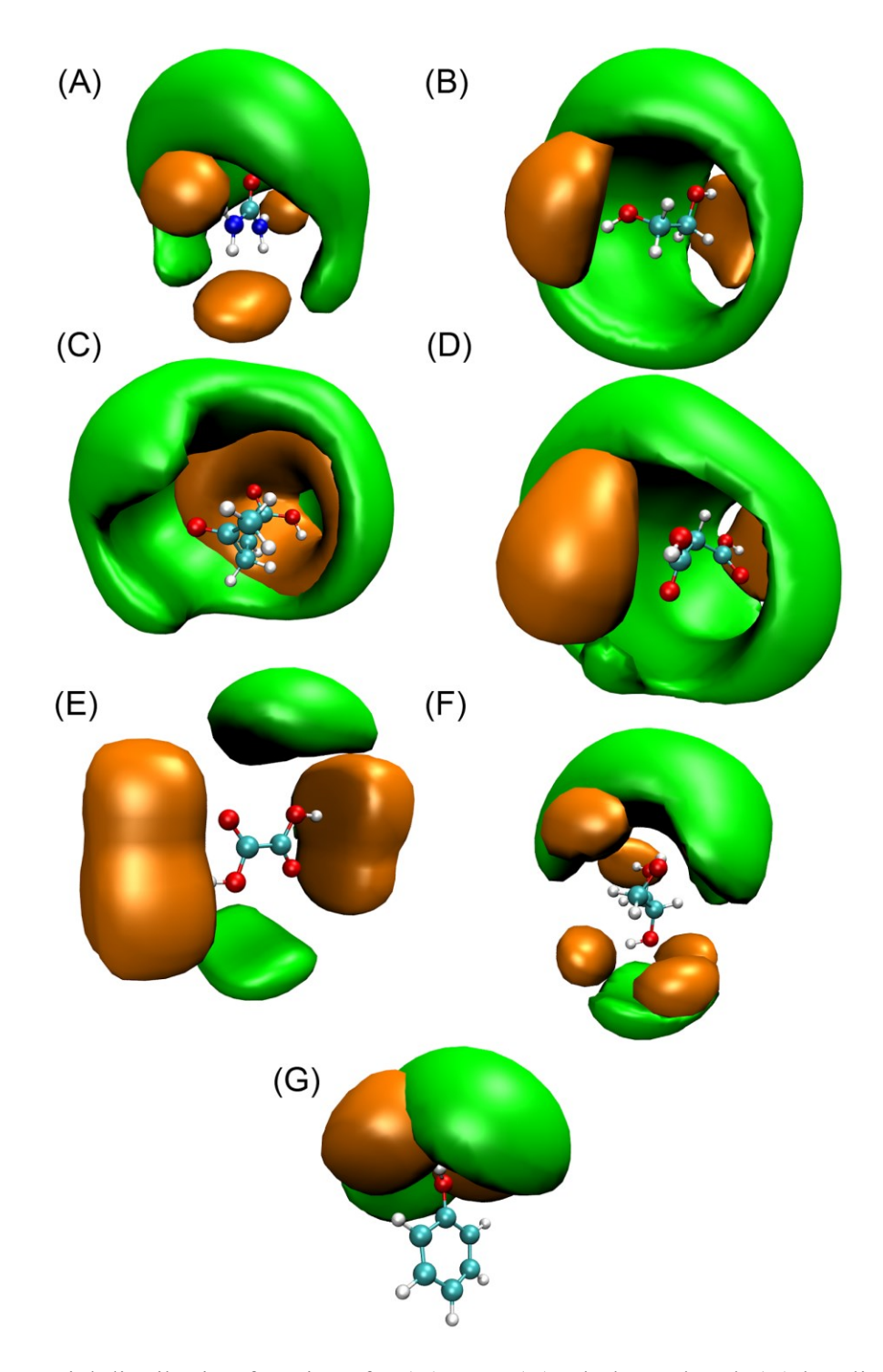


Figure 16. Spatial distribution functions for (A) urea, (B) ethylene glycol, (C) levulinic acid, (D) malonic acid, (E) oxalic acid, (F) glycerol, (G) phenol in choline chloride deep eutectic solvents. Orange denotes the position of the chloride anion, and the green depicts the choline cation. Reprint with permission from B. Doherty, O. Acevedo, *J. Phys. Chem. B*, **122**, (43), 9982-9993 (2018). OPLS Force Field for Choline Chloride-Based Deep Eutectic Solvents. Copyright 2018 American Chemical Society.

8 Application of DES through Simulation

8.1 Gas Sorption Studies on DES

The rapid increase of atmospheric pollutants through the combustion of fossil fuels has been linked to health effects as well as climate change, leading to the need for environmentally friendly gas capturing techniques. 183 DESs have been proposed as carbon capture sorbents due to their tunability and natural affinity for gas compounds such as CO₂. ^{12,57,184} Computational studies have been performed for the choline chloride phenylacetic acid system to investigate the binding modes between the DES components and CO₂ at both the vacuum surface and bulk liquid phase. ¹⁶³ Through DFT calculations, CO₂ was found to interact strongly with the COOH group of phenylacetic acid as well as Cl, while the choline cation stabilized the chloride anion through hydrogen bonding with its hydroxyl group. This binding motif matched previous DFT studies by the same group for CCLev (1:2 molar ratio) and CO₂.³⁷ In the bulk phase, MD simulations were performed at the DES interface where flue gas molecules (N2, H2O, CO2, and O2) were placed to fill the vacuum to monitor diffusion of each gas into the liquid. 163 Interestingly, CO₂ absorption was found to occur with very little volume expansion indicating minor rearrangement of the DES components was necessary to maintain the hydrogen bond network. Additionally, water was readily absorbed into the first layer and hindered the diffusion of CO₂ into the bulk region; future designs of DESs for CO₂ capture should take this observation into consideration.

The DES-based capture of SO₂ has also been studied both experimentally and computationally. Experimental studies for the eutectic mixtures of choline chloride with glycerol, ¹⁸⁵ levulinic acid, ¹⁸⁶ urea, thiourea, malonic acid, and ethylene glycol ¹⁸⁷ have all resulted in absorption capacities similar to ILs where the absorption process is reversible and showed no signs of decreasing capacity throughout the absorption-desorption cycle. Interactions between SO₂

and CCGly (1:1 molar ratio) have been studied using DFT¹⁸⁸ as well as AIMD¹⁷³ where both studies confirmed that the chloride anion binds to SO₂ which disrupted the OH-anion interactions with choline and glycerol causing the system to become more fluid. Weaker interactions between cation-glycerol and glycerol-glycerol were also disrupted with the addition of SO₂ due to dispersion-like interactions between the gas and the nonpolar groups of choline and glycerol.¹⁷³ Although these interactions are not as significant as the cation-anion and glycerol-anion interactions, Korotkevich et al.¹⁷³ suggested that future design of DESs tuned for SO₂ absorption may be able take advantage of this interaction by expanding the nonpolar regions.

8.2 DES interactions at Metal Surfaces

An attractive property that DESs have over traditional organic solvents is their high conductivity that can lead to catalytic behavior when involved in the electrodeposition of metals. $^{24,26-28,189-190}$ Understanding how DESs nucleate at the surface of metals is crucial for the design of DES-based materials and technology. Thus, studies have emerged focusing upon how DES species orient themselves around metal surfaces. $^{191-192}$ Experimentally, CCEtg has been studied on the surface of glassy carbon (GC) with the use of polarization modulation infrared reflection absorption spectroscopy. 193 This spectroscopic study suggested that decreasing the surface potential to -0.6 V caused the choline cation to absorb vertically to the surface by means of the N⁺(CH₃)₃ group, which resulted in a decrease of the molecular dipole moment. Conversely, when the potential was increased to E > +0.4 V, the choline cation was replaced by the chloride anion which formed an adlayer on the GC. In this case, the choline cation was still vertically oriented to maximize the electrostatic interaction with the anion. The electrodeposition of Cu²⁺ onto GC and Pt surfaces has also been investigated in a separate study by Vukmirovic, Adzic, and Akolkar. 24 Cyclic voltammetry studies revealed that nucleation rates were sluggish on GC

electrodes in relation to Pt, and is likely due to the nucleation structure on each surface. Although deposition of Cu²⁺ onto Pt in the CCEtg solvent medium exhibited faster kinetics relative to GC, a comparative study was performed replacing CCEtg with a 3M aqueous solution of NaCl to increase the chloride concentration that resulted in faster mass and charge transfer. This study highlights the importance that although DESs provide a large reduction potential that will ultimately increase cell voltage and energy density in energy storage devices, the kinetic limitations of charge and mass transfer at the electrode surface must first be overcome to compete with current aqueous electrolytes.

The absorption of choline into the (100) surface of a metal was also studied for CCLev on Ag, Al, and Pt using MD methods.⁵⁶ Two distinct absorption layers within 10 Å of the uncharged surfaces was computed for all 3 metals, where the first layer is primarily composed of levulinic acid and choline cations oriented in a parallel fashion to the surface and the second consisted of excess chloride anions and levulinic acid molecules. Within the absorbed layer, diffusion rates of the ions were significantly lower than that of the bulk solution further emphasizing the strong interactions present between the DES and the metal surface.

8.3 Proteins in DES

DESs have been utilized as cosolvents in enzymatic catalysis for completely green chemical processes. For example, DES systems have been shown to drive regioselectivity when combined with the potato epoxide hydrolase StEH1 for the hydrolysis of chiral (1,2)-trans-2-methylstyrene oxide.¹⁹⁴ Additionally, 8 different DES systems have been shown to stabilize Candida antarctica lipase B (CALB) and C. antarctica lipase A.¹⁹⁵ The DESs/enzymes provided a 30% enhancement to the production yield of α -monobenzoate glycerol through the esterification between benzoate and glycerol compared to commercially available biocatalysts.¹⁹⁶ Interestingly,

CALB has been shown to lose its activity by nearly 70% when pretreated with 10M urea due to protein denaturing. However, when pretreated with CCU, the activity loss was <1%. 197 The origin of why CALB remained active in a solvent that contained 66% urea was investigated by Monhemi et al. 39 through classical MD simulations. The CALB in an 8 M urea simulation found that urea molecules rapidly diffused into the α -Helix5 active site disrupting hydrogen bonding, which resulted in a denaturing process. In the CCU environment the urea molecules preferred to interact with the choline and Cl ions, allowing the α -Helix5 site to retain its intramolecular hydrogen bonds and remain active. Enzyme stability was also observed in the CCU mixture as the chloride anions formed hydrogen bonds with surface residues of the enzyme leading to the phenomenon known as "enzyme immobilization." This technique has also been reported for CALB in CCGly where no loss in enzyme activity was observed for up to 14 days. 196 The combination of DESs and biocatalysts is a rapidly developing and exciting field. However, many unanswered molecular level questions remain necessitating the future development and application of novel computational tools.

9. Summary

Provided in this chapter is a comprehensive overview of DESs and the methods used to study these systems through simulation. The majority of simulations have been performed on Type III DESs that contain choline chloride as the salt and a corresponding organic HBD at specific molar ratios. Ideally, due to the strong polarization present in each of the systems, *ab initio* methods such as DFT, FPMD, and AIMD would be utilized because of their explicit treatment of polarization and many body effects. While *ab initio* methods can provide valuable information such as solvation structure, charge transfer, and at times reactivity, limitations in their trajectory lengths and system sizes call for more computationally affordable methods. Considerable efforts

in the development of non-polarizable FFs for classical MD simulations have been reported that have provided in depth analysis into various DES properties such as density, thermal expansion coefficient, surface tension, heat capacity, enthalpy of vaporization, isothermal compressibility, viscosity, and self-diffusion coefficients. Due to the importance of parameter validation, this chapter provided an overview of how prominent DES FFs performed in reproducing bulk properties and liquid structures measured experimentally or computed using higher-theory *ab initio* methods.

Generally, most published non-polarizable FFs performed well in reproducing the bulk properties of DESs as outlined in Table 5. Significant improvement was noted when scaling the charges for the various DES systems to mimic charge transfer effects and polarization. In most cases, a uniform scaling factor between 0.7 and 0.9 was chosen due to reported success in previous applications to ILs. Alternatively, some groups have developed system specific charge models based on DFT calculation of small DES clusters or charge analysis from AIMD simulations. Success in reproducing bulk properties in MD simulations has also elucidated the structureproperty relationship of these solvents by highlighting the importance of the hydrogen bond network that is formed between each component. The hydrogen bond network greatly influences properties such as viscosity and diffusion coefficients, which can limit the application of some DESs as alternative solvents. A major challenge for non-polarizable FFs was the poor reproduction of self-diffusion coefficients; explicit treatment of polarization effects may be required to improve agreement. Additionally, a drawback of employing a scaled charge model is the treatment of additives that may alter the magnitude of charge transfer. Due to these concerns, a general and completely transferable non-polarizable FF may be difficult or even impossible to develop for DESs.

10. Acknowledgments

Gratitude is expressed to the National Science Foundation (CHE-1562205 for B.D. and O.A., SI2-1613155 for C.M.C and S.J.R.) and the University of Florida Preeminence Initiative for support of this research.

11. References

- 1. C. J. Clarke, W.-C. Tu, O. Levers, A. Bröhl, J. P. Hallett, *Chem. Rev.*, **118**, 747-800 (2018). Green and Sustainable Solvents in Chemical Processes.
- 2. D. V. Wagle, H. Zhao, G. A. Baker, *Acc. Chem. Res.*, **47**, 2299-2308 (2014). Deep Eutectic Solvents: Sustainable Media for Nanoscale and Functional Materials.
- 3. R. L. Vekariya, *J. Mol. Liq.*, **227**, 44-60 (2017). A Review of Ionic Liquids: Applications Towards Catalytic Organic Transformations.
- 4. M. Espino, M. de los Ángeles Fernández, F. J. V. Gomez, M. F. Silva, *Trends Analyt. Chem.*, **76**, 126-136 (2016). Natural Designer Solvents for Greening Analytical Chemistry.
- 5. M. C. Bubalo, S. Vidović, I. R. Redovniković, S. Jokić, *J. Chem. Technol. Biotechnol.*, **90**, 1631-1639 (2015). Green Solvents for Green Technologies.
- 6. H. Zhao, G. A. Baker, *J. Chem. Technol. Biotechnol.*, **88**, 3-12 (2012). Ionic Liquids and Deep Eutectic Solvents for Biodiesel Synthesis: A Review.
- 7. J. H. Clark, H. F. Sneddon, L. Summerton, L. C. Jones, *Green and Sustainable Medicinal Chemistry*, Royal Society of Chemistry, 2016.
- 8. Y. Medina-Gonzalez, S. Camy, J.-S. Condoret, *ACS Sustain. Chem. Eng.*, **2**, 2623-2636 (2014). Scco2/Green Solvents: Biphasic Promising Systems for Cleaner Chemicals Manufacturing.
- 9. J. I. García, H. García-Marín, E. Pires, *Green Chem.*, **16**, 1007-1033 (2014). Glycerol Based Solvents: Synthesis, Properties and Applications.
- 10. E. Knipping, C. Aucher, G. Guirado, L. Aubouy, *New J. Chem.*, **42**, 4693-4699 (2018). Room Temperature Ionic Liquids Versus Organic Solvents as Lithium–Oxygen Battery Electrolytes.
- 11. A. P. Abbott, G. Capper, D. L. Davies, H. L. Munro, R. K. Rasheed, V. Tambyrajah, *Chem. Commun.*, 2010-2011 (2001). Preparation of Novel, Moisture-Stable, Lewis-Acidic Ionic Liquids Containing Quaternary Ammonium Salts with Functional Side Chains.

- 12. A. Paiva, R. Craveiro, I. Aroso, M. Martins, R. L. Reis, A. R. C. Duarte, *ACS Sustain. Chem. Eng.*, **2**, 1063-1071 (2014). Natural Deep Eutectic Solvents Solvents for the 21st Century.
- 13. E. L. Smith, A. P. Abbott, K. S. Ryder, *Chem. Rev.*, **114**, 11060-11082 (2014). Deep Eutectic Solvents (Dess) and Their Applications.
- 14. T. Altamash, M. S. Nasser, Y. Elhamarnah, M. Magzoub, R. Ullah, B. Anaya, S. Aparicio, M. Atilhan, *ChemistrySelect*, **2**, 7278-7295 (2017). Gas Solubility and Rheological Behavior of Natural Deep Eutectic Solvents (Nades) Via Combined Experimental and Molecular Simulation Techniques.
- 15. D. V. Wagle, L. Adhikari, G. A. Baker, *Fluid Ph. Equilibria*, **448**, 50-58 (2017). Computational Perspectives on Structure, Dynamics, Gas Sorption, and Bio-Interactions in Deep Eutectic Solvents.
- 16. P. Liu, J.-W. Hao, L.-P. Mo, Z.-H. Zhang, *RSC Adv.*, **5**, 48675-48704 (2015). Recent Advances in the Application of Deep Eutectic Solvents as Sustainable Media as Well as Catalysts in Organic Reactions.
- 17. D. Z. Troter, Z. B. Todorović, D. R. Đokić-Stojanović, O. S. Stamenković, V. B. Veljković, *Renewable Sustainable Energy Rev.*, **61**, 473-500 (2016). Application of Ionic Liquids and Deep Eutectic Solvents in Biodiesel Production: A Review.
- 18. L. Wei, Y.-J. Fan, H.-H. Wang, N. Tian, Z.-Y. Zhou, S.-G. Sun, *Electrochim. Acta*, **76**, 468-474 (2012). Electrochemically Shape-Controlled Synthesis in Deep Eutectic Solvents of Pt Nanoflowers with Enhanced Activity for Ethanol Oxidation.
- 19. S. Sarmad, J.-P. Mikkola, X. Ji, *ChemSusChem*, **10**, 324-352 (2017). Carbon Dioxide Capture with Ionic Liquids and Deep Eutectic Solvents: A New Generation of Sorbents.
- 20. G. García, M. Atilhan, S. Aparicio, *J. Phys. Chem. C*, **119**, 21413-21425 (2015). Interfacial Properties of Deep Eutectic Solvents Regarding to Co2 Capture.
- 21. A. P. Abbott, A. Ballantyne, R. C. Harris, J. A. Juma, K. S. Ryder, G. Forrest, *Electrochim. Acta*, **176**, 718-726 (2015). A Comparative Study of Nickel Electrodeposition Using Deep Eutectic Solvents and Aqueous Solutions.
- 22. A. J. Goddard, R. C. Harris, S. Saleem, M. Azam, C. Hood, D. Clark, J. Satchwell, K. S. Ryder, *Transactions of the IMF*, **95**, 137-146 (2017). Electropolishing and Electrolytic Etching of Ni-Based Hip Consolidated Aerospace Forms: A Comparison between Deep Eutectic Solvents and Aqueous Electrolytes.
- 23. C. Li, J. Zhang, Z. Li, J. Yin, Y. Cui, Y. Liu, G. Yang, *Green Chem.*, **18**, 3789-3795 (2016). Extraction Desulfurization of Fuels with 'Metal Ions' Based Deep Eutectic Solvents (Mdess).
- 24. M. B. Vukmirovic, R. R. Adzic, R. Akolkar, *J. Phys. Chem. B*, **124**, 5465-5475 (2020). Copper Electrodeposition from Deep Eutectic Solvents-Voltammetric Studies Providing Insights into the Role of Substrate: Platinum Vs Glassy Carbon.

- 25. X. Shen, N. Sinclair, J. Wainright, R. Akolkar, R. F. Savinell, *J. Electrochem. Soc.*, **167**, 086509 (2020). Evaluating and Developing a Reliable Reference Electrode for Choline Chloride Based Deep Eutectic Solvents.
- 26. N. A. Shaheen, I. Mahesh, M. B. Vukmirovic, R. Akolkar, *Electrochem. commun.*, **115**, 106721 (2020). Hysteresis Effects and Roughness Suppression Efficacy of Polyethylenimine Additive in Cu Electrodeposition in Ethaline.
- 27. D. Shen, M. B. Vukmirovic, R. Akolkar, *J. Electrochem. Soc.*, **166**, E526-E532 (2019). Understanding the Role of Complexation in the Charge-Transfer Kinetics of the Cu2 E ↔ Cu1 Redox Reaction in Ethaline Deep Eutectic Solvent.
- 28. D. Shen, K. Steinberg, R. Akolkar, *J. Electrochem. Soc.*, **165**, E808-E815 (2018). Avoiding Pitfalls in the Determination of Reliable Electrochemical Kinetics Parameters for the $Cu2 \rightarrow Cu1$ Reduction Reaction in Deep Eutectic Solvents.
- 29. I. I. I. Alkhatib, D. Bahamon, F. Llovell, M. R. M. Abu-Zahra, L. F. Vega, *J. Mol. Liq.*, **298**, 112183 (2020). Perspectives and Guidelines on Thermodynamic Modelling of Deep Eutectic Solvents.
- 30. G. García, M. Atilhan, S. Aparicio, *Chem. Phys. Lett.*, **634**, 151-155 (2015). An Approach for the Rationalization of Melting Temperature for Deep Eutectic Solvents from Dft.
- 31. S. L. Perkins, P. Painter, C. M. Colina, *J. Chem. Eng. Data*, **59**, 3652-3662 (2014). Experimental and Computational Studies of Choline Chloride-Based Deep Eutectic Solvents.
- 32. S. Mainberger, M. Kindlein, F. Bezold, E. Elts, M. Minceva, H. Briesen, *Mol. Phys.*, **115**, 1309-1321 (2017). Deep Eutectic Solvent Formation: A Structural View Using Molecular Dynamics Simulations with Classical Force Fields.
- 33. C. R. Ashworth, R. P. Matthews, T. Welton, P. A. Hunt, *Phys. Chem. Chem. Phys.*, **18**, 18145-18160 (2016). Doubly Ionic Hydrogen Bond Interactions within the Choline Chloride–Urea Deep Eutectic Solvent.
- 34. S. Zahn, B. Kirchner, D. Mollenhauer, *Chemphyschem*, **17**, 3354-3358 (2016). Charge Spreading in Deep Eutectic Solvents.
- 35. B. Doherty, O. Acevedo, *J. Phys. Chem. B*, **122**, 9982-9993 (2018). Opls Force Field for Choline Chloride-Based Deep Eutectic Solvents.
- 36. Y. Zhang, D. Poe, L. Heroux, H. Squire, B. W. Doherty, Z. Long, M. Dadmun, B. Gurkan, M. E. Tuckerman, E. J. Maginn, *J. Phys. Chem. B*, **124**, 5251-5264 (2020). Liquid Structure and Transport Properties of the Deep Eutectic Solvent Ethaline.
- 37. R. Ullah, M. Atilhan, B. Anaya, M. Khraisheh, G. García, A. ElKhattat, M. Tariq, S. Aparicio, *Phys. Chem. Chem. Phys.*, **17**, 20941-20960 (2015). A Detailed Study of Cholinium Chloride and Levulinic Acid Deep Eutectic Solvent System for Co2 Capture Via Experimental and Molecular Simulation Approaches.

- 38. J. M. Rimsza, L. René Corrales, *Comput. Theor. Chem.*, **987**, 57-61 (2012). Adsorption Complexes of Copper and Copper Oxide in the Deep Eutectic Solvent 2:1 Urea—Choline Chloride.
- 39. H. Monhemi, M. R. Housaindokht, A. A. Moosavi-Movahedi, M. R. Bozorgmehr, *Phys. Chem. Chem. Phys.*, **16**, 14882-14893 (2014). How a Protein Can Remain Stable in a Solvent with High Content of Urea: Insights from Molecular Dynamics Simulation of Candida Antarctica Lipase B in Urea: Choline Chloride Deep Eutectic Solvent.
- 40. A. P. Abbott, G. Capper, D. L. Davies, R. K. Rasheed, V. Tambyrajah, *Chem. Commun.*, 70-71 (2003). Novel Solvent Properties of Choline Chloride/Urea Mixtures.
- 41. Q. Zhang, K. De Oliveira Vigier, S. Royer, F. Jérôme, *Chem. Soc. Rev.*, **41**, 7108-7146 (2012). Deep Eutectic Solvents: Syntheses, Properties and Applications.
- 42. A. P. Abbott, D. Boothby, G. Capper, D. L. Davies, R. K. Rasheed, *J. Am. Chem. Soc.*, **126**, 9142-9147 (2004). Deep Eutectic Solvents Formed between Choline Chloride and Carboxylic Acids: Versatile Alternatives to Ionic Liquids.
- 43. Y. Hou, Y. Gu, S. Zhang, F. Yang, H. Ding, Y. Shan, *J. Mol. Liq.*, **143**, 154-159 (2008). Novel Binary Eutectic Mixtures Based on Imidazole.
- 44. C. D'Agostino, R. C. Harris, A. P. Abbott, L. F. Gladden, M. D. Mantle, *Phys. Chem. Chem. Phys.*, **13**, 21383-21391 (2011). Molecular Motion and Ion Diffusion in Choline Chloride Based Deep Eutectic Solvents Studied by 1h Pulsed Field Gradient Nmr Spectroscopy.
- 45. E. O. Fetisov, D. B. Harwood, I. F. W. Kuo, S. E. E. Warrag, M. C. Kroon, C. J. Peters, J. I. Siepmann, *J. Phys. Chem. B*, **122**, 1245-1254 (2018). First-Principles Molecular Dynamics Study of a Deep Eutectic Solvent: Choline Chloride/Urea and Its Mixture with Water.
- 46. O. S. Hammond, D. T. Bowron, K. J. Edler, *Green Chem.*, **18**, 2736-2744 (2016). Liquid Structure of the Choline Chloride-Urea Deep Eutectic Solvent (Reline) from Neutron Diffraction and Atomistic Modelling.
- 47. C. Ruß, B. König, *Green Chem.*, **14**, 2969 (2012). Low Melting Mixtures in Organic Synthesis an Alternative to Ionic Liquids?
- 48. D. Carriazo, M. C. Serrano, M. C. Gutierrez, M. L. Ferrer, F. del Monte, *ChemInform*, **43**, no-no (2012). Cheminform Abstract: Deep-Eutectic Solvents Playing Multiple Roles in the Synthesis of Polymers and Related Materials.
- 49. A. P. Abbott, J. C. Barron, K. S. Ryder, D. Wilson, *Chem. Eur. J.*, **13**, 6495-6501 (2007). Eutectic-Based Ionic Liquids with Metal-Containing Anions and Cations.
- 50. L. I. N. Tomé, V. Baião, W. da Silva, C. M. A. Brett, *Appl. Mater. Today*, **10**, 30-50 (2018). Deep Eutectic Solvents for the Production and Application of New Materials.
- 51. B. Gurkan, H. Squire, E. Pentzer, *J. Phys. Chem. Lett.*, **10**, 7956-7964 (2019). Metal-Free Deep Eutectic Solvents: Preparation, Physical Properties, and Significance.

- 52. B. Chen, S. Mitchell, N. Sinclair, J. Wainright, E. Pentzer, B. Gurkan, *Mol. Syst. Des. Eng.*, (2020). Feasibility of Tempo-Functionalized Imidazolium, Ammonium and Pyridinium Salts as Redox-Active Carriers in Ethaline Deep Eutectic Solvent for Energy Storage.
- 53. J. M. Klein, H. Squire, W. Dean, B. E. Gurkan, *J. Phys. Chem. B*, (2020). From Salt in Solution to Solely Ions Solvation of Methyl Viologen in Deep Eutectic Solvents and Ionic Liquids.
- 54. H. Sun, Y. Li, X. Wu, G. Li, *J. Mol. Model.*, **19**, 2433-2441 (2013). Theoretical Study on the Structures and Properties of Mixtures of Urea and Choline Chloride.
- 55. S. L. Perkins, P. Painter, C. M. Colina, *J. Phys. Chem. B*, **117**, 10250-10260 (2013). Molecular Dynamic Simulations and Vibrational Analysis of an Ionic Liquid Analogue.
- 56. M. Atilhan, S. Aparicio, *J. Phys. Chem. C*, **120**, 10400-10409 (2016). Deep Eutectic Solvents on the Surface of Face Centered Cubic Metals.
- 57. G. García, S. Aparicio, R. Ullah, M. Atilhan, *Energy Fuels*, **29**, 2616-2644 (2015). Deep Eutectic Solvents: Physicochemical Properties and Gas Separation Applications.
- 58. S. Kristyán, P. Pulay, *Chem. Phys. Lett*, **229**, 175-180 (1994). Can (Semi)Local Density Functional Theory Account for the London Dispersion Forces?
- 59. J. Pérez-Jordá, A. D. Becke, *Chem. Phys. Lett*, **233**, 134-137 (1995). A Density-Functional Study of Van Der Waals Forces: Rare Gas Diatomics.
- 60. P. Hobza, J. Sponer, T. Reschel, *J. Comput. Chem.*, **16**, 1315-1325 (1995). Density Functional Theory and Molecular Clusters.
- 61. S. Grimme, *WIREs Comput Mol Sci*, **1**, 211-228 (2011). Density Functional Theory with London Dispersion Corrections.
- 62. S. Grimme, S. Ehrlich, L. Goerigk, *J. Comput. Chem.*, **32**, 1456-1465 (2011). Effect of the Damping Function in Dispersion Corrected Density Functional Theory.
- 63. D. V. Wagle, G. A. Baker, E. Mamontov, *J. Phys. Chem. Lett.*, **6**, 2924-2928 (2015). Differential Microscopic Mobility of Components within a Deep Eutectic Solvent.
- 64. Y. Zhao, D. G. Truhlar, *Theor. Chem. Acc.*, **120**, 215-241 (2008). The M06 Suite of Density Functionals for Main Group Thermochemistry, Thermochemical Kinetics, Noncovalent Interactions, Excited States, and Transition Elements: Two New Functionals and Systematic Testing of Four M06-Class Functionals and 12 Other Functionals.
- 65. Y. Zhao, D. G. Truhlar, *Acc. Chem. Res.*, **41**, 157-167 (2008). Density Functionals with Broad Applicability in Chemistry.
- 66. M. Walker, A. J. A. Harvey, A. Sen, C. E. H. Dessent, *J. Phys. Chem. A*, **117**, 12590-12600 (2013). Performance of M06, M06-2x, and M06-Hf Density Functionals for Conformationally Flexible Anionic Clusters: M06 Functionals Perform Better Than B3lyp for a Model System with Dispersion and Ionic Hydrogen-Bonding Interactions.

- 67. D. V. Wagle, C. A. Deakyne, G. A. Baker, *J. Phys. Chem. B*, **120**, 6739-6746 (2016). Quantum Chemical Insight into the Interactions and Thermodynamics Present in Choline Chloride Based Deep Eutectic Solvents.
- 68. P. Bultinck, C. Van Alsenoy, P. W. Ayers, R. Carbó-Dorca, *J. Chem. Phys.*, **126**, 144111 (2007). Critical Analysis and Extension of the Hirshfeld Atoms in Molecules.
- 69. S. Zahn, *Phys. Chem. Chem. Phys.*, **19**, 4041-4047 (2017). Deep Eutectic Solvents: Similia Similibus Solvuntur?
- 70. C. J. Martin, D. A. O'Connor, *J. Phys. C: Solid State Phys.*, **10**, 3521-3526 (1977). An Experimental Test of Lindemann's Melting Law.
- 71. J. Wang, R. M. Wolf, J. W. Caldwell, P. A. Kollman, D. A. Case, *J. Comput. Chem.*, **25**, 1157-1174 (2004). Development and Testing of a General Amber Force Field.
- 72. S. L. Mayo, B. D. Olafson, W. A. Goddard, *J. Phys. Chem.*, **94**, 8897-8909 (1990). Dreiding: A Generic Force Field for Molecular Simulations.
- 73. S. W. I. Siu, K. Pluhackova, R. A. Böckmann, *J. Chem. Theory Comput.*, **8**, 1459-1470 (2012). Optimization of the Opls-Aa Force Field for Long Hydrocarbons.
- 74. D. Kony, W. Damm, S. Stoll, W. F. Van Gunsteren, *J. Comput. Chem.*, **23**, 1416-1429 (2002). An Improved Opls-Aa Force Field for Carbohydrates.
- 75. S. V. Sambasivarao, O. Acevedo, *J. Chem. Theory Comput.*, **5**, 1038-1050 (2009). Development of Opls-Aa Force Field Parameters for 68 Unique Ionic Liquids.
- 76. J. N. Canongia Lopes, J. Deschamps, A. A. H. Pádua, *J. Phys. Chem. B*, **108**, 2038-2047 (2004). Modeling Ionic Liquids Using a Systematic All-Atom Force Field.
- 77. W. L. Jorgensen, D. S. Maxwell, J. Tirado-Rives, *J. Am. Chem. Soc.*, **118**, 11225-11236 (1996). Development and Testing of the Opls All-Atom Force Field on Conformational Energetics and Properties of Organic Liquids.
- 78. D. Shah, F. S. Mjalli, *Phys. Chem. Chem. Phys.*, **16**, 23900-23907 (2014). Effect of Water on the Thermo-Physical Properties of Reline: An Experimental and Molecular Simulation Based Approach.
- 79. T. A. Halgren, *J. Comput. Chem.*, **17**, 490-519 (1996). Merck Molecular Force Field. I. Basis, Form, Scope, Parameterization, and Performance of Mmff94.
- 80. T. A. Halgren, *J. Comput. Chem.*, **17**, 520-552 (1996). Merck Molecular Force Field. Ii. Mmff94 Van Der Waals and Electrostatic Parameters for Intermolecular Interactions.
- 81. T. A. Halgren, *J. Comput. Chem.*, **17**, 553-586 (1996). Merck Molecular Force Field. lii. Molecular Geometries and Vibrational Frequencies for Mmff94.
- 82. H. Sun, *J. Phys. Chem. B*, **102**, 7338-7364 (1998). Compass: An Ab Initio Force-Field Optimized for Condensed-Phase Applicationsoverview with Details on Alkane and Benzene Compounds.

- 83. H. Sun, *J. Comput. Chem.*, **15**, 752-768 (1994). Force Field for Computation of Conformational Energies, Structures, and Vibrational Frequencies of Aromatic Polyesters.
- 84. T. I. Morrow, E. J. Maginn, *J. Phys. Chem. B*, **107**, 9160-9160 (2003). Molecular Dynamics Study of the Ionic Liquid 1-N-Butyl-3-Methylimidazolium Hexafluorophosphate.
- 85. A. Chaumont, R. Schurhammer, G. Wipff, *J. Phys. Chem. B*, **109**, 18964-18973 (2005). Aqueous Interfaces with Hydrophobic Room-Temperature Ionic Liquids: A Molecular Dynamics Study.
- 86. G. Chevrot, R. Schurhammer, G. Wipff, *Phys. Chem. Chem. Phys.*, **8**, 4166-4174 (2006). Molecular Dynamics Simulations of the Aqueous Interface with the [Bmi][Pf6] Ionic Liquid: Comparison of Different Solvent Models.
- 87. B. L. Bhargava, S. Balasubramanian, *J. Chem. Phys.*, **127**, 114510 (2007). Refined Potential Model for Atomistic Simulations of Ionic Liquid [Bmim][Pf6].
- 88. H. Liu, E. Maginn, A. E. Visser, N. J. Bridges, E. B. Fox, *Industrial & Engineering Chemistry Research*, **51**, 7242-7254 (2012). Thermal and Transport Properties of Six Ionic Liquids: An Experimental and Molecular Dynamics Study.
- 89. V. Chaban, *Phys. Chem. Chem. Phys.*, **13**, 16055-16062 (2011). Polarizability Versus Mobility: Atomistic Force Field for Ionic Liquids.
- 90. K. Cui, A. Yethiraj, J. R. Schmidt, *J. Phys. Chem. B*, **123**, 9222-9229 (2019). Influence of Charge Scaling on the Solvation Properties of Ionic Liquid Solutions.
- 91. B. Doherty, X. Zhong, S. Gathiaka, B. Li, O. Acevedo, *J. Chem. Theory Comput.*, **13**, 6131-6145 (2017). Revisiting Opls Force Field Parameters for Ionic Liquid Simulations.
- 92. B. Doherty, X. Zhong, O. Acevedo, *J. Phys. Chem. B*, **122**, 2962-2974 (2018). Virtual Site Opls Force Field for Imidazolium-Based Ionic Liquids.
- 93. J. Rigby, E. I. Izgorodina, *Phys. Chem. Chem. Phys.*, **15**, 1632-1646 (2013). Assessment of Atomic Partial Charge Schemes for Polarisation and Charge Transfer Effects in Ionic Liquids.
- 94. G. García, M. Atilhan, S. Aparicio, *J. Mol. Liq.*, **211**, 506-514 (2015). The Impact of Charges in Force Field Parameterization for Molecular Dynamics Simulations of Deep Eutectic Solvents.
- 95. D. Bedrov, J.-P. Piquemal, O. Borodin, A. D. MacKerell, Jr., B. Roux, C. Schröder, *Chem. Rev.*, **119**, 7940-7995 (2019). Molecular Dynamics Simulations of Ionic Liquids and Electrolytes Using Polarizable Force Fields.
- 96. M. Atilhan, S. Aparicio, *J. Mol. Liq.*, **283**, 147-154 (2019). Molecular Dynamics Simulations of Mixed Deep Eutectic Solvents and Their Interaction with Nanomaterials.
- 97. E. E. L. Tanner, K. M. Piston, H. Ma, K. N. Ibsen, S. Nangia, S. Mitragotri, *ACS Biomater. Sci. Eng.*, **5**, 3645-3653 (2019). The Influence of Water on Choline-Based Ionic Liquids.

- 98. E. S. C. Ferreira, I. V. Voroshylova, C. M. Pereira, M. N. D S Cordeiro, *J. Phys. Chem. B*, **120**, 10124-10137 (2016). Improved Force Field Model for the Deep Eutectic Solvent Ethaline: Reliable Physicochemical Properties.
- 99. K. Górny, Z. Dendzik, M. Pabiszczak, Z. Gburski, *J. Non-Cryst. Solids*, **364**, 28-33 (2013). Non-Debye Dipolar Relaxation of Ethylene Glycol Embedded in Zsm-5 Zeolite Host Matrix Computer Simulation Study.
- 100. A. D. Mackerell, Jr., M. Feig, C. L. Brooks, 3rd, *J Comput Chem*, **25**, 1400-1415 (2004). Extending the Treatment of Backbone Energetics in Protein Force Fields: Limitations of Gas-Phase Quantum Mechanics in Reproducing Protein Conformational Distributions in Molecular Dynamics Simulations.
- 101. E. S. C. Ferreira, I. V. Voroshylova, N. M. Figueiredo, C. M. Pereira, M. N. D., *J. Mol. Liq.*, **298**, 111978 (2020). Computational and Experimental Study of Propeline: A Choline Chloride Based Deep Eutectic Solvent.
- 102. E. S. C. Ferreira, I. V. Voroshylova, V. A. Koverga, C. M. Pereira, M. N. D. S. Cordeiro, *J. Phys. Chem. B*, **121**, 10906-10921 (2017). New Force Field Model for Propylene Glycol: Insight to Local Structure and Dynamics.
- 103. A. K. Soper, E. W. Castner, A. Luzar, *Biophys. Chem.*, **105**, 649-666 (2003). Impact of Urea on Water Structure: A Clue to Its Properties as a Denaturant?
- 104. H. S. Salehi, M. Ramdin, O. A. Moultos, T. J. H. Vlugt, *Fluid Ph. Equilibria*, **497**, 10-18 (2019). Computing Solubility Parameters of Deep Eutectic Solvents from Molecular Dynamics Simulations.
- 105. K. Shahbaz, S. Baroutian, F. S. Mjalli, M. A. Hashim, I. M. AlNashef, *Thermochim. Acta*, **527**, 59-66 (2012). Densities of Ammonium and Phosphonium Based Deep Eutectic Solvents: Prediction Using Artificial Intelligence and Group Contribution Techniques.
- 106. R. B. Leron, M.-H. Li, *Thermochim. Acta*, **530**, 52-57 (2012). Molar Heat Capacities of Choline Chloride-Based Deep Eutectic Solvents and Their Binary Mixtures with Water.
- 107. R. B. Leron, D. S. H. Wong, M.-H. Li, *Fluid Ph. Equilibria*, **335**, 32-38 (2012). Densities of a Deep Eutectic Solvent Based on Choline Chloride and Glycerol and Its Aqueous Mixtures at Elevated Pressures.
- 108. Y. Xie, H. Dong, S. Zhang, X. Lu, X. Ji, *J. Chem. Eng. Data*, **59**, 3344-3352 (2014). Effect of Water on the Density, Viscosity, and Co2solubility in Choline Chloride/Urea.
- 109. F. Chemat, H. Anjum, A. M. Shariff, P. Kumar, T. Murugesan, *J. Mol. Liq.*, **218**, 301-308 (2016). Thermal and Physical Properties of (Choline Chloride Urea L-Arginine) Deep Eutectic Solvents.
- 110. C. Florindo, F. S. Oliveira, L. P. N. Rebelo, A. M. Fernandes, I. M. Marrucho, *ACS Sustain. Chem. Eng.*, **2**, 2416-2425 (2014). Insights into the Synthesis and Properties of Deep Eutectic Solvents Based on Cholinium Chloride and Carboxylic Acids.

- 111. A. Yadav, S. Pandey, *J. Chem. Eng. Data*, **59**, 2221-2229 (2014). Densities and Viscosities of (Choline Chloride + Urea) Deep Eutectic Solvent and Its Aqueous Mixtures in the Temperature Range 293.15 K to 363.15 K.
- 112. H. Shekaari, M. T. Zafarani-Moattar, B. Mohammadi, *J. Mol. Liq.*, **243**, 451-461 (2017). Thermophysical Characterization of Aqueous Deep Eutectic Solvent (Choline Chloride/Urea) Solutions in Full Ranges of Concentration at T= (293.15–323.15) K.
- 113. F. S. Mjalli, N. M. Abdel Jabbar, *Fluid Ph. Equilibria*, **381**, 71-76 (2014). Acoustic Investigation of Choline Chloride Based Ionic Liquids Analogs.
- 114. F. S. Mjalli, G. Vakili-Nezhaad, K. Shahbaz, I. M. AlNashef, *Thermochim. Acta*, **575**, 40-44 (2014). Application of the Eötvos and Guggenheim Empirical Rules for Predicting the Density and Surface Tension of Ionic Liquids Analogues.
- 115. O. Ciocirlan, O. Iulian, O. Croitoru, *Rev. Chim.*, **62**, 721-723 (2010). Effect of Temperature on the Physico-Chemical Properties of Three Ionic Liquids Containing Choline.
- 116. M. E. Senko, D. H. Templeton, *Acta Crystallographica*, **13**, 281-285 (1960). Unit Cells of Choline Halides and Structure of Choline Chloride.
- 117. K. Shahbaz, F. S. Mjalli, M. A. Hashim, I. M. AlNashef, *Thermochim. Acta*, **515**, 67-72 (2011). Prediction of Deep Eutectic Solvents Densities at Different Temperatures.
- 118. A. Yadav, J. R. Kar, M. Verma, S. Naqvi, S. Pandey, *Thermochim. Acta*, **600**, 95-101 (2015). Densities of Aqueous Mixtures of (Choline Chloride Ethylene Glycol) and (Choline Chloride Malonic Acid) Deep Eutectic Solvents in Temperature Range 283.15–363.15k.
- 119. A. P. Abbott, G. Capper, D. L. Davies, K. J. McKenzie, S. U. Obi, *J. Chem. Eng. Data*, **51**, 1280-1282 (2006). Solubility of Metal Oxides in Deep Eutectic Solvents Based on Choline Chloride.
- 120. R. Haghbakhsh, M. Taherzadeh, A. R. C. Duarte, S. Raeissi, *J. Mol. Liq.*, **307**, 112972 (2020). A General Model for the Surface Tensions of Deep Eutectic Solvents.
- 121. K. Shahbaz, F. S. Mjalli, M. A. Hashim, I. M. AlNashef, *Fluid Ph. Equilibria*, **319**, 48-54 (2012). Prediction of the Surface Tension of Deep Eutectic Solvents.
- 122. D. B. Macleod, *J. Chem. Soc. Faraday Trans.*, **19**, 38 (1923). On a Relation between Surface Tension and Density.
- 123. S. Sugden, *J. Chem. Soc., Trans.*, **125**, 32-41 (1924). Vi.—the Variation of Surface Tension with Temperature and Some Related Functions.
- 124. O. R. Quayle, *Chem. Rev.*, **53**, 439-589 (1953). The Parachors of Organic Compounds. An Interpretation and Catalogue.
- 125. S. A. Mumford, J. W. C. Phillips, *J. Chem. Soc.*, **0**, 2112-2133 (1929). Cclxxiv.—the Evaluation and Interpretation of Parachors.

- 126. T. A. Knotts, W. Vincent Wilding, J. L. Oscarson, R. L. Rowley, *J. Chem. Eng. Data*, **46**, 1007-1012 (2001). Use of the Dippr Database for Development of Qspr Correlations: Surface Tension†.
- 127. M. Deetlefs, K. R. Seddon, M. Shara, *Phys. Chem. Chem. Phys.*, **8**, 642-649 (2006). Predicting Physical Properties of Ionic Liquids.
- 128. R. L. Gardas, J. A. P. Coutinho, *Fluid Ph. Equilibria*, **265**, 57-65 (2008). Applying a Qspr Correlation to the Prediction of Surface Tensions of Ionic Liquids.
- 129. M. Lagache, P. Ungerer, A. Boutin, A. H. Fuchs, *Phys. Chem. Chem. Phys.*, **3**, 4333-4339 (2001). Prediction of Thermodynamic Derivative Properties of Fluids by Monte Carlo Simulation.
- 130. C. Cadena, Q. Zhao, R. Q. Snurr, E. J. Maginn, *J. Phys. Chem. B*, **110**, 2821-2832 (2006). Molecular Modeling and Experimental Studies of the Thermodynamic and Transport Properties of Pyridinium-Based Ionic Liquids.
- 131. K. E. Gutowski, B. Gurkan, E. J. Maginn, *Pure Appl. Chem.*, **81**, 1799-1828 (2009). Force Field for the Atomistic Simulation of the Properties of Hydrazine, Organic Hydrazine Derivatives, and Energetic Hydrazinium Ionic Liquids.
- 132. P. H. Berens, D. H. J. Mackay, G. M. White, K. R. Wilson, *J. Chem. Phys.*, **79**, 2375-2389 (1983). Thermodynamics and Quantum Corrections from Molecular Dynamics for Liquid Water.
- 133. M. Chen, R. Pendrill, G. Widmalm, J. W. Brady, J. Wohlert, *J. Chem. Theory Comput.*, **10**, 4465-4479 (2014). Molecular Dynamics Simulations of the Ionic Liquid 1-N-Butyl-3-Methylimidazolium Chloride and Its Binary Mixtures with Ethanol.
- 134. S.-T. Lin, M. Blanco, W. A. Goddard, *J. Chem. Phys.*, **119**, 11792-11805 (2003). The Two-Phase Model for Calculating Thermodynamic Properties of Liquids from Molecular Dynamics: Validation for the Phase Diagram of Lennard-Jones Fluids.
- 135. M. Taherzadeh, R. Haghbakhsh, A. R. C. Duarte, S. Raeissi, *J. Mol. Liq.*, **307**, 112940 (2020). Estimation of the Heat Capacities of Deep Eutectic Solvents.
- 136. S. Ravula, N. E. Larm, M. A. Mottaleb, M. P. Heitz, G. A. Baker, *ChemEngineering*, **3**, 42 (2019). Vapor Pressure Mapping of Ionic Liquids and Low-Volatility Fluids Using Graded Isothermal Thermogravimetric Analysis.
- 137. K. Shahbaz, F. S. Mjalli, G. Vakili-Nezhaad, I. M. AlNashef, A. Asadov, M. M. Farid, *J. Mol. Liq.*, **222**, 61-66 (2016). Thermogravimetric Measurement of Deep Eutectic Solvents Vapor Pressure.
- 138. K. A. Motakabbir, M. Berkowitz, *J. Phys. Chem.*, **94**, 8359-8362 (1990). Isothermal Compressibility of Spc/E Water.
- 139. J. H. Dymond, R. Malhotra, *Int. J. Thermophys.*, **9**, 941-951 (1988). The Tait Equation: 100 Years On.

- 140. J. K. Shah, J. F. Brennecke, E. J. Maginn, *Green Chem.*, **4**, 112-118 (2002). Thermodynamic Properties of the Ionic Liquid 1-N-Butyl-3-Methylimidazolium Hexafluorophosphate from Monte Carlo Simulations.
- 141. S. M. Hosseini, S. Aparicio, M. M. Alavianmehr, R. Khalifeh, *J. Mol. Liq.*, **266**, 751-761 (2018). On the Volumetric Properties of 2-Hydroxy Ethylammonium Formate Ionic Liquid under High-Pressures: Measurement and Molecular Dynamics.
- 142. M. P. Allen, M., D. J. Tildesley, T. Allen, D., *Computer Simulation of Liquids*, Oxford University Press, 1989.
- 143. C. L. Diel, V. F. Cabral, *J. Mol. Liq.*, **282**, 226-234 (2019). Equilibrium Properties of Protic Ionic Liquids Based on Metil-2-Hydroxyethylammonium Cation.
- 144. Z. Pouramini, A. Mohebbi, M. H. Kowsari, *J. Mol. Liq.*, **246**, 39-47 (2017). Atomistic Insights into the Thermodynamics, Structure, and Dynamics of Ionic Liquid 1-Hexyl-3-Methylimidazolium Hexafluorophosphate Via Molecular Dynamics Study.
- 145. H. Sakuma, M. Ichiki, *Geofluids*, **16**, 89-102 (2016). Density and Isothermal Compressibility of Supercritical H2o-Nacl Fluid: Molecular Dynamics Study from 673 to 2000 K, 0.2 to 2 Gpa, and 0 to 22 Wt% Nacl Concentrations.
- 146. E. S. Minina, E. S. Pyanzina, E. V. Novak, S. S. Kantorovich, *Eur. Phys. J. E Soft Matter*, **41**, 67 (2018). Compressibility of Ferrofluids: Towards a Better Understanding of Structural Properties.
- 147. B. Szefczyk, M. N. D. S. Cordeiro, *J. Phys. Chem. B*, **115**, 3013-3019 (2011). Physical Properties at the Base for the Development of an All-Atom Force Field for Ethylene Glycol.
- 148. W. Guo, Y. Hou, S. Ren, S. Tian, W. Wu, *J. Chem. Eng. Data*, **58**, 866-872 (2013). Formation of Deep Eutectic Solvents by Phenols and Choline Chloride and Their Physical Properties.
- 149. A. P. Abbott, R. C. Harris, K. S. Ryder, *J. Phys. Chem. B*, **111**, 4910-4913 (2007). Application of Hole Theory to Define Ionic Liquids by Their Transport Properties.
- 150. R. Stefanovic, M. Ludwig, G. B. Webber, R. Atkin, A. J. Page, *Phys. Chem. Chem. Phys.*, **19**, 3297-3306 (2017). Nanostructure, Hydrogen Bonding and Rheology in Choline Chloride Deep Eutectic Solvents as a Function of the Hydrogen Bond Donor.
- 151. R. Zwanzig, *Annu. Rev. Phys. Chem.*, **16**, 67-102 (1965). Time-Correlation Functions and Transport Coefficients in Statistical Mechanics.
- 152. C. Rey-Castro, L. F. Vega, *J. Phys. Chem. B*, **110**, 14426-14435 (2006). Transport Properties of the Ionic Liquid 1-Ethyl-3-Methylimidazolium Chloride from Equilibrium Molecular Dynamics Simulation. The Effect of Temperature.
- 153. M. H. Kowsari, S. Alavi, M. Ashrafizaadeh, B. Najafi, *J. Chem. Phys.*, **130**, 014703 (2009). Molecular Dynamics Simulation of Imidazolium-Based Ionic Liquids. Ii. Transport Coefficients.

- 154. M. Atilhan, J. Jacquemin, D. Rooney, M. Khraisheh, S. Aparicio, *Ind. Eng. Chem. Res.*, **52**, 16774-16785 (2013). Viscous Behavior of Imidazolium-Based Ionic Liquids.
- 155. L. Zhao, X. Wang, L. Wang, H. Sun, *Fluid Ph. Equilibria*, **260**, 212-217 (2007). Prediction of Shear Viscosities Using Periodic Perturbation Method and Opls Force Field.
- 156. J. Ma, Z. Zhang, Y. Xiang, F. Cao, H. Sun, *Mol. Simul.*, **43**, 1502-1512 (2017). On the Prediction of Transport Properties of Ionic Liquid Using 1-N-Butylmethylpyridinium Tetrafluoroborate as an Example.
- 157. B. Hess, *J. Chem. Phys.*, **116**, 209 (2002). Determining the Shear Viscosity of Model Liquids from Molecular Dynamics Simulations.
- 158. S. H. Jamali, R. Hartkamp, C. Bardas, J. Söhl, T. J. H. Vlugt, O. A. Moultos, *J. Chem. Theory Comput.*, **14**, 5959-5968 (2018). Shear Viscosity Computed from the Finite-Size Effects of Self-Diffusivity in Equilibrium Molecular Dynamics.
- 159. I.-C. Yeh, G. Hummer, *J. Phys. Chem. B*, **108**, 15873-15879 (2004). System-Size Dependence of Diffusion Coefficients and Viscosities from Molecular Dynamics Simulations with Periodic Boundary Conditions.
- 160. Y. Zhang, A. Otani, E. J. Maginn, *J. Chem. Theory Comput.*, **11**, 3537-3546 (2015). Reliable Viscosity Calculation from Equilibrium Molecular Dynamics Simulations: A Time Decomposition Method.
- 161. F. Müller-Plathe, *Phys. Rev. E*, **59**, 4894 (1999). Reversing the Perturbation in Nonequilibrium Molecular Dynamics: An Easy Way to Calculate the Shear Viscosity of Fluids.
- 162. M. S. Kelkar, E. J. Maginn, *J. Phys. Chem. B*, **111**, 4867-4876 (2007). Effect of Temperature and Water Content on the Shear Viscosity of the Ionic Liquid 1-Ethyl-3-Methylimidazolium Bis(Trifluoromethanesulfonyl)Imide as Studied by Atomistic Simulations.
- 163. T. Altamash, M. Atilhan, A. Aliyan, R. Ullah, G. García, S. Aparicio, *RSC Adv.*, **6**, 109201-109210 (2016). Insights into Choline Chloride–Phenylacetic Acid Deep Eutectic Solvent for Co 2 Absorption.
- 164. A. González de Castilla, J. P. Bittner, S. Müller, S. Jakobtorweihen, I. Smirnova, *J. Chem. Eng. Data*, (2019). Thermodynamic and Transport Properties Modeling of Deep Eutectic Solvents: A Review on G E -Models, Equations of State, and Molecular Dynamics.
- 165. R. Haghbakhsh, S. Raeissi, K. Parvaneh, A. Shariati, *J. Mol. Liq.*, **249**, 554-561 (2018). The Friction Theory for Modeling the Viscosities of Deep Eutectic Solvents Using the Cpa and Pc-Saft Equations of State.
- 166. R. Haghbakhsh, K. Parvaneh, S. Raeissi, A. Shariati, *Fluid Ph. Equilibria*, **470**, 193-202 (2018). A General Viscosity Model for Deep Eutectic Solvents: The Free Volume Theory Coupled with Association Equations of State.
- 167. J. O. Lloret, L. F. Vega, F. Llovell, *Fluid Ph. Equilibria*, **448**, 81-93 (2017). Accurate Description of Thermophysical Properties of Tetraalkylammonium Chloride Deep Eutectic Solvents with the Soft-Saft Equation of State.

- 168. A. P. Abbott, R. C. Harris, K. S. Ryder, C. D'Agostino, L. F. Gladden, M. D. Mantle, *Green Chem.*, **13**, 82-90 (2011). Glycerol Eutectics as Sustainable Solvent Systems.
- 169. H. Zhao, Z.-C. Liang, F. Li, *J. Mol. Liq.*, **149**, 55-59 (2009). An Improved Model for the Conductivity of Room-Temperature Ionic Liquids Based on Hole Theory.
- 170. M. G. Del Pópolo, G. A. Voth, *J. Phys. Chem. B*, **108**, 1744-1752 (2004). On the Structure and Dynamics of Ionic Liquids.
- 171. M. Francisco, A. van den Bruinhorst, M. C. Kroon, *Angew. Chem. Int. Ed Engl.*, **52**, 3074-3085 (2013). Low-Transition-Temperature Mixtures (Lttms): A New Generation of Designer Solvents.
- 172. M. Gilmore, L. M. Moura, A. H. Turner, M. Swadźba-Kwaśny, S. K. Callear, J. A. McCune, O. A. Scherman, J. D. Holbrey, *J. Chem. Phys.*, **148**, 193823 (2018). A Comparison of Choline:Urea and Choline:Oxalic Acid Deep Eutectic Solvents at 338 K.
- 173. A. Korotkevich, D. S. Firaha, A. A. H. Padua, B. Kirchner, *Fluid Ph. Equilibria*, **448**, 59-68 (2017). Ab Initio Molecular Dynamics Simulations of So 2 Solvation in Choline Chloride/Glycerol Deep Eutectic Solvent.
- 174. Y. Dai, J. van Spronsen, G.-J. Witkamp, R. Verpoorte, Y. H. Choi, *Anal. Chim. Acta*, **766**, 61-68 (2013). Natural Deep Eutectic Solvents as New Potential Media for Green Technology.
- 175. R. Ahmadi, B. Hemmateenejad, A. Safavi, Z. Shojaeifard, A. Shahsavar, A. Mohajeri, M. Heydari Dokoohaki, A. R. Zolghadr, *Phys. Chem. Chem. Phys.*, **20**, 18463-18473 (2018). Deep Eutectic-Water Binary Solvent Associations Investigated by Vibrational Spectroscopy and Chemometrics.
- 176. A. H. Turner, J. D. Holbrey, *Phys. Chem. Chem. Phys.*, (2019). Investigation of Glycerol Hydrogen-Bonding Networks in Choline Chloride/Glycerol Eutectic-Forming Liquids Using Neutron Diffraction.
- 177. S. Kaur, S. Sharma, H. K. Kashyap, *J. Chem. Phys.*, **147**, 194507 (2017). Bulk and Interfacial Structures of Reline Deep Eutectic Solvent: A Molecular Dynamics Study.
- 178. V. Migliorati, F. Sessa, P. D'Angelo, *Chemical Physics Letters: X*, **2**, 100001 (2019). Deep Eutectic Solvents: A Structural Point of View on the Role of the Cation.
- 179. F. L. Hirshfeld, *Theor. Chem. Acc.*, **44**, 129-138 (1977). Bonded-Atom Fragments for Describing Molecular Charge Densities.
- 180. P. Wernet, D. Nordlund, U. Bergmann, M. Cavalleri, M. Odelius, H. Ogasawara, L. A. Näslund, T. K. Hirsch, L. Ojamäe, P. Glatzel, L. G. M. Pettersson, A. Nilsson, *Science*, **304**, 995-999 (2004). The Structure of the First Coordination Shell in Liquid Water.
- 181. L. P. Silva, C. F. Araújo, D. O. Abranches, M. Melle-Franco, M. A. R. Martins, M. M. Nolasco, P. J. A. Ribeiro-Claro, S. P. Pinho, J. A. P. Coutinho, *Phys. Chem. Chem. Phys.*, **21**, 18278-18289 (2019). What a Difference a Methyl Group Makes Probing Choline–Urea Molecular Interactions through Urea Structure Modification.

- 182. M. E. Tuckerman, A. Chandra, D. Marx, *J. Chem. Phys.*, **133**, 124108 (2010). A Statistical Mechanical Theory of Proton Transport Kinetics in Hydrogen-Bonded Networks Based on Population Correlation Functions with Applications to Acids and Bases.
- 183. F. Perera, *Int. J. Environ. Res. Public Health*, **15**, (2017). Pollution from Fossil-Fuel Combustion Is the Leading Environmental Threat to Global Pediatric Health and Equity: Solutions Exist.
- 184. T. J. Trivedi, J. H. Lee, H. J. Lee, Y. K. Jeong, J. W. Choi, *Green Chem.*, **18**, 2834-2842 (2016). Deep Eutectic Solvents as Attractive Media for Co2 Capture.
- 185. D. Yang, M. Hou, H. Ning, J. Zhang, J. Ma, G. Yang, B. Han, *Green Chem.*, **15**, 2261 (2013). Efficient So2 Absorption by Renewable Choline Chloride–Glycerol Deep Eutectic Solvents.
- 186. D. Deng, G. Han, Y. Jiang, *New J. Chem.*, **39**, 8158-8164 (2015). Investigation of a Deep Eutectic Solvent Formed by Levulinic Acid with Quaternary Ammonium Salt as an Efficient So 2 Absorbent.
- 187. S. Sun, Y. Niu, Q. Xu, Z. Sun, X. Wei, *Ind. Eng. Chem. Res.*, **54**, 8019-8024 (2015). Efficient So 2 Absorptions by Four Kinds of Deep Eutectic Solvents Based on Choline Chloride.
- 188. H. Li, Y. Chang, W. Zhu, C. Wang, C. Wang, S. Yin, M. Zhang, H. Li, *Phys. Chem. Chem. Phys.*, **17**, 28729-28742 (2015). Theoretical Evidence of Charge Transfer Interaction between So₂ and Deep Eutectic Solvents Formed by Choline Chloride and Glycerol.
- 189. O. S. Hammond, K. J. Edler, D. T. Bowron, L. Torrente-Murciano, *Nat. Commun.*, **8**, (2017). Deep Eutectic-Solvothermal Synthesis of Nanostructured Ceria.
- 190. L. Wei, Z.-Y. Zhou, S.-P. Chen, C.-D. Xu, D. Su, M. E. Schuster, S.-G. Sun, *Chem. Commun.*, **49**, 11152-11154 (2013). Electrochemically Shape-Controlled Synthesis in Deep Eutectic Solvents: Triambic Icosahedral Platinum Nanocrystals with High-Index Facets and Their Enhanced Catalytic Activity.
- 191. A. P. Abbott, J. C. Barron, G. Frisch, K. S. Ryder, A. F. Silva, *Electrochim. Acta*, **56**, 5272-5279 (2011). The Effect of Additives on Zinc Electrodeposition from Deep Eutectic Solvents.
- 192. N. M. Pereira, P. M. V. Fernandes, C. M. Pereira, A. Fernando Silva, *J. Electrochem. Soc.*, **159**, D501-D506 (2012). Electrodeposition of Zinc from Choline Chloride-Ethylene Glycol Deep Eutectic Solvent: Effect of the Tartrate Ion.
- 193. L. Vieira, R. Schennach, B. Gollas, *Phys. Chem. Chem. Phys.*, **17**, 12870-12880 (2015). In Situ Pm-Irras of a Glassy Carbon Electrode/Deep Eutectic Solvent Interface.
- 194. D. Lindberg, M. de la Fuente Revenga, M. Widersten, *J. Biotechnol.*, **147**, 169-171 (2010). Deep Eutectic Solvents (Dess) Are Viable Cosolvents for Enzyme-Catalyzed Epoxide Hydrolysis.
- 195. J. T. Gorke, F. Srienc, R. J. Kazlauskas, *Chem. Commun.*, 1235-1237 (2008). Hydrolase-Catalyzed Biotransformations in Deep Eutectic Solvents.

196. N. Guajardo, K. Ahumada, P. Domínguez de María, R. A. Schrebler, *Biocatal. Biotransformation*, **37**, 106-114 (2019). Remarkable Stability of Candida Antarctica Lipase B Immobilized Via Cross-Linking Aggregates (Clea) in Deep Eutectic Solvents.